

THE EFFECTS OF OXYGEN ON THE FORMATION OF
Ni, Pd and Pt SILICIDES

Thesis by
David Martin Scott

In Partial Fulfillment of the Requirements
for the Degree of
Doctor of Philosophy

California Institute of Technology
Pasadena, California

1982

(Submitted March 3, 1982)

ACKNOWLEDGEMENTS

It is a very moving experience to acknowledge the people who have contributed to the successful completion of my work at Caltech. First and foremost I would like to express my appreciation to my advisor, Professor Marc-A. Nicolet for the guidance, support and encouragement he has given me throughout my stay at Caltech. I am deeply indebted to him. I would also like to thank Professor James W. Mayer for his thoughtful advice and encouragement. It has been a very rewarding experience to work in their solid state group.

Several people have contributed to the technical aspect of this work. I would like to give special thanks to Dr. Paula J. Grunthaler for her collaboration on the XPS work. I also wish to thank Dr. Bor-Yeu Tsaur for his assistance at the start of this work and also Drs. Silvanus S. Lau, Leszek S. Wielunski and Professor Charles A. Barnes for their interest and many fruitful discussions.

The collaboration of Thomas C. Banwell on the contact resistivity work and especially during meV/atom Pb implantations is gratefully acknowledged. I would also like to express my appreciation to Rob Gorris, Rouel Fernandez, Daniel G. Tonn and Jeff J. Mallory for their outstanding technical help and also to Wilfred Schick for his assistance with the 3 MeV accelerator. Thanks to Mrs. Michell L. Parks for her friendship and skillful typing and also to Linda Dozsa for her friendship throughout my stay here. Thanks also to Vivian Davies for her excellent work on this manuscript.

Of the people outside the Caltech community who also contributed to the successful completion of my graduate work, I am most deeply indebted to Dr. Judy Swerling for her friendship and support. I am also indebted to John Krenzalek for his support and understanding both as landlord and as a good friend. I especially wish to express my deepest appreciation to Jennette Johnson for her love and support. The concern and advice of Dr. Fernando Morinigo is also gratefully appreciated. I would also like to thank my mom, Janice V. Scott for her support and encouragement and my fiancée Anne E. Ludvigsen for her love, encouragement and patient understanding. Finally, I would like to acknowledge the Calculator (Toy) Division of Hewlett-Packard for making the work reported here not only easier but much more enjoyable.

ABSTRACT

A systematic study of the effects of implanted oxygen on the formation of Ni, Pt and Pd silicides has been carried out using $^4\text{He}^+$ backscattering spectrometry (BS), $^{16}\text{O}(d,\alpha)^{14}\text{N}$ nuclear reaction analysis (NRA) and x-ray photoelectron spectroscopy (XPS) for the analysis. A detailed presentation of the NRA technique is given as this technique was central to this study and is not as generally known as are BS and XPS (Chapter II). The depth resolution of this technique is found to be ~ 150 to 200 \AA in Ni. The oxygen sensitivity is essentially limited by measurement time (~ 10 hrs) to $\sim 10^{19}$ to 10^{20} O/cm^2 .

The effect of oxygen on the formation of Ni_2Si is shown to vary with the initial location of the oxygen (Chapter III). Ni is the dominant diffusing species in Ni_2Si formation. Oxygen initially located in the Ni film is found to build up during annealing at the Ni- Ni_2Si interface until a diffusion barrier to the Ni is formed. The XPS data shows this barrier to be SiO_2 . Oxygen picked up during annealing from the ambient also plays a role in the buildup of this barrier. Once Ni_2Si growth is halted, the second phase NiSi begins to nucleate and grow. The result is the simultaneous presence of Ni, Ni_2Si and NiSi in the implanted samples. The threshold dose ϕ_{th} necessary for barrier formation is $\sim 1.2 \times 10^{16} \text{ O/cm}^2$. This is equivalent to $\sim 26 \text{ \AA}$ of stoichiometric fused quartz if present as a layer. For the oxygen initially present in the Si, the oxygen is incorporated into the Ni_2Si layer without an interfacial accumulation taking place. The relative reduction in oxygen density parallels that of the Si density as Si forms Ni_2Si .

We model these observations in terms of the asymmetries that are present in this system with regard to the moving species in Ni_2Si formation and with regard to the chemical reactivity of oxygen with Ni and Si.

The effects of implanted oxygen on NiSi formation are studied for the case of the oxygen initially present in the Ni_2Si film on a Si $\langle 100 \rangle$ substrate. Upon annealing, NiSi grows with square root of time in both implanted and unimplanted samples. This disagrees with the linear rate previously reported. The growth is slightly slower for implanted samples. The slowing is uncorrelated with the amount of oxygen, suggesting that a structural change due to ion implantation is the cause. During NiSi formation, oxygen is incorporated into the NiSi film without interfacial accumulation, but the oxygen distribution is seen to move towards the surface. This motion is explained in terms of a simple model based on the chemical affinity of oxygen to Si and Ni and the fact that Ni is the moving species in NiSi growth. The shift in the oxygen peak position during NiSi formation enables the implanted oxygen to act as a diffusion marker. This confirms that Ni is the diffusing species in NiSi formation. The use of implanted oxygen as a diffusion marker in thin film studies is briefly explored.

We have also studied the effect of impurity oxygen initially present in a Pt film on Pt_2Si formation (Chapter IV). We found that the redistribution of the oxygen during annealing, subsequent barrier formation and threshold oxygen dose were all identical to that of the corresponding Ni case. This result is shown to be consistent with the asymmetries present in the chemistry of oxygen relative to Pt and Si and in the initial

location of the oxygen relative to the moving species (Pt). The case of oxygen initially located in the Si was not investigated as this case most likely is also identical to the corresponding Ni case.

For the impurity oxygen initially present in a Pd film on a Si $\langle 100 \rangle$ substrate (Chapter V), we found that the oxygen is incorporated into the Pd₂Si without a diffusion barrier being formed. The implanted oxygen has no effect on the growth of Pt₂Si. We find oxygen to be mobile in the Pd at an annealing temperature of only 250°C. Upon annealing the oxygen diffuses to the Pd-Pt₂Si interface, to react and form SiO₂ there. Simultaneously Si diffuses through the Pd₂Si layer and forms additional silicide at the Pd-Pd₂Si interface thereby incorporating the SiO₂ into the Pd₂Si. Thus barrier formation does not occur. We also show that our results identify Si as the dominant diffusing species during Pd₂Si formation rather than both Pd and Si as previously reported.

Generalizing from the result of our study of the effects of impurity oxygen on the formation of the silicides of Ni, Pt and Pd we present a conceptual framework for impurity effects in metal silicide formation (Chapter VI). This model relies on the asymmetries present with regard to the initial location of the impurity relative to the moving species and with regard to the chemical affinities of the impurity relative to the reacting species. The results for impurity N in the Ni-Si system are briefly compared with predictions of the model and shown to agree.

Further work suggested by this model is summarized next (Chapter VII). The cases covered are impurity N in the Ni-Si, Pt-Si and Pd-Si systems along with impurity C in the Ni-Si and Pt-Si systems. Also covered are the preliminary results of contact resistivity measurements

after barrier formation has occurred for the cases of impurity N and O in the Ni-Si system. The results of this additional work are shown to be consistent with the model.

Some parts of this thesis have already been published under the following titles:

1. "The Effect of Oxygen on the Growth Kinetics of Nickel Silicides," D. M. Scott, P. J. Grunthaner, B. Y. Tsauro, M-A. Nicolet and J. W. Mayer, in *Proceedings of the Symposium on Thin Film Interfaces and Interactions*, J. E. E. Baglin and J. M. Poate, eds., (The Electrochemical Soc. Princeton, Vol. 80-2, 148 (1980))
2. "Modification of Nickel Silicide Formation by Oxygen Implantation," D. M. Scott and M-A. Nicolet, *Nucl. Inst. Meth.* 182/183, 655 (1981)
3. "Implanted Oxygen in NiSi Formation," D. M. Scott and M-A. Nicolet, *Phys. Stat. Sol. (a)*, 66, 773 (1981)
4. "Oxygen Impurity Effects at Metal/Silicide Interfaces: Formation of Silicon Oxide and Suboxides in the Ni/Si System," P. J. Grunthaner, F. J. Grunthaner, D. M. Scott, M-A. Nicolet, and J. W. Mayer,, *J. Vac. Sci. Tech.* 19, 641 (1981)
5. "Alteration of Ni Silicide Formation by N Implantation," L. Wielunski, D. M. Scott, M-A. Nicolet and H. von Seefeld, *Appl. Phys. Lett.*, 38, 106 (1981)
6. "Retardation and Suppression of Nickel Silicide Formation by N⁺ Implantation," D. M. Scott, L. Wielunski, H. von Seefeld and M-A. Nicolet, *Nucl. Inst. Meth.*, 182/183 661 (1981)

TABLE OF CONTENTS

ACKNOWLEDGEMENTS	ii
ABSTRACT	iv
TABLE OF CONTENTS	viii
CHAPTER I. INTRODUCTION	1
REFERENCES	3
CHAPTER II. EXPERIMENTAL METHODS	4
A. Introduction	4
B. $^{16}\text{O}(d,\alpha)^{14}\text{N}$ Nuclear Reaction Analysis	5
1. Introduction	5
2. Radiation Safety	6
3. Geometry	6
4. Depth Scale	9
5. Oxygen Concentration	9
6. Stopping Power	12
7. Cross Section	14
8. Charge Normalization	15
9. Resolution	17
10. Geometrical Effects	18
11. Straggling	19
12. Interferences	21
13. Results and Discussion	24
14. Sensitivity	26
15. Resolution	27
16. Summary	27
REFERENCES	29
CHAPTER III. IMPURITY OXYGEN IN NICKEL SILICIDE FORMATION	31
A. Introduction	31
B. Experimental Procedures	33
1. Initial Oxygen in Ni	33
2. Initial Oxygen in Si	35
3. Initial Oxygen in Ni_2Si	36
C. Oxygen in Ni	38
1. Experimental Results	38
2. Discussion	48
D. Oxygen in Silicon	52
1. Experimental Results	52
2. Discussion	55
E. Oxygen in Ni_3Si	58
1. Experimental Results	58
2. Discussion	60
F. Summary and Conclusion	65
REFERENCES	67

Table of Contents (Cont'd)

CHAPTER IV. IMPLANTED OXYGEN IN Pt SILICIDE FORMATION	68
A. Introduction	68
B. Experimental Procedures	70
C. Experimental Results	72
D. Discussion	80
E. Conclusion	88
REFERENCES	90
CHAPTER V. OXYGEN IN Pd ₂ Si FORMATION	92
A. Introduction	92
B. Experimental	94
C. Experimental Results	95
D. Discussion	98
E. Conclusion	104
REFERENCES	105
CHAPTER VI. GENERAL MODEL	106
A. Introduction	106
1. Model	106
REFERENCES	110
CHAPTER VII. SUMMARY OF ADDITIONAL WORK	111
A. Introduction	111
B. N in Ni, Pt and Pd Silicide Formation	112
1. N Effects on Ni Silicide Formation	112
2. N Effects on Pt Silicide Formation	113
3. N Effects on Pd Silicide Formation	114
C. C in Ni and Pt Silicide Formation	115
1. C Effects on Ni Silicide Formation	115
2. C Effects on Pt Silicide Formation	116
D. Diffusion Barrier Effects on Contact Resistivity of Nickel .	
Silicide	117
1. O Effects on Contact Resistivity	117
2. N Effects on Contact Resistivity	117
REFERENCES	119
CHAPTER VIII. CONCLUSION AND OUTLOOK	120
A. Conclusion	120
B. Outlook	123

CHAPTER I

INTRODUCTION

Metal silicides are important in the manufacture of semiconductor devices since they are used extensively to form contacts and Schottky barriers. Invariably these metal silicides are formed by a solid phase reaction between the Si substrate and a thin deposited metal film. No process is perfectly clean however, and therefore some contamination by impurities is inevitable. There are clear cases in the literature that show that impurities can greatly alter or even control the formation of these silicides [1]-[6]. An understanding of the role of impurities is important to avoid unwanted effects and also may lead to the possibility of using impurities to control silicide growth.

Aside from these technological incentives, the effects of an impurity on silicide formation is also of scientific interest because the mechanisms responsible for impurity effects are not known.

Thus far no systematic investigation of the effects of impurities on metal silicide formation has been made. In this thesis we present a systematic study on the effects of impurity oxygen on the formation of Ni, Pt and Pd silicide. Oxygen was selected as the impurity element both because it is a highly reactive and ubiquitous impurity element and because there is a good analytical technique for the detection of oxygen, $^{16}\text{O}(d,\alpha)^{14}\text{N}$ nuclear reaction analysis (NRA) (Chapter II, 7,8). Ni, Pt and Pd were selected as the silicide forming metals since their silicide formations are well characterized [5],[9]-[11] and they are important

contact materials used in semiconductor devices. The alternative is to look at early transition metal silicides; however, they are so reactive that the pure case is difficult to achieve or maintain. Ni, Pd and Pt are not prone to this difficulty; in addition, these metals form silicides at low temperatures ($\sim 300^{\circ}\text{C}$) which may enhance the effect an impurity has on the reaction.

REFERENCES

- [1] R. J. Blattner, C. A. Evans Jr., S. S. Lau, J. W. Mayer and B. M. Ullrich, *J. Electrochem. Soc.* 122, 1732 (1975)
- [2] J. B. Bindell, J. W. Colby, D. R. Wonsidler, J. M. Poate, D. K. Conly and T. C. Tisone, *Thin Solid Films*, 37, 441 (1976)
- [3] C. Canali, F. Catellani, G. Ottaviani and M. Prudenziati, *Appl. Phys. Lett.* 33, 187 (1978)
- [4] H. Kräutle, M-A. Nicolet and J. W. Mayer, *J. Appl. Phys.* 8, 3304 (1974)
- [5] C. Canali, C. Catellani and M. Prudenziati, W. H. Wadlin and C. A. Evans Jr., *Appl. Phys. Lett.* 31, 43 (1977)
- [6] M. Severi, E. Gabilli, S. Guerri and G. Celotti, *J. Appl. Phys.*, 48, 1998 (1977)
- [7] S. T. Picraux, *Nuc. Inst. Meth.*, 149, 289 (1978)
- [8] A. Turos, L. Wielunski and A. Barcz, *Nuc. Inst. Meth.* 111, 605 (1973)
- [9] J. O. Olowolafe, M-A. Nicolet and J. W. Mayer, *Thin Solid Films*, 38, 143 (1976)
- [10] R. W. Bower, D. Sigurd and R. E. Scott, *Solid State Elect.*, 16, 1461 (1973)
- [11] N. W. Cheung, M-A. Nicolet, M. Wittmer, C. A. Evans Jr., and T. T. Sheng, *Thin Solid Films*, 79, 51 (1981)

CHAPTER II

EXPERIMENTAL METHODS

A. INTRODUCTION

The work reported in this thesis has used three complementary techniques to investigate the effects of impurity elements on the silicide forming reactions of the near noble metals. These techniques are Rutherford backscattering spectrometry (BS), $^{16}\text{O}(d,\alpha)^{14}\text{N}$ nuclear reaction analysis (NRA), and x-ray photoelectron spectroscopy (XPS). BS was used to quantitatively determine the atomic composition as a function of depth. A limitation of this technique is its inability to measure low Z elements contained in a high Z matrix. This may be overcome for specific elements such as oxygen with NRA. A nuclear reaction is sensitive to only one element and therefore is insensitive to the matrix composition. Neither BS or NRA yield information about the chemical environment of an atom. This important information was obtained using the last of the three complementary techniques, XPS. The complementary nature of the information obtained by these three techniques was an essential part in obtaining an understanding of impurity effects on metal silicide formation.

In this chapter the NRA technique is presented as this technique was central to this study and is not as generally known as are BS and XPS. Excellent detailed treatments of BS [1] and XPS [2], [3], [4] may be found elsewhere.

B. $^{16}\text{O}(d,\alpha)^{14}\text{N}$ NUCLEAR REACTION ANALYSIS

1. Introduction

There are other methods of profiling oxygen such as AES and SIMS. The $^{16}\text{O}(d,\alpha)^{14}\text{N}$ nuclear reaction technique was used here because it offers good sensitivity and depth resolution, is quantitative and is directly adaptable to our existing backscattering setup. The practical sensitivity of ~ 1 at. % is comparable with AES although not as good as SIMS which has typically 0.001 at. % sensitivity [5]. An advantage is that the $^{16}\text{O}(d,\alpha)^{14}\text{N}$ method is nondestructive as compared to AES or SIMS which rely on ion milling to obtain depth profiles. The $^{16}\text{O}(d,\alpha)^{14}\text{N}$ technique is an ideal complementary technique for BS to profile low concentrations of oxygen.

The $^{16}\text{O}(d,\alpha)^{14}\text{N}$ nuclear reaction profiling technique is similar yet distinct from BS [6],[7],[8]. As in BS, the energy loss that an ion experiences in penetrating solid matter sets the depth scale. The major difference lies in the origin of the detected particle. In BS the reaction between incoming ion and target atom is an elastic collision and the incoming and outgoing particles are the same. In the $^{16}\text{O}(d,\alpha)^{14}\text{N}$ nuclear reaction the initial particles are an oxygen target atom and an incident deuteron whereas the final particles are a nitrogen atom and an outgoing α particle. In addition, 3.115 MeV is released in the reaction giving the outgoing α 's much higher energy than that of the incoming deuteron, which eliminates interferences between the signal of the α 's and the much stronger signal of the elastically scattered deuterons. As in BS, energy analysis of the outgoing particle gives the oxygen profile. This

similarity enables an existing BS setup to use this reaction with only minor changes such as detector bias and amplifier gains.

2. Radiation Safety

Some nuclear reactions that take place with deuterium produce hazardous radiation. In our accelerator the $^{12}\text{C}(d,n)^{13}\text{N}$ reaction, which produces neutrons, is the main radiation source. Only a small fraction of the D^+ beam leaving the ion source actually reaches the target. The rest impinges on the walls of the beam line or upon the beam defining slits. The hydrocarbon film everpresent on these surfaces provides the carbon for this reaction. No shielding is possible in our system since the controls and beam line share the same room. Thus to avoid excessive neutron production the energy of the incident neutron must be kept in a region where the reaction probability, the total cross section σ_T , is low. σ_T increases rapidly from 0.5 to 2 MeV, however [9]. At 2.0 MeV D^+ energy, the average neutron level in the control/beam line room was ~ 10 mr/hr and rose to 250-300 mr/hr near the slits and analyzing magnet. By lowering the energy to 0.90 MeV the average level went to only 2 mr/hr. Since the Nuclear Regulatory Agency sets 2.5 mr/hr as the maximum a radiation worker may receive on a 40/hr week, 50 week/year basis, 0.90 MeV was the maximum energy used in this study. With this precaution the requirements of radiation safety were satisfied, however careful attention must be paid to the radiation levels whenever a deuterium beam is present.

3. Geometry

The experimental layout used for this technique is illustrated in Fig. 1. The normals to the sample, incident beam and detector are

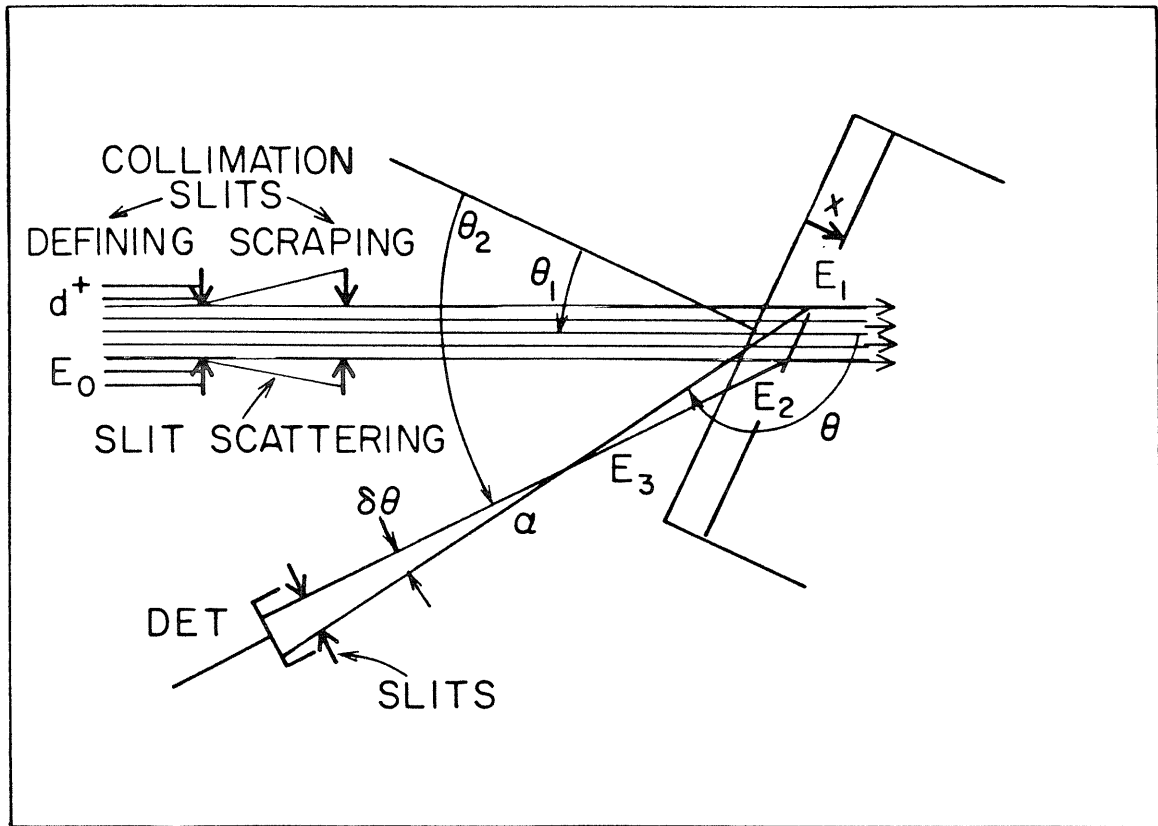


Fig. 1 The experimental layout for the $^{16}\text{O}(d,\alpha)^{14}\text{N}$ nuclear reaction technique. The beam direction, detector and surface normal are coplanar. The d^+ beam passes through defining slits to set the beam spot size then through scraping slits that remove the particles scattered from the defining slits. The d^+ beam impinges on the sample tilted at θ_1 degrees to the beam. The exiting α particles enter the detector placed at θ with a small angular divergence $\delta\theta$. The initial energy of the d^+ is E_0 , just before the reaction at a depth x it is E_1 . Just after the reaction the α particle has energy E_2 and after leaving the sample arrives at the detector with energy E_3 .

coplanar. The sample may be tilted with respect to the incident beam to lengthen the incoming and outgoing paths and thus to enhance the depth resolution. A Si surface barrier detector is at an angle θ to the incident deuterium beam which has energy E_0 . After penetrating into the sample a distance $x/\cos\theta_1$ the deuterons have an energy E_1 given by

$$E_1(x) = E_0 - \int_0^{x/\cos\theta_1} S_d dx, \quad (1)$$

where $S_d \equiv \left(\frac{dE}{dx}\right)_d$ is the rate of energy loss of deuterium in the sample.

Right after the reaction takes place the α particle exiting at an angle θ has an energy E_2 given by

$$E_2(E_1) = \frac{m_1 m_2 E_1}{(M+m_2)^2} \left(2 \cos^2\theta + \frac{M(m_2+M)}{m_1 m_2} \left(\frac{Q}{E_1} - \frac{m_1}{M} + 1 \right) \right. \\ \left. + 2 \cos\theta \left(\cos^2\theta + \frac{M(m_2+M)}{m_1 m_2} \left(\frac{Q}{E_1} - \frac{m_1}{M} + 1 \right) \right)^{\frac{1}{2}} \right) \quad (2)$$

where m_1 , m_2 and M are the masses of the incident particle, outgoing particle and recoiling atom, respectively, and Q is the energy liberated in the reaction. Eq. (2) is the kinematics formula usually derived in nuclear physics texts [10], [11]. Finally after leaving the sample the outgoing α particle has energy E_3 given by

$$E_3(x) = E_2(E_1) - \int_0^{x/\cos\theta_2} S_\alpha dx \quad (3)$$

4. Depth Scale

If the variation of E_2 with E_1 is not too great

$$E_2(E_1) = E_2(E_0) - \left. \frac{\partial E_2}{\partial E_1} \right|_{E_0} (E_0 - E_1) . \quad (4)$$

For sample depths small enough we may take S_α and S_d to be constant. Eqs. (1) and (3) then may be integrated and combined with Eq. (4) to obtain

$$E_3(x=0) - E_3(x) = \left[\left. \frac{\partial E_2}{\partial E_1} \right|_{E_0} \frac{S_d}{\cos\theta_1} + \frac{S_\alpha}{\cos\theta_2} \right] x \quad (5)$$

Letting the expression in brackets equal $[S_r]$ we have

$$E_3(x=0) - E_3(x) = [S_r] x \quad (6)$$

This represents a linear depth scale and greatly simplifies the calculations. At greater depths the approximations break down and an exact expression must be used. A comparison of the exact energy to depth relation to the linear approximation for a Ni target is shown in Figure 2. For tilt angles up to 55° the approximation is within 10% of the exact value up to depths of 5000 Å.

5. Oxygen Concentration

To obtain the oxygen concentration it is necessary to recall from backscattering analysis the expression for the height of a spectrum [1]

$$H = \frac{N_0 \tau}{\cos\theta_1} \sigma(E_1) \Omega Q \quad (7)$$

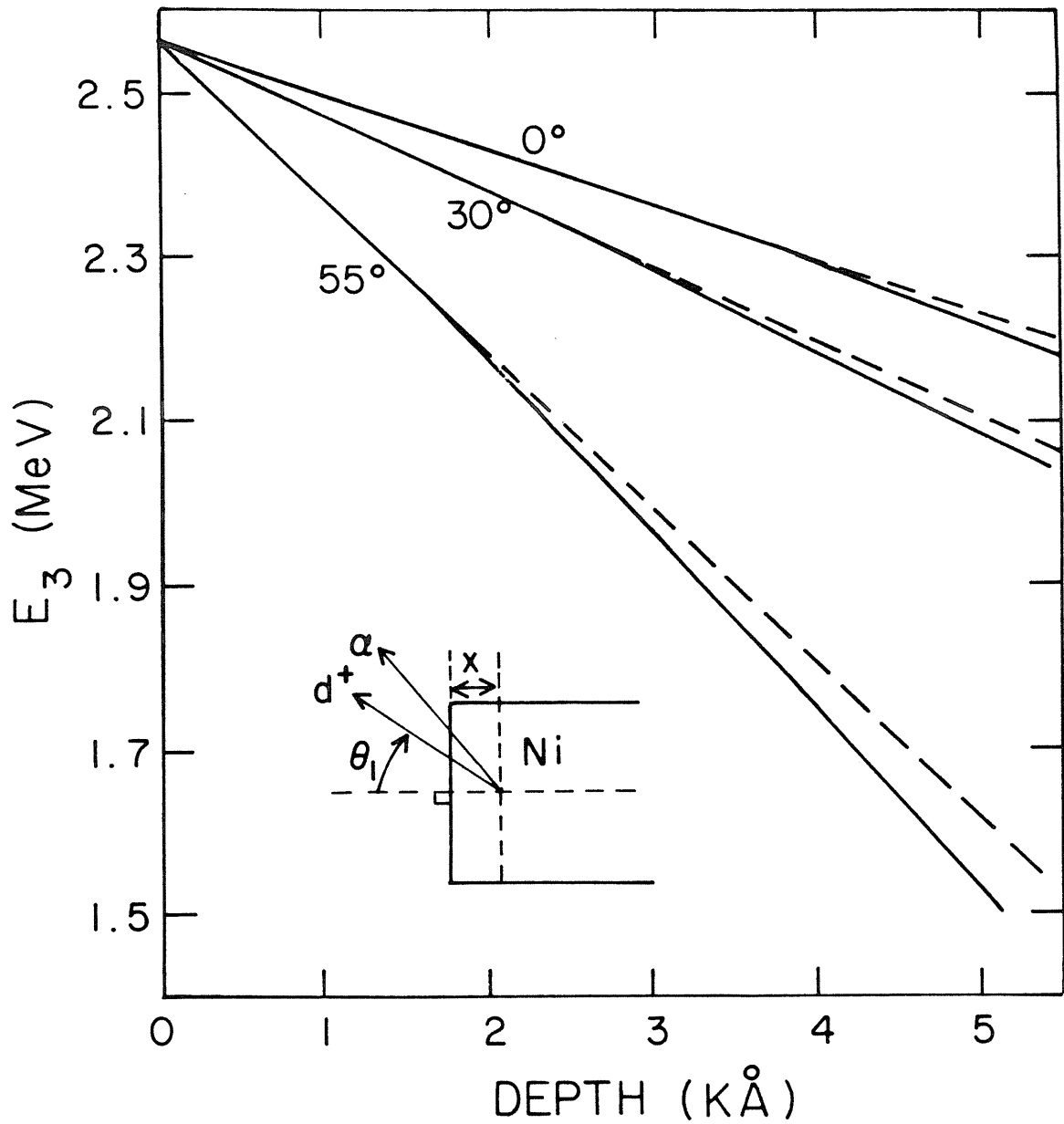


Fig. 2. Plot of the linear depth scale (dashed line) compared with the exact depth scale (solid line) obtained numerically for three tilt angles. The material is Ni, E_0 is 900 keV and the detector angle is 164° to the incident beam. The linear approximation is within 10% of the exact value for Ni films up to 5 kÅ thick.

where H = the number of counts per channel

$\sigma(E)$ = differential cross section (for the $^{16}_0(d,\alpha)^{14}_N$ reaction
in this case)

Ω = the detector solid angle

Q = number of incident particles

τ = the depth increment corresponding to the energy width of one
channel

N_0 = the atomic density of oxygen in the sample.

Rewriting Eq. (7) explicitly for N_0 and dividing through by N_M , the matrix
atomic density of the sample, we obtain

$$\frac{N_0}{N_M} = \frac{H \cos\theta_1}{\sigma(E_1)\Omega Q N_M \tau} \quad (8)$$

The depth increment τ corresponding to the energy width per channel, ϵ ,
must be determined. At a depth x the energy width ϵ' that will send the
outgoing particles into one channel is related to τ using (6) by

$$\epsilon' = [S_r] \tau \quad (9)$$

We may relate ϵ' to ϵ by noting that at a depth x the outward path length
is given by

$$\frac{x}{\cos\theta_2} = \int_{E_3}^{E_2} \frac{dE}{S_\alpha} \quad (10)$$

Using Eq. (9) we have that a particle from a depth $x+\tau$ will arrive at x
with energy $E_2 - \epsilon'$ and will exit with energy $E_3 - \epsilon$. Thus

$$\frac{x}{\cos\theta_2} = \int_{E_3-\epsilon}^{E_2-\epsilon'} \frac{dE}{S_\alpha} \quad (11)$$

Equating the integrals in Eqs. (10) and (11) and subtracting overlapping parts we obtain

$$\int_{E_3-\epsilon}^{E_3} \frac{dE}{S_\alpha} = \int_{E_2-\epsilon'}^{E_2} \frac{dE}{S_\alpha} \quad (12)$$

Since ϵ and ϵ' are small compared to E_2 and E_3 we have

$$\frac{\epsilon}{S_\alpha(E_3)} = \frac{\epsilon'}{S_\alpha(E_2)} \quad (13)$$

Substituting Eqs. (9) and (13) into Eq. (8) we finally obtain

$$\frac{N_0}{N_M} = \frac{H \cos\theta_1 [S_r] S_\alpha(E_3)}{\sigma(E_1) \Omega Q N_M \epsilon S_\alpha(E_2)} \quad (14)$$

From this we have that the atomic percent concentration is simply

$$\text{at. \% oxygen} = \frac{1}{1 + \frac{N_M}{N_0}} \times 100 \quad (15)$$

Some of the quantities in Eq. (14) must be known a priori. These are the stopping powers S_d and S_α , the cross section $\sigma(E)$ and also the product of detector solid angle and integrated charge ΩQ .

6. Stopping Power

S_α is available in the form of semiempirical data [12]. Unfortunately no such data are available for S_d . At our energies, however,

only the electronic contribution S_e to S_d is important. S_e has the generic form [1]

$$S_e = N_M Z_2 (Z_1 e^2)^2 f\left(\frac{E}{m}\right) \quad (16)$$

where

N_M = atomic density of the sample

$Z_1 e$ = charge of the incident particle

$Z_2 e$ = charge of the target nucleus

$f\left(\frac{E}{m}\right)$ is a function depending only on the velocity squared of the incident particle.

This equation tells us that

$$S_d(E) = \frac{1}{4} S_\alpha(2E) . \quad (17)$$

This relationship between stopping powers enables us to use S_α data to obtain S_d . A compilation of proton stopping powers S_p has also been made [13]. Using these proton values and the relationship

$$S_d(E) = S_p(E/2) \quad (18)$$

another independent estimate of S_d can be obtained. The values of S_d derived from S_α and S_p differ by less than 0.7%. Such good agreement for different estimates supports the validity of the procedure, and S_d has been taken from those estimates. In this work $S_d^{\text{Ni}}(0.90 \text{ MeV}) = 6.48 \text{ eV/\AA}$ and $S_d^{\text{Si}}(0.90 \text{ MeV}) = 16.5 \text{ eV/\AA}$. S_d for other elements and energies were calculated using Eq. (17). $S_\alpha(2E)$ was obtained using Table V of [11], a table of coefficients to a 5th order polynomial least squares fit to ^4He

stopping cross sections ϵ_α . ($S_\alpha = N_M \epsilon_\alpha$). For compound samples and for samples containing large amounts of oxygen S is computed using Bragg's rule [14],

$$\frac{S_{m n}^{A B}}{N_{m n}^{A B}} = m \frac{S^A}{N^A} + n \frac{S^B}{N^B} \quad (19)$$

where $N_{m n}^{A B}$ and $S_{m n}^{A B}$ are the molecular density of compound $A_m B_n$ and energy loss rate for $A_m B_n$, respectively, and N^A is the atomic density of element A, etc.

S_α and $[S_r]$ in Eq. (14) depend on all the elements present in the sample through Bragg's rule. One of the elements that must be considered is the oxygen which is initially present in unknown quantities. Therefore, initially N_O/N_m is computed with the oxygen concentration set to zero for the calculations of S_α and $[S_r]$. This first value of N_O/N_m is then used to refine the values of the S 's which are used to calculate a better value of N_O/N_m , and so on. This iteration must be done for each data point. The matrix may also change with depth. For each point, the local composition must be used to calculate the initial S 's.

7. Cross Section

Another important parameter left to be determined in Eq. (14) is the reaction cross section $\sigma(E)$. This cross section, unlike the Rutherford scattering cross section, is not given by a known formula and therefore must be found experimentally. Measurements have been made for a few angles and energies however, [15], [16], and from these possibilities $\theta = 164^\circ$ was selected. The kinematic angle θ is 164° in all of the $^{16}_0(d,\alpha)^{14}_N$

measurements in this thesis. The published values of $\sigma(E)$ for this angle disagree by some 30% [15], [16]. However, the cross section used here is that measured by Kim et al [15] and was verified by measuring an SiO_2 sample. This cross section is shown in Figure 3. The ideal energy is 1.25 MeV since the cross section is quite constant from 1.20 to 1.25 MeV. However, 0.90 MeV was chosen to minimize the background neutron radiation hazard which is a relatively strong function of energy. The cross section between 0.8 and 0.9 MeV changes uniformly. In this work, however, the cross section was taken to be a constant (8.0 mb/sr) since S_d is very low.

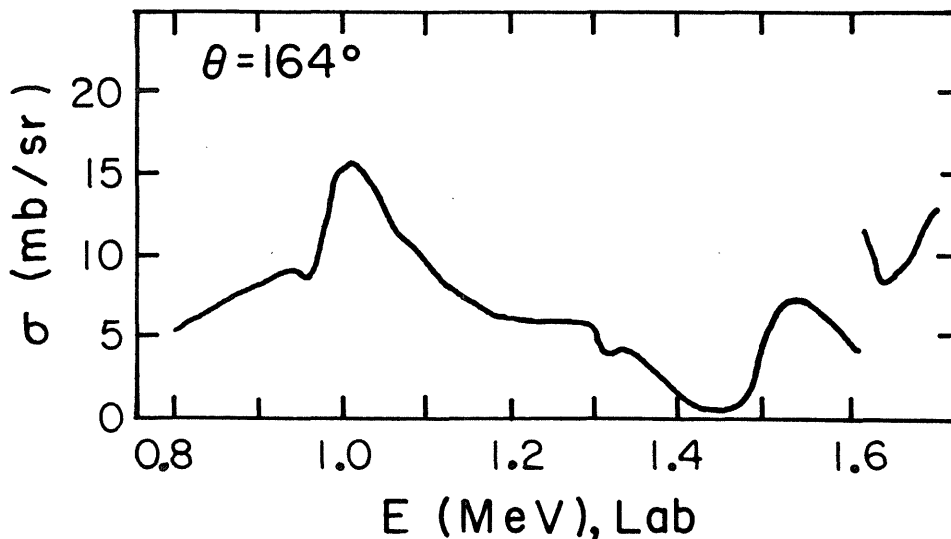


Fig. 3. A plot of the cross section versus incident deuteron energy in the laboratory frame for the $^{16}\text{O}(d,\alpha)^{14}\text{N}$ nuclear reaction. From Kim et al [15]. The angle detection θ is 164° .

8. Charge Normalization

The remaining term in Eq. (14) yet to be discussed is the product ΩQ . While Ω can be measured fairly accurately, Q is obtained by integrating

the charge that falls on the target and this process is not very reliable [17]. Secondary electron and neutral beam effects cause large errors that vary with time. A method to avoid these errors uses the signal of the deuterons that are elastically backscattered from the matrix during the measurement. The surface height H_s of this matrix signal is, using Eq. (7)

$$H_s = \frac{N_m \tau_0}{\cos \theta_1} \sigma_R(E_0) \Omega Q \quad (20)$$

where $\sigma_R(E_0)$ is the Rutherford cross section for the elastic scattering of deuterons from the target matrix and subscript 0 refers to near-surface values.

For elastic scattering we use Eq. (2) for the incoming and outgoing particles as deuterons the recoiling nucleus as that of a matrix atom and $Q = 0$. Then the energy to depth relationship Eq. (6) becomes

$$E_3(x=0) - E_3(x) = [S_d]x \quad (21)$$

where $[S_d]$ is the energy loss factor for deuterons in the sample Eq. (21) tells us that

$$\tau_0 = \frac{E}{[S_d]} \quad (22)$$

Using (22) and (20) we have that

$$\Omega Q = \frac{H_s [S_d] \cos \theta_1}{E \sigma_R(E_0) N_m} \quad (23)$$

which yields the value of ΩQ in terms of H_s and known values, thus avoiding the charge integration problems. The major uncertainty in (23) comes from the energy loss factor $[S_d]$ and is on the order of 5%. Using Eq. (23), Eq. (14) becomes

$$\frac{N_O}{N_M} = \left(\frac{H[S_r(x)]s_\alpha(E_3)}{\sigma(E_1)S_\alpha(E_2)} \right) \left(\frac{\sigma_R(E_0)}{H_S[S_d]} \right) \quad (24)$$

The first factor comes from the matrix containing the oxygen and the second factor comes from normalization to the surface height of some element in the sample but not necessarily from the oxygen bearing matrix. In the general case for an oxygen bearing matrix $A_m B_n$ and taking the normalization from element C of $C_p D_q$ we have that

$$\frac{N_O}{N_{A_m B_n}} = \left(\frac{H[S_r(x)]^{A_m B_n}}{\sigma(E_1)(m+n)} \frac{S_\alpha^{A_m B_n}(E_3)}{S_\alpha^{A_m B_n}(E_2)} \right) \left(\frac{\sigma_R^C(E_0)p}{H_S^C[S_d]_{C_p D_q}} \right) \quad (25)$$

where $[S_d]$ is the deuteron energy loss factor for elastic scattering from element C in compound $C_p D_q$ with $\sigma_R^C(E_a)$ the elastic scattering cross section for element C and H_S^C is the surface height of element C. $S^{A_m B_n}$ is $\frac{dE}{dx}$ of this outgoing particle in $A_m B_n$ and $[S_r]^{A_m B_n}$ is the nuclear reaction energy loss factor for a matrix $A_m B_n$.

9. Resolution

An important question is that of depth resolution. The depth resolution of this technique is determined by the energy broadening effects

present. If approximately Gaussian distributions for these effects are assumed the fwhm of the system energy resolution δE is given by

$$\delta E^2 = \delta E_b^2 + \delta E_d^2 + \delta E_s^2 + \delta E_g^2 \quad (26)$$

where δE_b , δE_d , δE_s and δE_g are the fwhm of the beam spread (a few kev and negligible), detector resolution (a constant for the experiment ≈ 18 kev), straggling and geometrical effects, respectively. The depth resolution then follows from Eq. (9)

10. Geometrical Effects $\delta x = \frac{\delta E}{[S_r]} . \quad (27)$

There are two contributions due to experimental geometry that tend to degrade the energy resolution. Referring to Fig. 1, the finite size of the beam spot and detector aperture allows particles with a range $\delta\theta$ of angles to enter the detector. This causes energy broadening due to both variations in the kinematic factor and also to variations in the exiting particles path length. The energy spreading due to geometry is given by

$$\delta E_g = \frac{\partial E_3}{\partial \theta} \delta \theta \quad (28)$$

Using Eq. (5) we obtain

$$\frac{\partial E_3}{\partial \theta} = \frac{\partial E_3(x=0)}{\partial \theta} - \frac{\partial^2 E_2}{\partial \theta \partial E_1} \frac{xS_d}{\cos \theta_1} - \frac{\partial}{\partial \theta} \frac{xS_\alpha}{\cos \theta_2} \quad (29)$$

The first term in Eq. (29) is computed using (2)

$$\frac{\partial E_3(x=0)}{\partial \theta} \approx -2E_0 \sin\theta \left[\frac{Mm_1m_2}{(M+m_2)^3} \left(\frac{Q}{E} - \frac{M_1}{M} + 1 \right) \right] = -A \sin\theta \quad . \quad (30)$$

$\partial^2 E_2 / \partial \theta \partial E_1$ is on the order of 10^{-3} , therefore the second term in Eq. (29) may be neglected. Therefore we have

$$\partial E_g = [-A \sin\theta + xS_\alpha \frac{\sin\theta_2}{\cos^2\theta_2}] \delta\theta \quad (31)$$

The first term in Eq. (26) arises from the variation in the kinematic factor and the second reflects length differences in the outgoing path. The one remaining term in Eq. (26) is that due to straggling δE_s .

11. Straggling

The energy width of a beam of particles broadens as it penetrates solid matter due to the statistical nature of the energy loss process. This straggling process results in an increase in δE_s with depth. A reasonable estimate of straggling comes from the Bohr theory [18], [19]

$$\delta E_s^2 = (5.55) 4\pi(Z_1 e^2)^2 N_m^A N_n^B (mZ_A + nZ_B) x \quad , \quad (32)$$

where the target composition is $A_m B_n$ and Z_1 , Z_A and Z_B are the atomic numbers of the outgoing particle and target atoms A and B, respectively. Using Eqns. (26), (31) and (32) we can calculate the depth resolution of this method. Fig. 4 shows the result of this calculation for 900 keV d^+ incident on a Ni matrix ($N^{Ni} = 9.14 \times 10^{22}$ atoms/cm³). $\delta\theta$ and δE_d were taken to be 2° and 18 keV, respectively. For each depth there is a

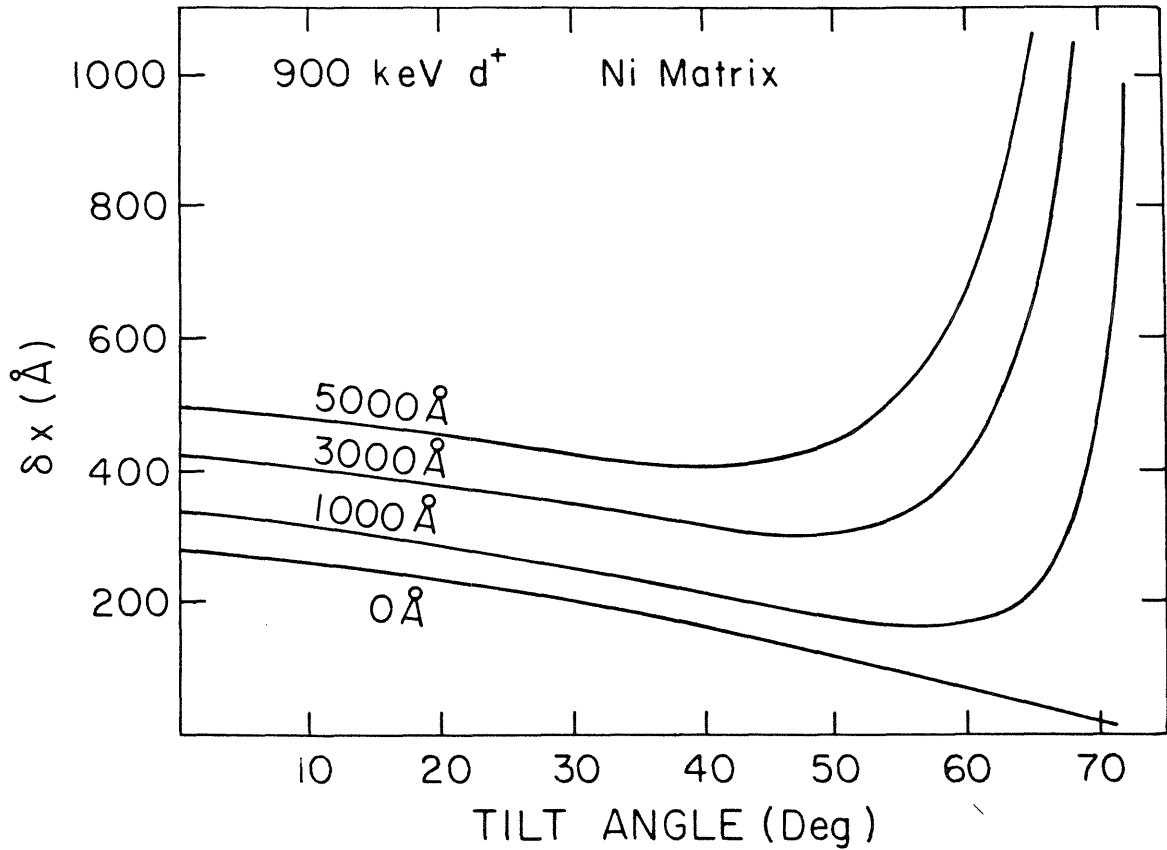


Fig. 4. A plot of depth resolution in Ni versus tilt angle (θ_1) for various depths. In the calculation $\delta\theta$, δE_d and N^{Ni} were taken to be 2° , 18 keV and 9.12×10^{22} atoms/cm³, respectively. The detection angle θ is 164° . The best resolution is seen to be near 50° for films less than 300 Å thick.

minimum in the depth resolution which occurs when the two terms in Eq. (31) cancel. For Ni films a few kÅ thick the minimum is between 40° to 60° of tilt. Since we are limited to ~ 1500 Å Ni films in order to prevent signal overlapping in backscattering measurements, a higher tilt angle is favored, typically 55° . The depth resolution for a fixed tilt angle may be conveniently displayed by a rearrangement of Fig. 4. This is shown in Fig. 5 keeping the same parameters as in Fig. 4. We see that for thick films 55° is not optimal. A better resolution may be achieved by only tilting 30° for film depths greater than 3500 Å. For 55° and films of less than 2k Å the depth resolution is less than 200 Å. This is directly comparable with usual backscattering. In all the work reported here the tilt angle θ_1 was 55° .

12. Interferences

It is due to low background levels that the $^{16}\text{O}(d,\alpha)^{14}\text{N}$ technique owes its high sensitivity; therefore overlapping signals from other nuclear reactions must be avoided. Two such reactions are shown in Fig. 6 top. $^{12}\text{C}(d,p_0)^{13}\text{C}$ has a signal 0.36 MeV above the $^{16}\text{O}(d,\alpha)^{14}\text{N}$ signal and $^{16}\text{O}(d,p_0)^{17}\text{O}$ has a signal 0.22 MeV below it. For thick samples or high tilt angles the oxygen signal width may easily overlap this lower signal. As carbon does build up on the sample surface during the long measurement (~ 3 to 4 hours), this $^{12}\text{C}(d,p_0)^{13}\text{C}$ signal can easily overlap the high energy part of oxygen signal. Both interferences can be eliminated by reducing the depletion layer width of the surface barrier detector to ≈ 35 μm . As shown in Fig. 6 bottom, the maximum energy a proton can deposit in this layer is only ~ 2.1 MeV. Thus the upper signal is eliminated entirely and the lower interference is moved to ≈ 0.5 MeV below the oxygen

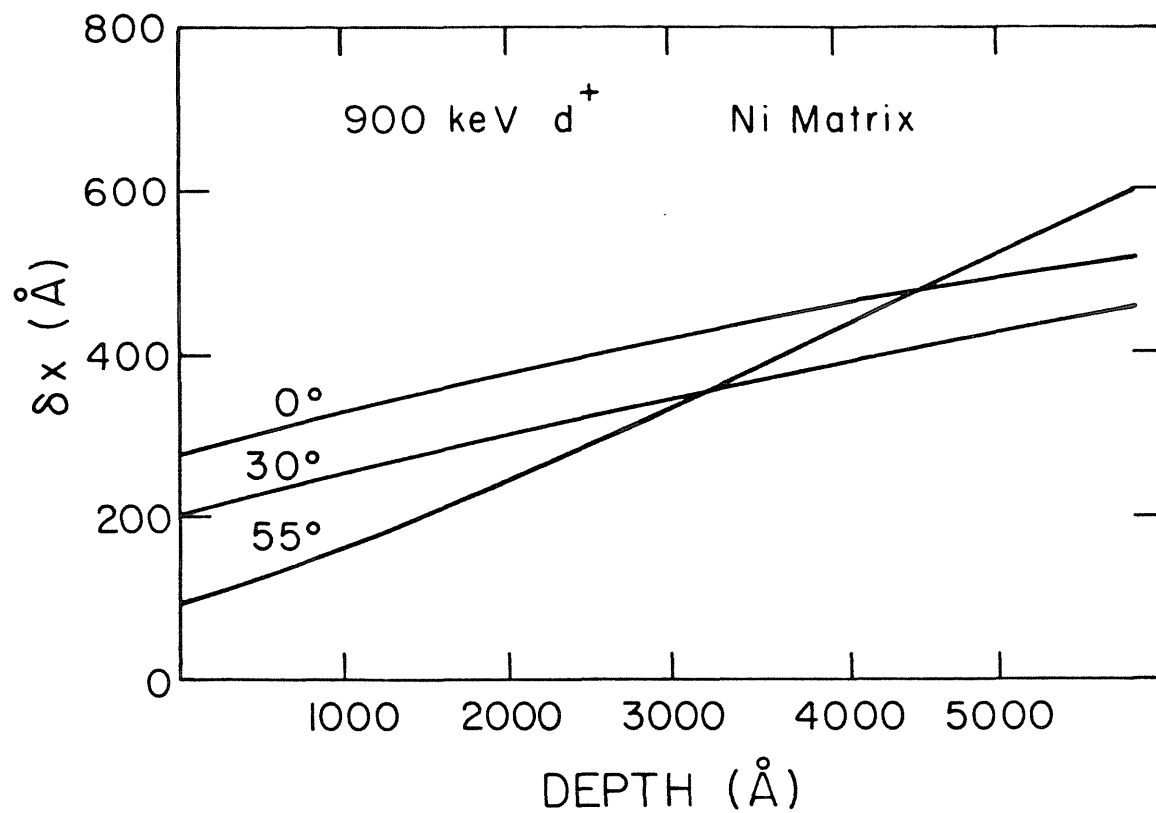


Fig. 5. A plot of depth resolution in Ni versus depth for a few tilt angles. The same parameters were used as in Fig. 4. A high tilt angle will improve depth resolution for thin films but will degrade resolution at depths greater than ~ 3000 \AA .

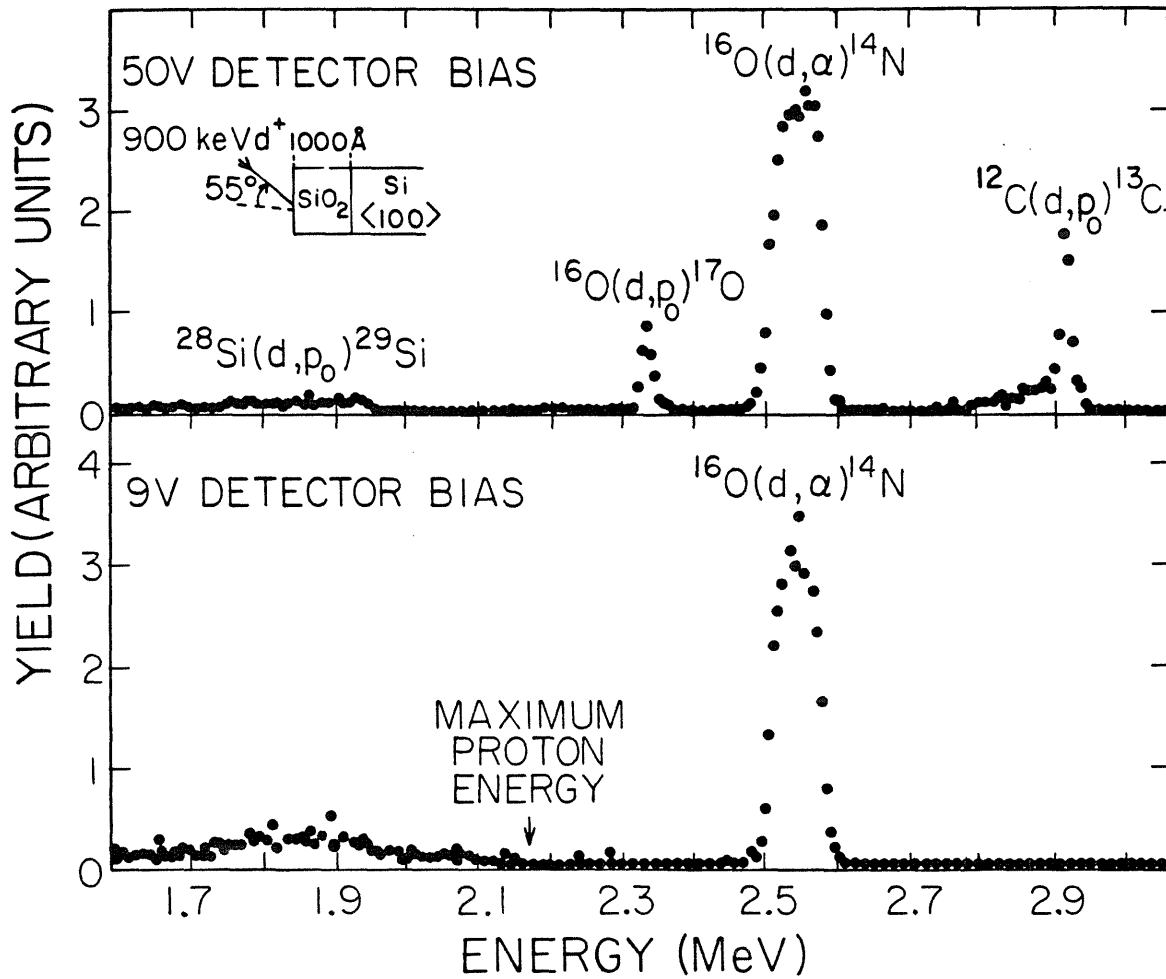


Fig. 6. TOP: A spectrum obtained by the $^{16}\text{O}(d,\alpha)^{14}\text{N}$ nuclear reaction technique of a 1000 Å SiO_2 film on a Si substrate. Two interferences to the $^{16}\text{O}(d,\alpha)^{14}\text{N}$ signal are seen due to competing nuclear reactions.

BOTTOM: A spectrum obtained using the $^{16}\text{O}(d,\alpha)^{14}\text{N}$ technique showing the effect of reducing the detector depletion width. The two interferences have been removed. In both spectra the detector angle θ was 164° , the solid angle of the detector Ω was 0.54 mSr, the tilt angle θ_1 was 55° and the dose was ~ 1 mC.

signal. A disadvantage is that a low bias degrades the detector resolution. This effect is reduced for low resistivity detectors; therefore a 600 Ω cm rather than a more usual 2500 Ω cm detector was used (Ortec BA-14-25-100-S).

Other sources of background counts are due to scattering from the beam collimation slits and beam halo effects. Low angle forward scattered particles from the defining slits and the beam halo can hit the target holder. To minimize these effects a second set of scraping slits, a phosphor screen to facilitate their proper adjustment, and a 1 cm aperture to eliminate the beam halo were added. The beam definition slits were located 84 cm from the target. The scraping slits were 45 cm down beam from the defining slits followed by the aperture 9 cm further, 30 cm from the target. With this arrangement, the background obtained from single crystal Si used as a low oxygen containing target was reduced to 0.02 of its prior value. This is a much lower background level than obtained with the evaporated metal films and indicates the presence of residual oxygen in these films.

13. Results and Discussion

Fig. 7 shows a typical spectrum for this technique. The 900 keV d^+ beam was incident on a 1500 Å Ni film, implanted with 2.3×10^{16} O/cm² at 80 keV/atom, on a Si substrate. The sample tilt angle θ_1 was 55°, detector angle θ , detector solid angle Ω and bias were 164°, 0.54 mSr and 10 V, respectively. The average beam current i was ~ 100 nA. The integrated charge Q was 2.0 mC resulting in a measurement time of ~ 330 min. Comparison of the product ΩQ using this integrated charge, 1.08 mC-mSr to that using Eq. (23), 1.05 mC-mSr, shows quite good agreement.

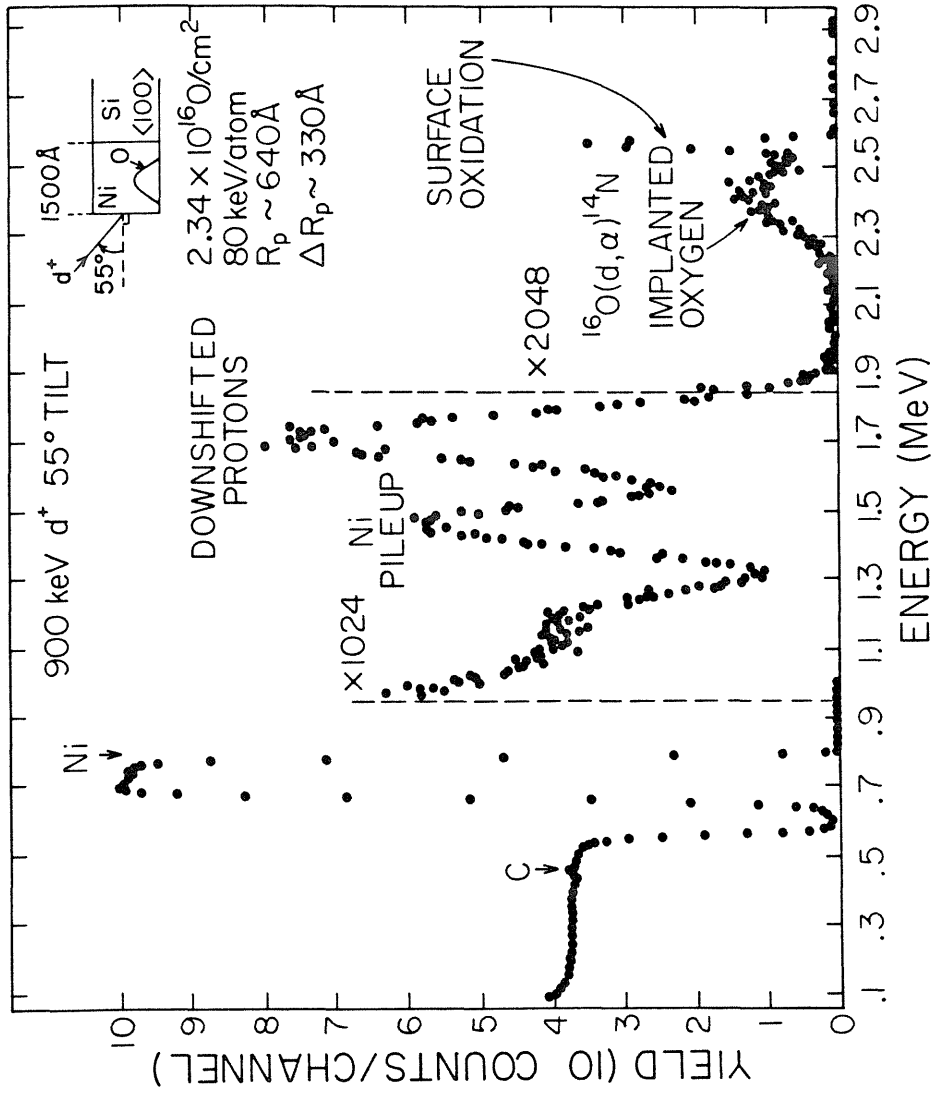


Fig. 7. A spectrum obtained for a 1500 Å Ni film implanted with 2.3×10^{16} O/cm² on a Si substrate. The broad peak located ~ 2.4 MeV is due to the implanted oxygen. The detector angle θ was 164°, detector solid angle Ω was 0.54 mSr, the tilt angle θ_1 was 55° and the dose was 2.0 mC.

The factors used in Eq. (23) are $H_s = 9.85 \times 10^5$, $[Sd]^{Ni}/N^{Ni} = 85.12 \times 10^{-18}$ keV - cm²/atom, $\sigma_R(0.90 \text{ MeV}) = 1.30 \times 10^{-24}$ cm², the energy width of a channel $E = 5.63$ keV and $\theta_1 = 55^\circ$. Using Fig. 7 we next discuss the sensitivity of the technique to oxygen and also compare the resolution with that predicted in Figs. 4 and 5.

14. Sensitivity

The sensitivity of this method relies on low backgrounds rather than a large cross section, i.e., compared to the implanted oxygen signal height, the Ni elastic backscattering is over 17,000 times greater. The oxygen signal background is ~ 2 to 3 counts/channel corresponding to ~ 0.1 at. % oxygen or $\sim 10^{20}$ O/cm³. This is due to residual oxygen in the evaporated Ni film, however, and does not represent the method's detection limit. For a single crystal Si target a total background of 5 counts was observed over the 141 channels of the oxygen signal region. This corresponds to a detection limit of ~ 0.001 at. % Si or $\sim 7 \times 10^{17}$ O/cm³ and represents a lower limit to the method's sensitivity. This lower limit is not attainable in practice since the beam current is limited by pileup considerations to ~ 200 nA and good statistics ($\sim 10\%$) 1mC-at. % oxygen require about 1 mC-at. % oxygen. Thus for 0.001 at. % oxygen requires ~ 1 C which would take ~ 1000 hours of continuous measurement. Practical limits are ~ 10 hrs of measurement time with target current of ~ 200 nA. Therefore ~ 0.1 at. % or between 10^{19} to 10^{20} O/cm³ constitutes a realistic sensitivity limit.

15. Resolution

The surface oxygen peak is due to both the surface oxidation of Ni that takes place when it is exposed to the atmosphere and surface contamination by oxygen containing organic vapors such as diffusion pump oils, etc. The energy width of this peak provides a convenient measure of the system resolution at the sample surface. As shown in Fig. 7 the energy width of the surface peak is ~ 28 keV. This corresponds to a depth resolution of ~ 150 Å of Ni. This increase over the calculated value of ~ 100 Å shown in Figs. 4 and 5 is most likely due largely to the accumulation of a carbon overlayer during the long (~ 6 hrs) measurement time.

A last method of improving depth resolution is that of numerically deconvoluting the spectra with the resolution function of the system. A simple deconvolution routine was tried but due to the statistical fluctuations in the original spectra, nonphysical highly oscillatory results were obtained. More advanced schemes involving the introduction of a priori information to avoid the statistics problem have been published [20] but were not tried here. It may be possible to further improve the depth resolution by such a scheme.

16. Summary

In this section the $^{16}\text{O}(d,\alpha)^{14}\text{N}$ nuclear reaction technique for profiling oxygen has been described in detail to explain the origin of oxygen profile spectra presented later and also enough practical considerations have been given to clarify the actual use of the method. Resolution was shown to be quite good (~ 200 Å) for film thickness of a few thousand Angstroms. While in concept the sensitivity of this method

can rival SIMS, which is currently the most sensitive technique of all profiling methods, practical considerations are shown to reduce that sensitivity by two orders of magnitude to the order obtainable by AES. This sensitivity is still very acceptable, as the $^{16}\text{O}(d,\alpha)^{14}\text{N}$ technique is inherently quantitative and does not need secondary standards for its use. The disadvantage that the matrix composition be known independently can be easily overcome with BS and these two techniques ideally complement each other. The $^{16}\text{O}(d,\alpha)^{14}\text{N}$ nuclear reaction technique has been found very adequate to study the effect of impurity oxygen.

REFERENCES

- [1] W-K. Chu, J. W. Mayer and M-A Nicolet, *Backscattering Spectrometry* Academic Press, NY, (1978)
- [2] T. Carlson, *Photoelectron and Auger Spectroscopy*, Plenum Press, NY, (1975)
- [3] M. Cardona, L. Ley, *Topics in Applied Physics*, Springer-Verlag, NY, 26, (1978)
- [4] C. S. Fadley in *Electron Spectroscopy: Theory, Techniques and Applications*, , C. R. Brundle and A. D. Baker, eds., Academic Press, NY, 2, (1975)
- [5] G. Mezy, E. Kotai, T. Nagy, L. Lohner, A. Manuaba, J. Gyulai, V. R. Deline, R. J. Blattner and C. A. Evans, Jr., *Nucl. Inst. and Meth.*, 167, 279 (1979)
- [6] G. Amsel, J. P. Nadai, E. D'Artemare, D. David, E. Girard and J. Moulin, *Nucl. Inst. and Meth*, 92, 481 (1971)
- [7] A. Tuross, L. Wielunski and A. Barcz, *Nucl. Inst. and Meth.*, 111, 605 (1973)
- [8] S. T. Picraux, *Nucl. Inst. and Meth.*, 149, 289 (1978)
- [9] K. Wohlleben and E. Schuster, *Radiochim*, 8, 78 (1967)
- [10] F. K. Richtmeyer, E. H. Kennard and J. N. Cooper, *Introduction to Modern Physics*, 6th ed. McGraw-Hill, NY, (1969)
- [11] J. B. Marion and F. C. Young, *Nuclear Reaction Analysis: Graphs and Tables*, North-Holland, Amsterdam, (1968)
- [12] J. F. Ziegler and W. K. Chu, *Atomic Data Nucl. Data Tables* 13, 463 (1974)
- [13] H. H. Anderson and J. F. Ziegler, *Hydrogen: Stopping Powers and Ranges in All Elements*, Pergamon, Elmsford, NY, (1979)
- [14] W. H. Bragg and R. Kleeman, *Phil. Mag.* 10, 5318 (1905)
- [15] H. C. Kim, R. F. Seiler, D. F. Herring and K. W. Jones, *Nucl. Phys.* 57, 526 (1964)
- [16] G. Amsel, Thesis, (1963), *Ann. Phys. (Paris)* 9, 247 (1964)
- [17] S. Matteson and M-A. Nicolet, *Nucl. Inst. and Meth.* 160, 301 (1979)
- [18] N. Bohr, *Phil. Mag.* 30, 581 (1915)
- [19] W-K. Chu, *Phys. Rev. A.* 13, 2057 (1976)

References (Cont'd)

- [20] A. Barcz, B. Cichocki, A. Turos and L. Wielunski, *Acta Physica Polonica*, A53, 485 (1978)

CHAPTER III

IMPURITY OXYGEN IN NICKEL SILICIDE FORMATION

A. INTRODUCTION

The growth of Ni silicides formed by solid-phase reactions has been studied before [1],[2],[3]. It is known that for impurity-free Ni films deposited on impurity-free Si substrates and annealed in vacuum ($200^{\circ}\text{C} \leq T$) the metal rich phase Ni_2Si forms first and grows as a layer between the Ni and the Si. The Ni_2Si grows with the square root of the annealing time eventually to consume all of the Ni film. Thereafter the second phase NiSi begins to nucleate and grow. NiSi also forms as a layer between the Ni_2Si and the Si. However, NiSi growth has been reported to be linear with annealing time [4]. NiSi grows until all of the Ni_2Si has been converted to NiSi and is the final phase formed for annealing temperatures below $\sim 750^{\circ}\text{C}$. At no time during this growth sequence are Ni, Ni_2Si and NiSi simultaneously present. However for samples annealed in a N_2 ambient rather than in vacuum, formation of NiSi at the Ni_2Si -Si interface was observed with unreacted Ni still present on the surface [3].

It was suggested that this effect is caused by impurities from the ambient diffusing through the Ni to the Ni- Ni_2Si interface so that growth of the first phase ceases and the second phase appears [3].

There are thus two sequences of Ni silicide growth that have been observed. The first sequence is characterized by the complete consumption of the Ni film by the first phase before second phase growth is initiated. The second case is characterized by the simultaneous presence of Ni and both silicides. The available evidence suggests that this second sequence is associated with and caused by impurities. This chapter is a detailed study of these effects when oxygen is used as the impurity.

This choice introduces two major asymmetries that should be recognized at the outset; they will turn out to be of major importance. First, oxygen bonds very strongly to Si ($\Delta G_f^\circ(\text{SiO}_2) = -205.5 \text{ kcal/mol}$) and rather weakly to Ni ($\Delta G_f^\circ(\text{NiO}) = -58.4 \text{ kcal/mol}$) [5]. Second, marker studies show that Ni is the moving species in Ni_2Si and NiSi formation [1],[6]-[10]. Thus the case where oxygen is initially present in the Ni film differs basically from that where oxygen is initially present in the Si.

In this chapter we investigate the effects of impurity oxygen on Ni_2Si formation for both the case where the impurity oxygen is initially located in the Ni film and where the oxygen is initially located in the Si.

For semiconductor applications, it is the final phase NiSi rather than Ni_2Si that is important. An interesting question is what effects impurity oxygen has on the reaction that transforms Ni_2Si to NiSi. Therefore we complete this study by investigating the effects oxygen has on the NiSi reaction when the oxygen is initially located in the Ni_2Si film.

B. EXPERIMENTAL PROCEDURES

There are three basic types of samples used in this study. Since their preparation and subsequent processing vary substantially, an individual description will be given for each type. In the first type the impurity oxygen is present only in a Ni film deposited on a single crystal Si substrate.

1. Initial Oxygen in Ni

Commercially prepared and polished Si <100> wafers (Wacker) were cleaned ultrasonically with TCE, acetone and methanol then rinsed in doubly distilled H₂O. The wafers were then etched for one min. in a 1:1 HF:H₂O solution and immediately loaded into our oil-free e-beam evaporation system. Ni films 1300 to 1700 Å thick were then deposited at a rate of ~ 35 Å/sec with the pressure held below 4×10^{-7} torr during evaporation. Half of the wafers were then implanted with O₂⁺ at 80 keV/atom to doses of 0.76, 1.54 and 2.34×10^{16} O/cm². According to range tables [11], this places the peak of the oxygen concentration (1,2 and 3 at. % respectively) at $R_p \sim 640$ Å with $\Delta R_p \sim 330$ Å in the Ni film. The sample temperature during implantation was monitored by a chromel-alumel thermocouple attached to the sample holder. Good thermal contact between the sample and the sample holder was made via silicone heat sink compound (Dow-Corning 340) to eliminate beam heating effects. The sample temperature was kept at ~ 20°C during implantation.

After implantation the samples used for the kinetics study were diced and loaded into a quartz-tube vacuum annealing furnace. Unimplanted

and implanted samples were annealed simultaneously at 290°C with the background pressure kept to $\sim 5 \times 10^{-7}$ torr.

The samples used for XPS were further cleaned to remove a carbon surface layer formed during implantation. We attribute this overlayer to a pump oil contamination which has subsequently been polymerized by the bombardment of the ion beam. This carbon overlayer was found to be impervious to a variety of common solvents (TCE, acetone, MEK, ethanol) and acids (HF, HCL). Plasma oxidation, however, was successful in removing this layer.

The XPS samples were placed into a flowing N₂ dry box containing a plasma cleaner and the input port to the XPS system. The samples were rinsed with ethanol and loaded into the plasma cleaner. The samples were exposed to a ~ 10 W O₂ plasma for 10 min. The O₂ pressure was ~ 50 m torr. The nickel oxide that formed during plasma oxidation was etched off by spinning the sample at 3600 rpm and adding dropwise 500 μ l of 1:1 HCL:ethanol and 1 ml of ethanol as a final rinse. After each cleaning step the samples were loaded into the XPS system, a modified HP 5950A ESCA spectrometer [12] to monitor and verify this cleaning procedure. This procedure was found to remove all of the carbon overlayer and nickel oxide.

After cleaning, the samples were annealed in situ at $\sim 280^\circ\text{C}$ in the analyzing chamber of the XPS system. This temperature is sufficient to allow Ni₂Si to form. As this reaction proceeds the Ni-Ni₂Si interface moves towards the sample surface. Either the Si 2p or O 1s core level was continuously monitored during this annealing. As the reaction brings the Ni-Ni₂Si interface within the depth range accessible to the analyzer

($\leq 50 \text{ \AA}$), the intensity of the core level begins to increase. The reaction was considered complete when the intensity had reached a plateau. The sample was then cooled to room temperature to allow extended data accumulation (Ni2p, O1s and Si2p lines) on the final product.

The composition and distribution of the silicide phases present in both XPS and kinetics samples was studied using 2.0 MeV $^4\text{He}^+$ backscattering spectroscopy [13]. The detector angle was 170° with the He beam incident along the sample normal. The chemical identity of Ni_2Si and NiSi was inferred from the signal height ratios of Ni to Si in the backscattering spectra, without recourse to x-ray diffraction analysis, because the Ni-Si system has been very well characterized in previous studies [1],[2],[3]. The oxygen distribution was measured by $^{16}\text{O}(d,\alpha)^{14}\text{N}$ nuclear reaction analysis as described in Chapter II. The detector angle was 164° with the D^+ beam incident at 55° to the sample normal. The cross section used is that of Kim et al [14].

2. Initial Oxygen in Si

In the second type of sample the impurity oxygen is present only in the single crystal Si substrate and the impurities in the deposited Ni film are kept to a minimum.

The Si $\langle 100 \rangle$ substrates (Wacker) were cleaned ultrasonically with TCE, acetone and methanol before loading into the implanter. The substrates were implanted with O_2^+ at 30 keV/atom to a dose of $7.0 \times 10^{15} \text{ O/cm}^2$. According to range tables [11], this places the peak of 2 at. % of the oxygen concentration at $R_p \sim 720 \text{ \AA}$ into the Si with $\Delta R_p \sim 270 \text{ \AA}$. The wafers were tilted 7° to the incident O_2^+ beam to avoid channeling effects.

Lattice damage caused by the implantation was removed by thermal annealing in vacuum at 550°C for ~ 2600 min. The wafers were then plasma-oxidized in 100 m torr of O₂ for 80 min. with ~ 10 W of RF power to remove the carbon layer formed during implantation. The SiO₂ formed during this oxidation step was removed by etching for one min. in a 1:1 HF:H₂O solution just prior to loading into our oil-free e-beam evaporation system. Ni films 1300 to 1500 Å thick were then deposited at ~ 35 Å/sec with the pressure kept below 4×10⁻⁷ torr during evaporation. These thicknesses will combine with from 1190 to 1375 Å of Si, twice the depth of the implanted O, in forming Ni₂Si.

The wafers were then diced and loaded into our quartz-tube vacuum annealing furnace. Unimplanted and implanted samples were annealed simultaneously at ~ 290°C with the background pressure kept to ~ 5×10⁻⁷ torr.

The silicide composition and growth kinetics were studied by 2.0 MeV He⁴ backscattering spectroscopy [13]. The oxygen distribution was studied by the ¹⁶O(d,α)¹⁴N nuclear reaction technique. The parameters for these measurements are the same as in the previous samples.

3. Initial Oxygen in Ni₂Si

In the third type of sample the impurity oxygen is initially located in a Ni₂Si film on a single crystal Si substrate.

The Si <100> wafers (Wacker) were cleaned ultrasonically with organic solvents as in the previous two cases. Immediately following a one min. etch in a 1:1 HF:H₂O solution, the wafers were loaded into our oil-free e-beam evaporation system. Ni films 1500 Å thick were evaporated

onto the silicon substrates at ~ 40 Å/sec with the vacuum kept at $\sim 3 \times 10^{-7}$ torr during the evaporation. Following Ni deposition, the wafers were annealed in our quartz-tube vacuum furnace at 293°C for 90 min. plus 291°C for 50 min. with the background pressure kept below 1×10^{-6} torr. This annealing is sufficient to react the Ni film completely with the Si substrate to form Ni_2Si yet does not allow for appreciable second phase NiSi formation. For Ni films initially 1500 Å thick, this corresponds to the formation of ~ 2300 Å of Ni_2Si .

One-half of these samples were then implanted with either 2 or 3×10^{16} O/cm² at 100 keV/atom. An estimate based on range tables [11], places the peak oxygen concentration at $R_p = \sim 1000$ Å into the Ni_2Si layer with the width $\Delta R_p = \sim 400$ Å. For a dose of 1×10^{16} O/cm², this estimate implies a peak volume concentration of oxygen of 1.1 atomic percent ($\rho_{\text{Ni}_2\text{Si}} = 8.94 \times 10^{22}$ atoms/cm³). Glancing angle x-ray diffraction measurements using a Read camera of the as-grown and the 2×10^{16} O/cm² implanted samples were taken before further annealing. The samples were then again loaded into the quartz-tube vacuum furnace and both the implanted and unimplanted samples were annealed simultaneously at 325°C for various times with the background pressure kept below 1×10^{-6} torr.

The silicide growth kinetics and composition were measured using MeV $^4\text{He}^+$ backscattering and the oxygen distribution were measured using the $^{16}\text{O}(d,\alpha)^{14}\text{N}$ nuclear reaction as in the previous two cases.

C. OXYGEN IN NI

If the impurity oxygen is initially located in the Ni film, the oxygen may form at best only weak bonds with the Ni atoms. Further reaction with Si is energetically very favorable. In addition, the oxygen finds itself in the moving species in Ni₂Si formation and thus substantial redistribution of the oxygen may be anticipated. In this section we present the effects of impurity oxygen on Ni₂Si formation when the oxygen is initially located in the Ni film.

1. Experimental Results

Figure 1 shows a plot of Ni silicide thickness squared versus annealing time at 290°C for unimplanted samples and for samples implanted with 2.3×10^{16} O/cm² half way into the Ni film. At the peak of its distribution, oxygen reaches a concentration of 3 at. % of Ni. In the unimplanted samples, Ni₂Si grows with square root of time until all unreacted Ni is consumed. The growth rate agrees with published data [2]. Then the second phase NiSi begins to grow, also with square root of time, which results in a parabolic decrease in Ni₂Si thickness squared. For the implanted samples, the Ni₂Si growth ceases after only ~ 1250 Å have formed. The Ni₂Si thickness squared decreases linearly and some NiSi begins to form but growth is much slower than in the unimplanted samples. The total amount of Ni in the Ni₂Si and NiSi layers slowly increases during subsequent annealing. This also confirmed by backscattering spectra which shows that the amount of unreacted Ni on the surface decreases. The effect of a reduced oxygen dose is shown in Fig. 2.

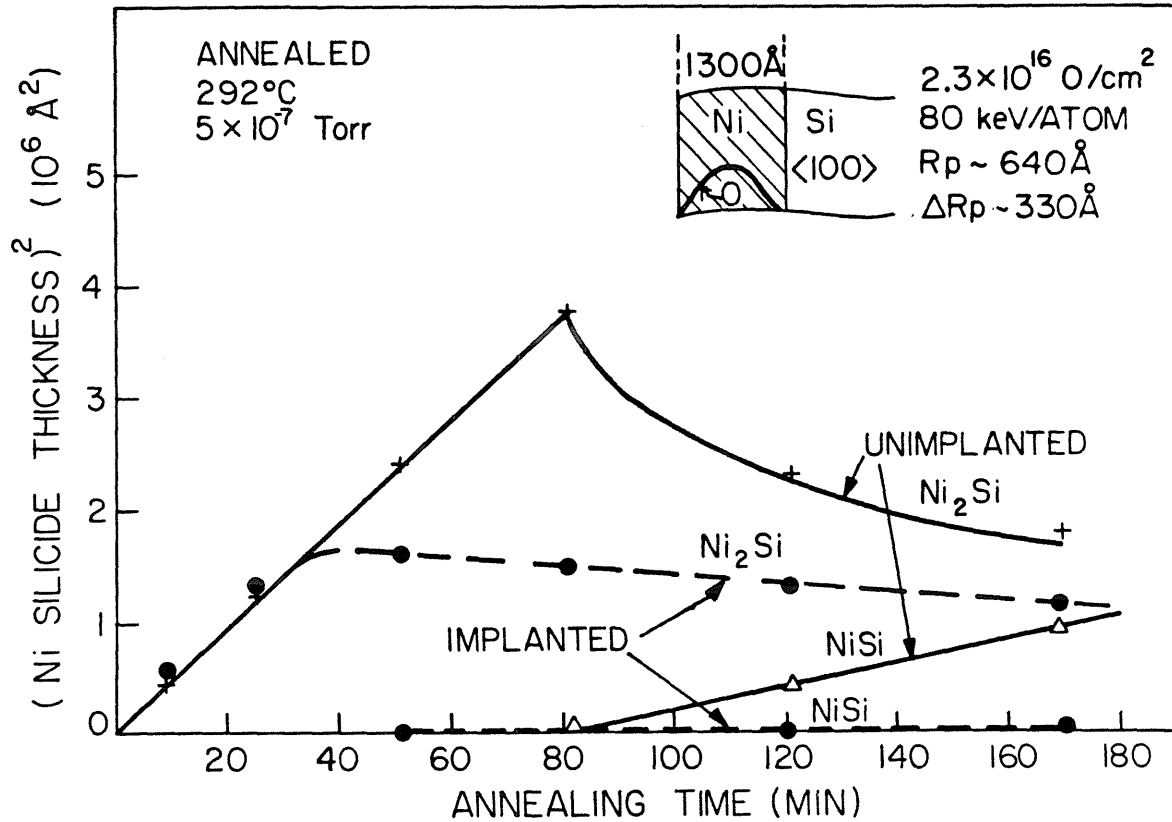


Fig. 1. Plot of Ni_2Si thickness squared versus annealing time at 292°C for unimplanted samples and for samples with 2.3×10^{16} O/cm² (3 at. % of Ni peak) implanted initially halfway into the Ni film. Barrier formation in the implanted samples stops Ni_2Si growth before the Ni is completely consumed. In comparison to the parabolic decrease in Ni_2Si thickness squared seen for unimplanted samples, the linear decrease indicates the presence of a partial barrier to the silicide formation process.

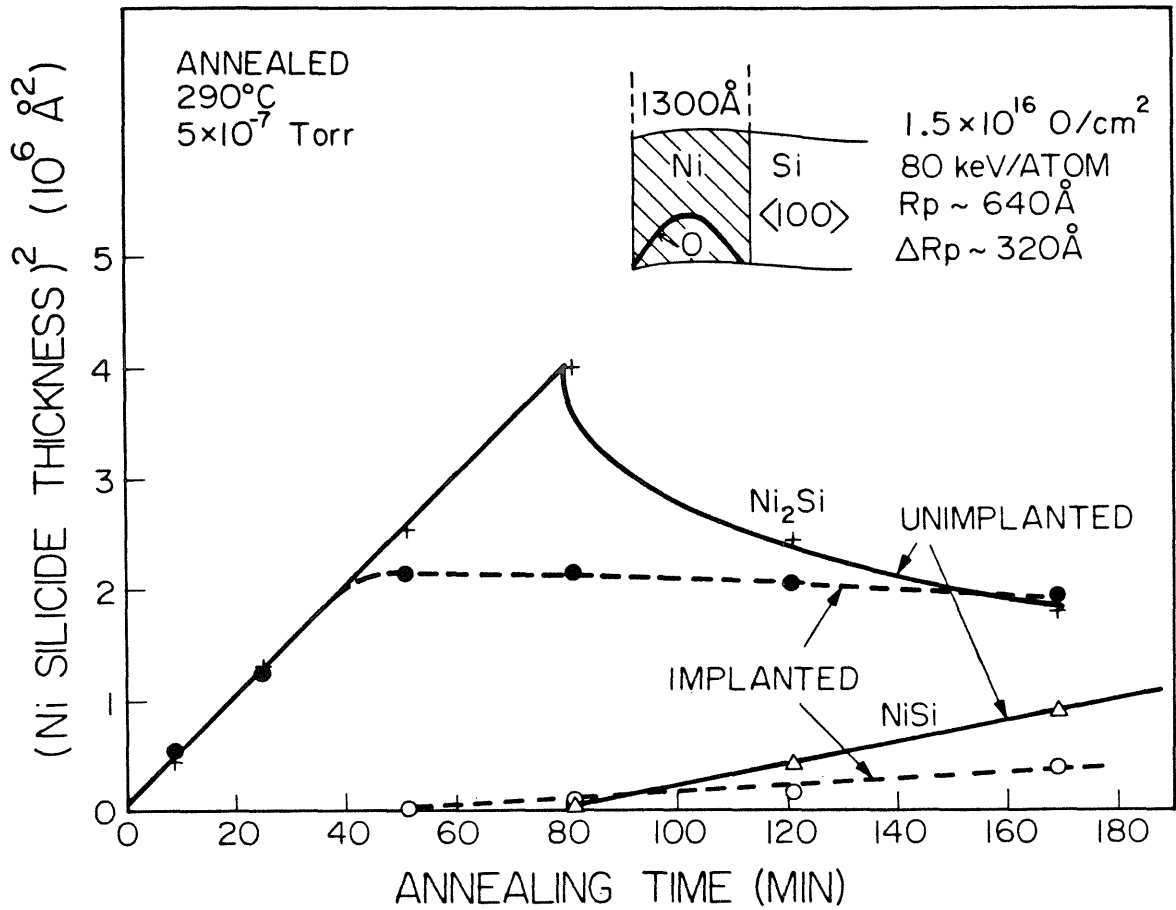


Fig. 2. Plot of Ni₂Si thickness squared versus annealing time at 290°C for unimplanted samples and for samples implanted with 1.5×10^{16} O/cm² (2 at. % of Ni peak) halfway into the Ni film. Barrier formation is delayed due to the lower dose. The linear decrease in NiSi thickness squared indicates the presence of a partial barrier to Ni₂Si formation.

One may expect that for a lower oxygen dose more Ni_2Si will form. Fig. 2 shows a plot of Ni silicide thickness squared versus annealing time at 290°C for unimplanted samples and for samples implanted with 1.6×10^{16} O/cm^2 . At the peak of its distribution, the oxygen reaches 2 at. % of Ni. Upon annealing 1470 \AA of Ni_2Si forms in the implanted samples before growth ceases. NiSi begins to form then, but at a faster rate than in the previous case although still slower than for unimplanted samples. The effects of a still lower oxygen dose are shown in Fig. 3. Figure 3 shows a plot of Ni silicide thickness squared versus annealing time at 290°C for unimplanted samples and samples implanted with for 0.76×10^{16} O/cm^2 . The peak of the oxygen distribution reaches only 1 at. % of Ni. The growth rate of Ni_2Si is the same in both implanted and unimplanted samples. Ni_2Si continues to form until all unreacted Ni is consumed. Then NiSi begins to nucleate and grow. No slowing of NiSi growth in the implanted samples is seen; NiSi growth rates for both implanted and unimplanted samples are evidently unimpeded.

Figure 4a shows the as-implanted oxygen distribution obtained from the $^{16}\text{O}(\text{d},\alpha)^{14}\text{N}$ nuclear reaction technique for a sample with a dose of 1.6×10^{16} O/cm^2 . The measured peak of the implanted oxygen distribution R_p is located at $\sim 630 \text{ \AA}$ into the Ni film, very close to the calculated value of 640 \AA . ΔR_p is $\sim 370 \text{ \AA}$ only slightly larger than the calculated value of 330 \AA . The maximum oxygen concentration is 2.3 at. % which is 15% higher than the 2.0 at. % calculated. The total amount of oxygen in this peak (from 150 \AA to 1400 \AA) is 1.7×10^{16} O/cm^2 . This is very close to the value obtained by charge integration during ion implantation. The narrow peak located at the Ni surface is mainly due to oxidation of the Ni surface during processing. Since this peak represents 3.3×10^{15} O/cm^2

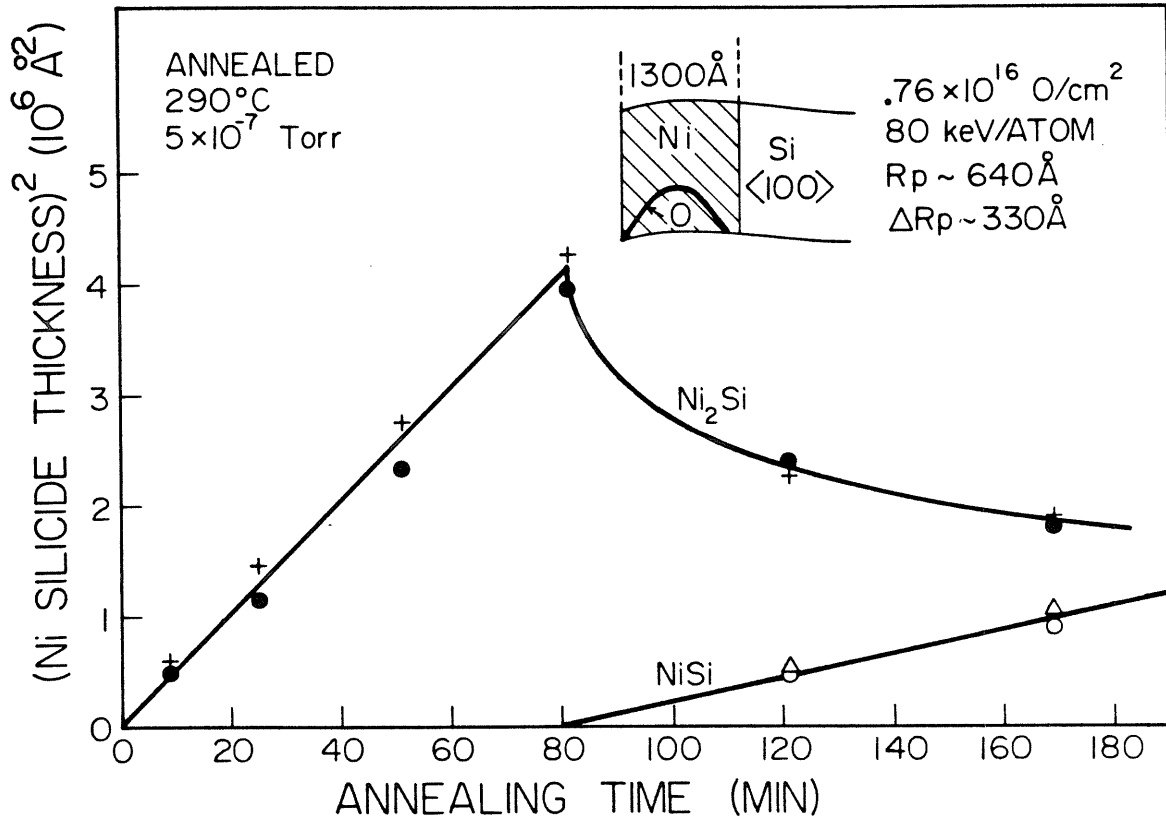


Fig. 3. Plot of Ni₂Si thickness squared versus annealing time at 290°C for unimplanted samples and for samples implanted with 0.76×10^{16} O/cm² (1 at. % of Ni peak) halfway into the Ni film. The implanted oxygen dose is below the threshold dose for barrier formation. The reaction proceeds to completion unhindered in both unimplanted and implanted samples.

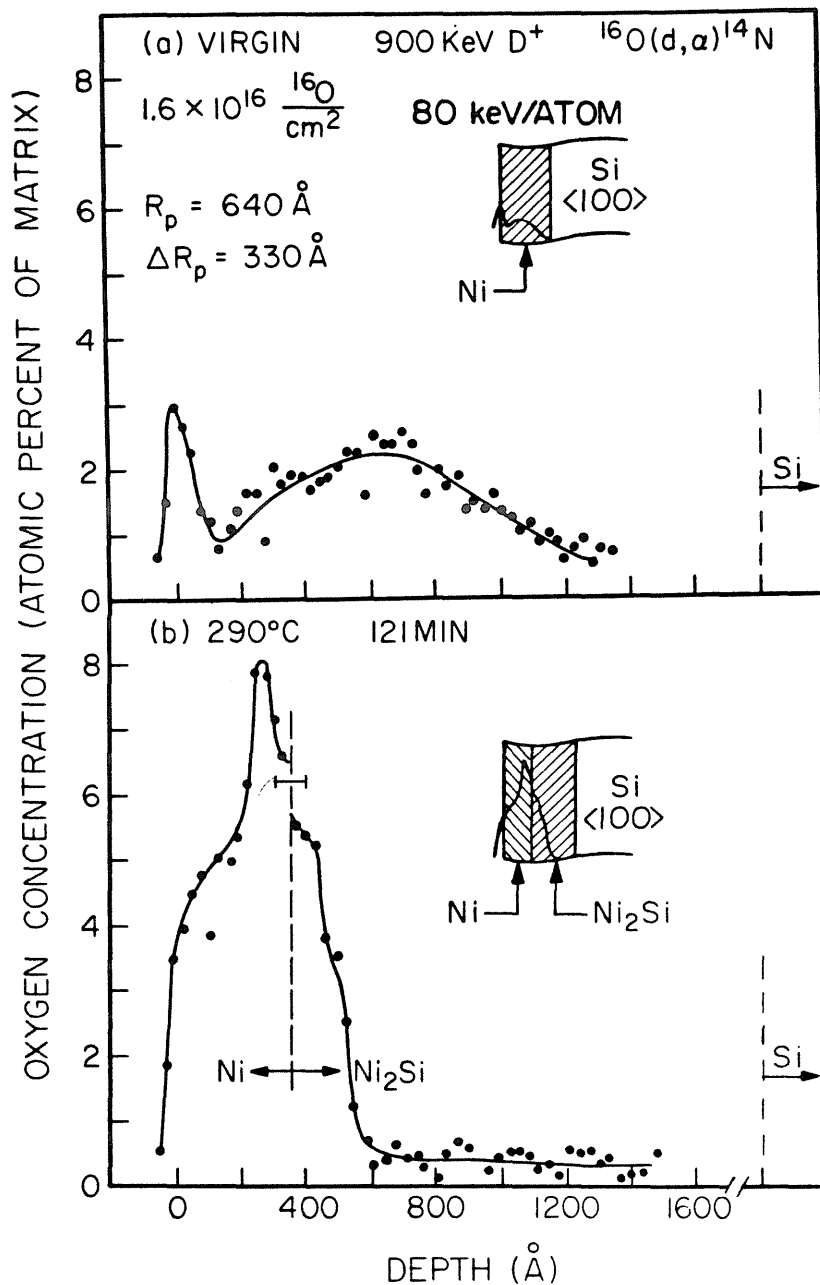


Fig. 4. Oxygen distribution obtained by the $^{16}\text{O}(d,\alpha)^{14}\text{N}$ nuclear reaction for a sample: a) as-implanted, and b) after annealing at 290°C for 121 min. The dashed lines are interface positions determined independently by $^4\text{He}^+$ backscattering. After annealing, the oxygen distribution peaks at the Ni-Ni₂Si interface. No oxygen is found in the Ni₂Si.

the total amount of oxygen in this sample is $\sim 2.0 \times 10^{16}$ O/cm². The position of the interfaces in Figs. 4a and b were obtained independently using ⁴He backscattering. Figure 4b shows the oxygen distribution after annealing at 290°C for 121 min. The implanted oxygen has built up at the Ni-Ni₂Si interface and is rejected from the silicide. The total amount of oxygen increases during annealing from 2.0 to 3.2×10^{16} O/cm². This additional oxygen is most likely introduced during annealing in the imperfect vacuum.

A very similar increase is observed during annealing of the sample with 2.3×10^{16} O/cm²; after 169 min. at 290°C the oxygen content rises to 3.3×10^{16} O/cm². The amount of oxygen within ± 100 Å of the Ni-Ni₂Si interface is 1.2×10^{16} O/cm². The discontinuity of the profile at the Ni-Ni₂Si interface is due to the atomic density change from 9.14 to 8.98×10^{22} atoms/cm³ going from Ni to Ni₂Si.

Figure 5 shows the Ni 2p and Si 2p signals after in situ annealing for unimplanted samples and for samples implanted with 1.54×10^{16} O/cm² (2 at. % of Ni) halfway into the Ni film. The position of these signals for various chemical states is shown by the labeled arrows. The position of the Ni 2p signal in both the unimplanted (5a) and implanted samples (5b) corresponds only to Ni₂Si. No signal from Ni oxide is found even though the oxygen was initially present in the Ni film. The Si 2p signal for the unimplanted samples (5c) also shows a large peak corresponding to Ni₂Si. This line is broader than the Ni 2p line due to overlapping Si 2p 1/2 and Si 2p 3/2 spin-orbit components. A low broad peak is present upfield of the Ni₂Si peak. Its position indicates the presence of some Si⁺⁴, SiO₂, along with Si⁺³ and Si⁺² suboxides Si₂O₃ and SiO [15].

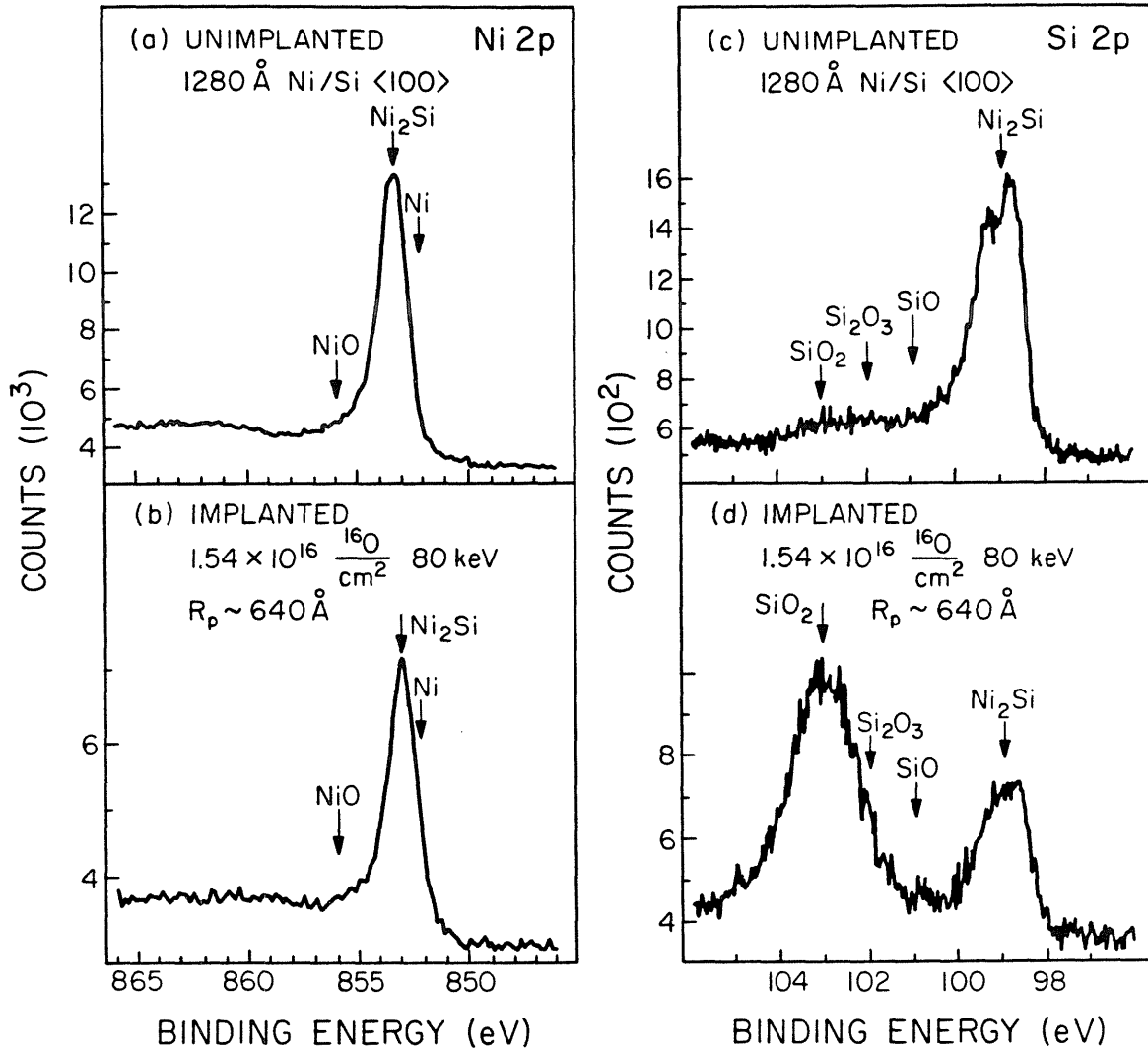


Fig. 5. XPS spectra for Ni-Ni₂Si interface showing the Ni2p and Si2p core levels for a) and c) unimplanted samples and b) and d), samples implanted with $1.5 \times 10^{16} \text{ O/cm}^2$ halfway into the Ni film. The position of the signals corresponds to Ni₂Si and SiO₂.

The Si 2p signal in the implanted case (5d) shows a large peak corresponding to SiO_2 , larger than the Ni_2Si signal. Similar spectra were also obtained after in situ annealing for the samples implanted with 0.76 and $2.34 \times 10^{16} \text{ O/cm}^2$ (1 and 3 at. %). If all the oxygen present in the film is bound as SiO_2 , the O 1s intensity should be completely accounted for by the Si 2p oxide intensity. In the lower curves in Fig. 6, the O 1s and Si 2p oxide intensities are plotted as a function of in situ annealing time. The initial decrease in the O 1s signal is due to the desorption of oxygen containing impurities on the sample surface as heating begins. During the first 45 min. no O or Si signal is detected. After 45 min., the O 1s signal begins to increase rapidly followed by the Si 2p oxide signal at 55 min. Both signals reach nearly full intensity after ~ 90 min. and remain constant for the remainder of the experiment. Since the kinetic energy of the Si 2p photoelectron is greater than that of the O 1s photoelectron one would not expect to observe the O 1s signal first. This suggests there is a front of oxygen preceding the advancing Si. The middle curve of Fig. 6 shows the stoichiometry ratio of O to Si versus anneal time. This curve was obtained by calibrating the intensity ratio O 1s/Si 2p of the oxide lines against a thick SiO_2 layer thermally grown on Si. The use of a calibration standard allows the estimation of the stoichiometry since such unknown factors as the photoelectron cross-sections and electron escape depths are intrinsically included. The initial dip in the O/Si curve indicates the presence of Si suboxides. The O/Si ratio, once the O and Si intensities reach a plateau, is two indicating the presence of SiO_2 with no excess oxygen. The O 1s and Si 2p oxide binding energies in the upper set of curves in Fig. 6 also show a shift from low to high binding energies as the initial signals appear.

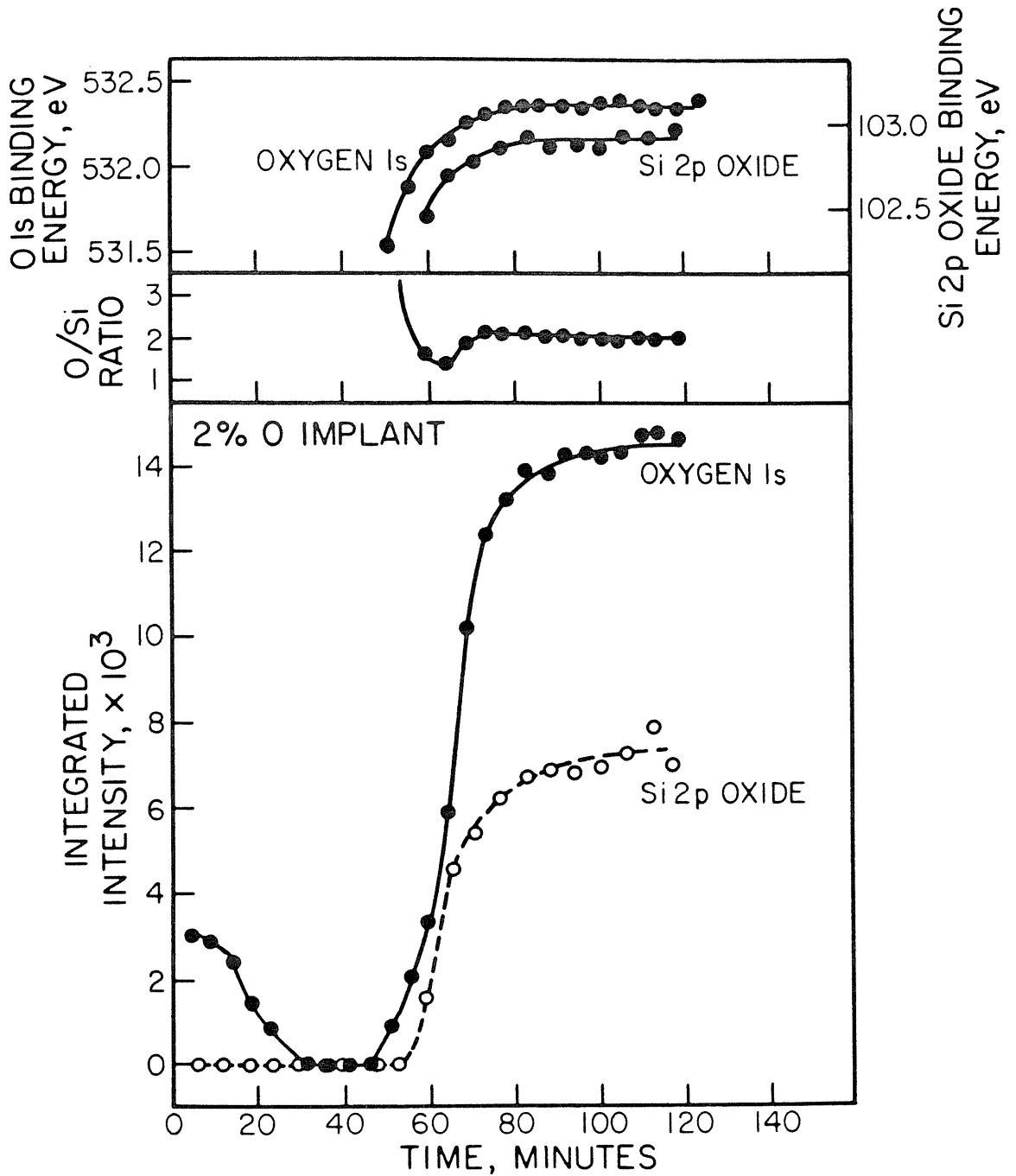


Fig. 6. Composite plot giving the core line intensities, O/Si stoichiometries, and binding energy maxima versus annealing time for the 2% oxygen implant dosage.

This also indicates the initial presence of Si suboxides followed by SiO_2 formation.

2. Discussion

Marker experiments have shown that Ni is the dominant diffusing species in Ni_2Si growth [1], [6]-[10]. The growth sequence of the unimplanted samples shows that as long as there is a supply of Ni atoms to the Ni_2Si -Si interface, the first phase Ni_2Si will continue to grow. Once the supply of Ni atoms is cut off, as when the Ni film is completely consumed, the second phase begins to nucleate and grow. That the suppression of the metal supply leads to the formation of a second silicide phase has been observed and stated before [3]. The implantation of 2 or 3 at. % oxygen (1.54 or 2.34×10^{16} O/cm^2 respectively) into the Ni film is sufficient to cause the second phase to nucleate and grow before all the unreacted Ni is consumed. Evidently, this presence of oxygen leads to the formation of a barrier to Ni diffusion, during annealing. Since the oxygen is seen to build up at the Ni- Ni_2Si interface and since the XPS results show this oxygen to have formed SiO_2 , this barrier is SiO_2 that has accumulated at the Ni- Ni_2Si interface. If only 1 at. % oxygen (0.76×10^{16} O/cm^2) is implanted into the Ni film a barrier to Ni diffusion does not form even though XPS measurements show the oxygen still forms SiO_2 . There is, therefore, a threshold oxygen dose necessary for barrier formation. For annealing of 290°C , this dose is between 0.76 and 1.5×10^{16} O/cm^2 or in terms of SiO_2 , between 16 \AA and 32 \AA of SiO_2 is necessary to block Ni diffusion. Since the barrier is SiO_2 at the Ni- Ni_2Si interface, the actual threshold dose can be estimated from the amount of oxygen present close to the interface. The threshold dose is,

taking the oxygen within $\pm 100 \text{ \AA}$ of the Ni-Ni₂Si interface, $1.2 \times 10^{16} \text{ O/cm}^2$ or $\sim 25 \text{ \AA}$ of SiO₂. Using the ratio of the intensity of the Si 2p oxide line I_{ox} to the Si 2p silicide line I_{sil} the thickness of the SiO₂ barrier may be independently estimated from the XPS results using:

$$\frac{I_{\text{ox}}}{I_{\text{sil}}} = \frac{N_{\text{Si}}^{\text{SiO}_2}}{N_{\text{Si}}^{\text{Ni}_2\text{Si}}} \frac{\lambda_{\text{ox}}}{\lambda_{\text{sil}}} \left(e^{-\frac{x}{(\lambda_{\text{ox}} \sin \sigma)}} - 1 \right)$$

where $N_{\text{Si}}^{\text{SiO}_2}$ and $N_{\text{Si}}^{\text{Ni}_2\text{Si}}$ are the atomic densities of Si in the oxide and silicide respectively; λ_{ox} and λ_{sil} are the electron escape depths in the oxide and silicide respectively and θ is the angle between the plane of the sample and the electron detector (38.5°). If we allow λ_{ox} to be 36 \AA [16] and let λ_{sil} be a "metallic like" 15 \AA [17] we find that $\sim 24 \text{ \AA}$ of SiO₂ is the threshold necessary to form the barrier.

24 \AA of SiO₂ amounts to $1.1 \times 10^{16} \text{ O/cm}^2$. This is within the range 0.76 to 1.5×10^{16} as it should be and also agrees with the value obtained previously. Thus the threshold dose necessary for barrier formation is $\sim 1.2 \times 10^{16} \text{ O/cm}^2$.

These results are consistent with a sequence of events that is summarized in Fig. 7. The moving species in Ni₂Si formation is Ni. Presumably implanted oxygen binds with Ni atoms to form nickel oxide complexes that are apparently immobile in Ni. As the Ni atoms diffuse into the silicide (represented by arrows) upon annealing, these oxygen complexes (represented by the solid dots) are moved toward the Ni-Ni₂Si interface. Oxygen bonds rather weakly to Ni ($\Delta G_f^\circ (\text{NiO}) = 51.7 \text{ kcal/mol}$) and very strongly to Si ($\Delta G_f^\circ (\text{SiO}_2) = -204.8 \text{ kcal/mol}$ [5]). Because of

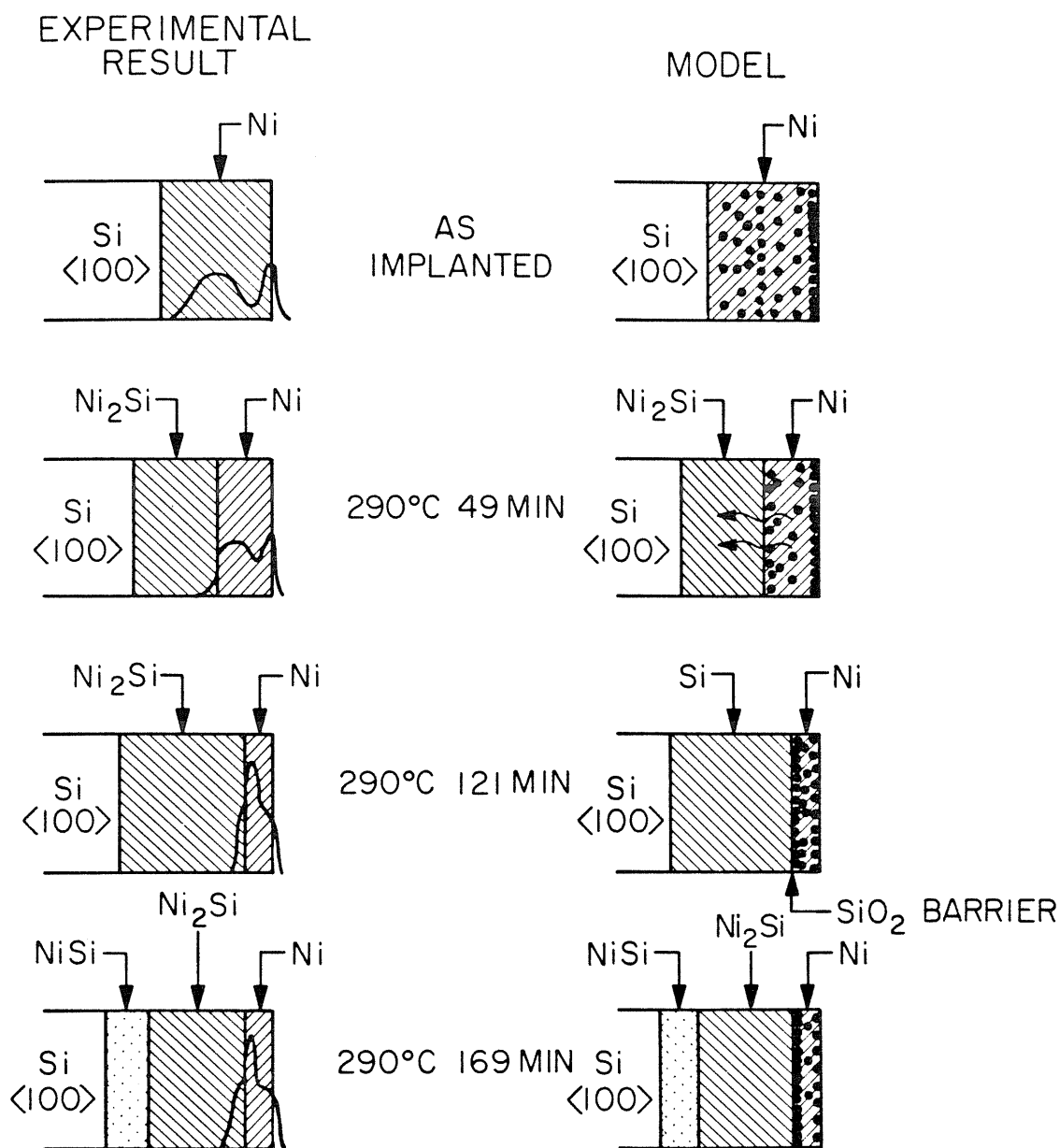


Fig. 7. Model of SiO₂ barrier formation. The black dots represent oxygen complexes in the Ni film. Upon annealing Ni diffuses into the silicide, represented by the curved arrows, exposing the oxygen to the Si present at the Ni-Ni₂Si interface. Oxygen reacts there to form SiO₂. When all Ni diffusion paths are blocked, the second phase NiSi begins to form.

this asymmetry in the chemical affinity of oxygen to Si and Ni, Si reduces the nickel oxides and forms silicon oxides when the Ni diffusion exposes them to Si at the Ni-Ni₂Si interface. The oxygen initially forms Si suboxides. As further Ni diffusion brings increasing amounts of oxygen to the Ni-Ni₂Si interface, the suboxides become SiO₂. SiO₂ is not mobile relative to Ni₂Si and therefore remains at the Ni-Ni₂Si interface. Thus, as oxygen-bearing Ni diffuses into the Ni₂Si, the oxygen builds up at the interface in the form of SiO₂ until further Ni diffusion is blocked. Ni diffusion is blocked after $\sim 25 \text{ \AA}$ of SiO₂ has accumulated at the Ni-Ni₂Si interface, thus at least $1.2 \times 10^{16} \text{ O/cm}^2$ must be initially present in the Ni film before subsequent barrier formation can take place. When the Ni supply ceases the second phase NiSi begins to form converting the Ni₂Si to NiSi. The NiSi growth rate, even though the impurity oxygen has been rejected from the Ni₂Si layer, leaving this layer impurity free, still remains dependent on the initial oxygen dose present in the Ni film. That this effect may be caused by the incorporation of small amounts of oxygen into the silicide layer is unlikely. In Section E of this chapter we investigate the effect of impurity oxygen initially present in the Ni₂Si layer on NiSi growth and show that even large amounts of oxygen have little effect. In that section we present arguments that a structural change in the Ni₂Si layer caused by ion implantation damage may be responsible for the slowing in NiSi growth observed there. A similar effect may be present here. The resolution of this question may require additional diagnostic techniques, in particular, TEM.

D. OXYGEN IN SILICON

If the oxygen is initially present in the Si rather than the Ni, the effect of oxygen is not expected to be the same, because oxygen is placed at once in the medium (Si) with the lowest free energy of reaction (SiO_2), so that a reaction with Ni is now energetically unfavorable. The oxygen is also located in the non-diffusing species. In this section we present the effects of impurity oxygen on Ni_2Si growth when the oxygen is initially present in the Si substrate.

1. Experimental Results

Figure 8 shows a plot of Ni_2Si thickness squared versus annealing time at 290°C for 1440 \AA Ni films on Si $\langle 100 \rangle$ substrates that were implanted with $7.0 \times 10^{15} \text{ O/cm}^2$ to a depth of $\sim 700 \text{ \AA}$ in the Si. At the peak of its distribution, the oxygen concentration reaches 1 at. % of Si. In comparison with the unimplanted samples in which Ni_2Si grows as usual, the implanted samples show a slight drop in growth rate after ~ 64 min of annealing. Ni_2Si continues to form, however.

Figure 9a shows the as-implanted oxygen distribution obtained from the $^{16}\text{O}(d,\alpha)^{14}\text{N}$ nuclear reaction. The Ni-Si interface position, obtained independently by backscattering spectrometry, is located at 1440 \AA . The broad peak located near 2200 \AA is due to the implanted oxygen and corresponds to a depth in the Si of $\sim 780 \text{ \AA}$. This agrees reasonably well with the calculated range of 715 \AA . The total amount of implanted oxygen determined from this oxygen signal (1000 \AA to 3500 \AA) is $8.9 \times 10^{15} \text{ O/cm}^2$ and agrees well with the value of $7.0 \times 10^{15} \text{ O/cm}^2$ measured during the

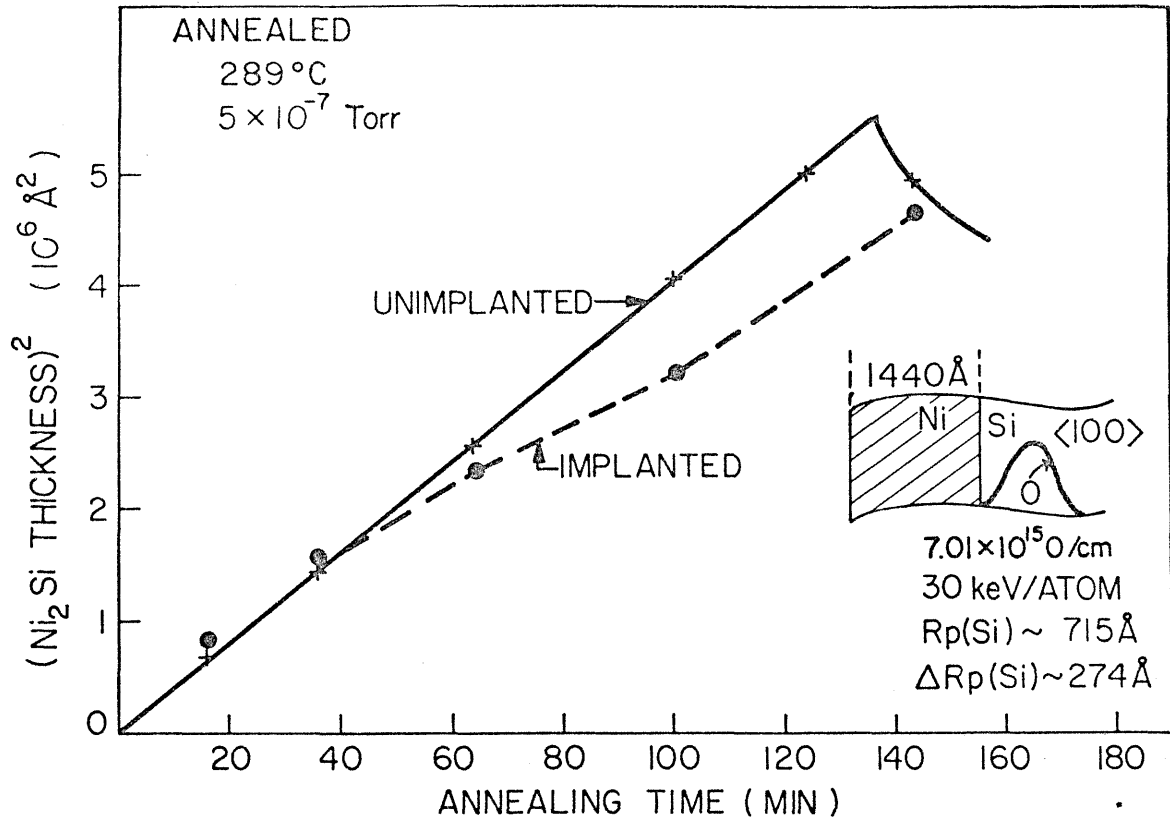


Fig. 8. Plot of Ni₂Si thickness squared versus annealing time at 289°C for unimplanted samples and samples implanted with 7.0×10^{15} O/cm² approximately 715 Å into the Si substrate. No barrier forms and Ni₂Si grows until all unreacted Ni is consumed.

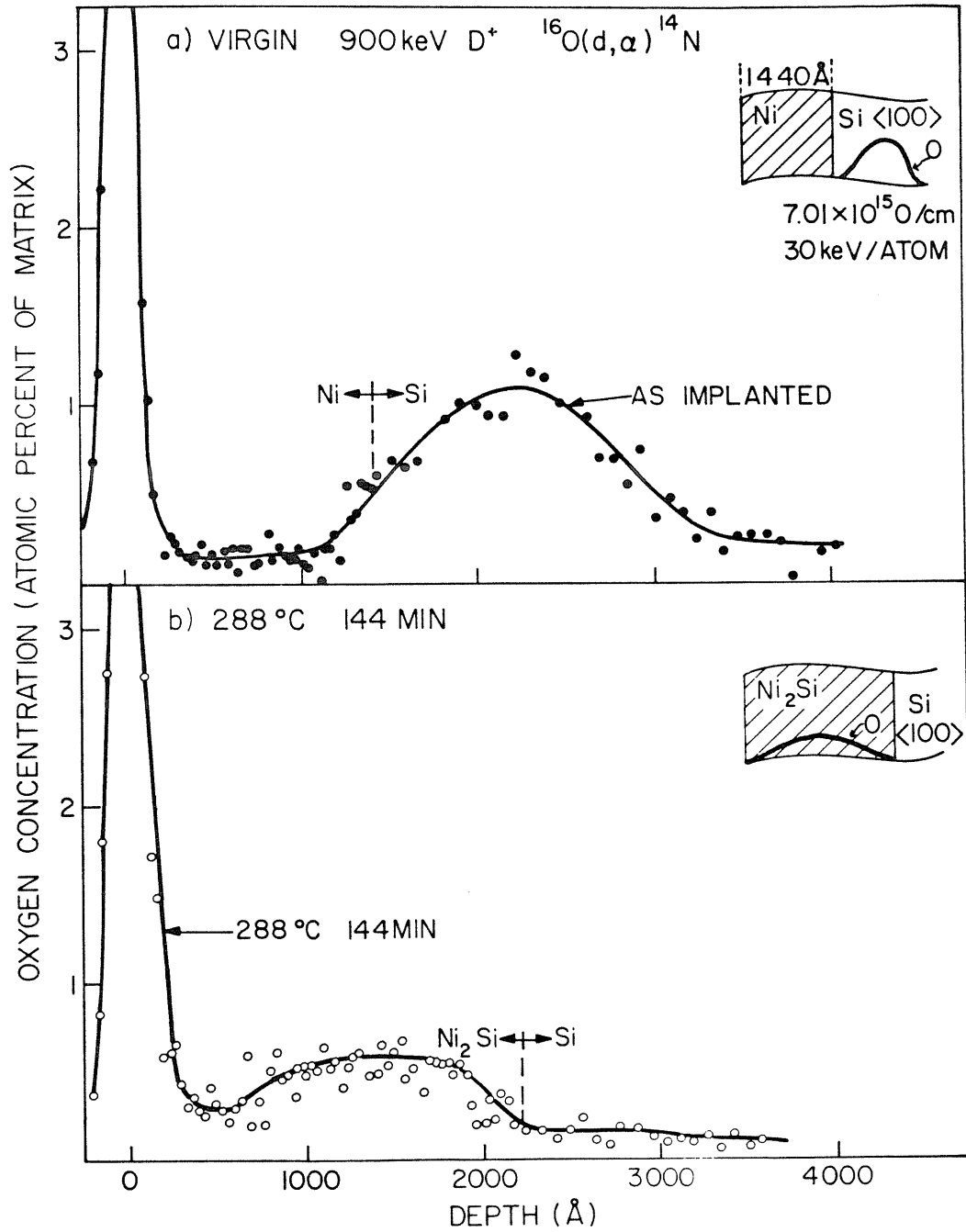


Fig. 9. Oxygen distribution obtained by the $^{16}\text{O}(d,\alpha)^{14}\text{N}$ nuclear reaction for a sample: a) as-implanted, and b) after annealing at 288°C for 144 min. No barrier formation is seen. The oxygen is incorporated into the Ni_2Si . The oxygen density is lowered similar to that of the Si as the Si formed Ni_2Si .

implantation. Figure 9b shows the oxygen distribution after annealing at 288°C for 144 min. The oxygen has been incorporated into the Ni₂Si with only a lowering and some broadening of its initial distribution. The decrease in oxygen concentration deduced from this plot is approximately 40%. An interfacial accumulation of oxygen is not observed. The total amount of oxygen in the annealed sample is 8.1×10^{15} O/cm² and differs insignificantly from the 8.9×10^{15} O/cm² measured initially. Evidently, oxygen from the ambient is not able to enter the silicide. As in the case when the implanted oxygen is initially in the Ni film, such oxygen will be swept out as the Ni-Ni₂Si interface moves through the Ni to the surface.

2. Discussion

It is clear from the results that a barrier to Ni diffusion does not form when the oxygen is initially located in the Si. Instead, the impurity oxygen is incorporated into the Ni₂Si without an interfacial accumulation taking place. The decrease in oxygen concentration during incorporation into the Ni₂Si is ~ 40%. Since this value is also that of the density change of Si when Ni₂Si is formed, we conclude that oxygen and silicon do not alter their relative positions as Ni₂Si formation proceeds. This is in marked contrast to the case when oxygen is initially in the Ni and no oxygen is found in the Ni₂Si after annealing.

The effects observed on the Ni₂Si growth when oxygen is initially in the Si are summarized in Fig. 10. The oxygen distribution for the as-implanted case is approximately gaussian and located within the Si that will be consumed in Ni₂Si formation. Oxygen bonds very strongly to Si ($\Delta G_f^\circ(\text{SiO}_2) = -204.8$ kcal/mol) and very weakly to Ni ($\Delta G_f^\circ(\text{NiO}) = -51.7$ kcal/mol) [5]. Thus, since Ni cannot reduce Si oxides the oxygen will

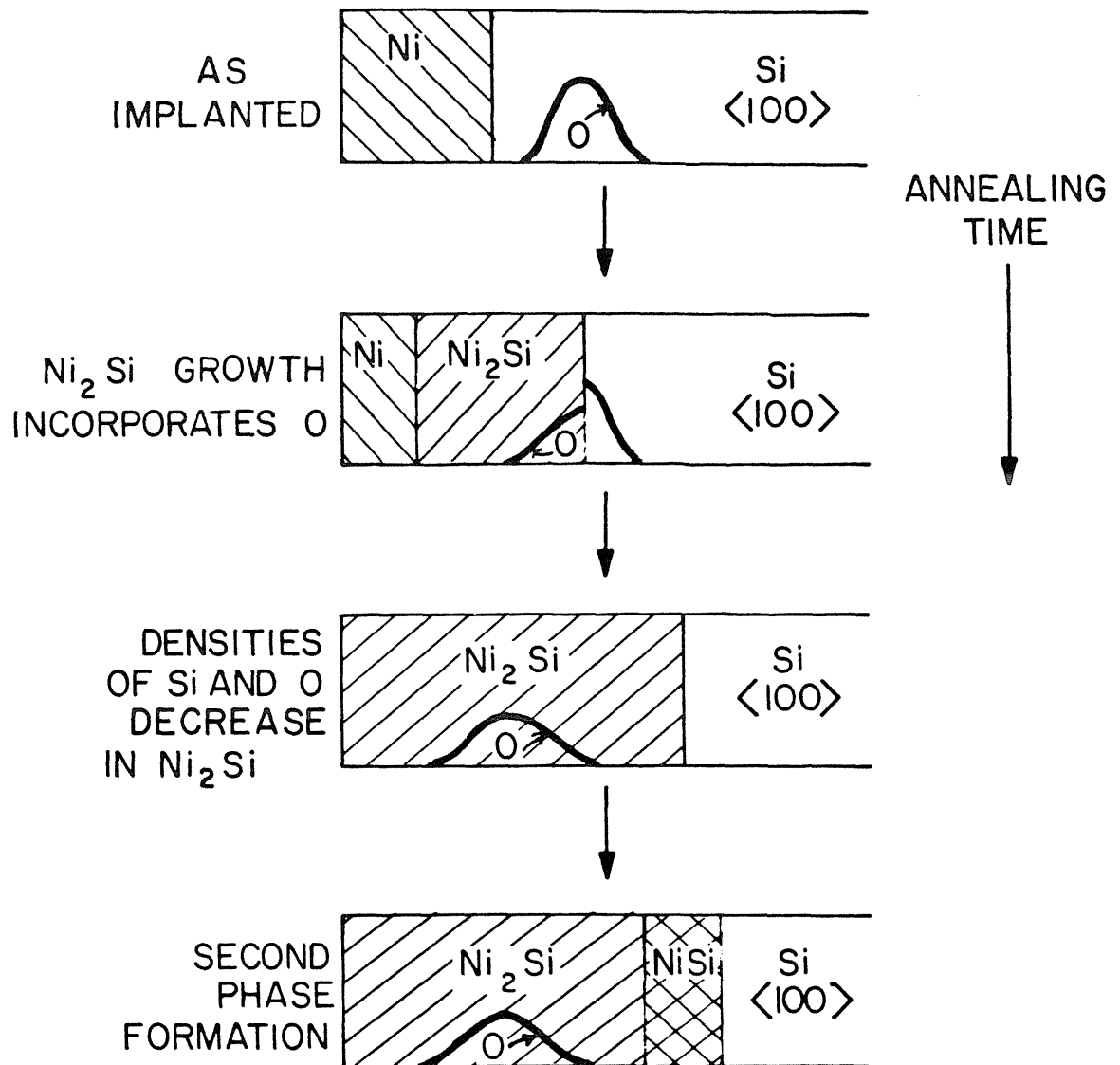


Fig. 10. Model of oxygen incorporation into Ni_2Si without barrier formation. Oxygen binds to the silicon initially and remains bound to it during Ni_2Si formation. The Ni diffuses around Si-O complexes in forming Ni_2Si , diluting the oxygen density in the same ratio as the Si density.

remain bound to the Si during Ni_2Si formation. Presumably, SiO_2 (or a Si suboxide) is not mobile with respect to Ni_2Si , and therefore it will be incorporated into the silicide along with the Si during Ni_2Si growth. Si undergoes a density decrease from 5.0 to $3.0 \times 10^{16} \text{ Si/cm}^2$ in forming Ni_2Si . The oxygen in the Si will change its density by the same ratio, decreasing and broadening, unless sufficient oxygen is present to form a glassy substructure that would resist density changes. The oxygen in Si decreases the growth rate, however, as the presence of oxygen in the Ni_2Si and at the $\text{Ni}_2\text{Si-Si}$ interface interferes with the Ni diffusion and the formation of new Ni_2Si . This interference is not sufficient to significantly alter the reaction process and Ni_2Si is still the phase formed. Nucleation and growth of the second phase NiSi does not take place until all of the unreacted Ni film has been consumed by Ni_2Si growth.

E. OXYGEN IN Ni₂Si

In Section C we found that the growth rate of the second phase NiSi strongly depends on the initial oxygen dose implanted into the Ni film. While an oxygen dose of 1 at. % of Ni had no effect on the NiSi growth rate, doses of 2 and 3 at. % reduced the growth rate (NiSi thickness squared/annealing time) from $9.9 \times 10^3 \text{ \AA}^2/\text{min}$ to 3.2×10^3 and $4.2 \times 10^2 \text{ \AA}^2/\text{min}$ respectively. An interesting question is if this effect is due to the incorporation of impurities into the Ni₂Si layer.

In this section we investigate the effects that implanted oxygen has on the NiSi reaction when oxygen is initially located in the Ni₂Si film.

1. Experimental Results

Figure 11a shows a plot of NiSi thickness squared versus annealing time for unimplanted samples and for samples implanted with 2 or $3 \times 10^{16} \text{ O/cm}^2$ into the Ni₂Si film for an annealing temperature of 325°C. X-ray diffraction patterns taken from a sample before and after the $2 \times 10^{16} \text{ O/cm}^2$ implantation show the presence of Ni₂Si in both cases. However, there is a significant broadening of the lines in the implanted case indicating that structural changes have taken place. This sample remains polycrystalline, however, damage has occurred possibly enough to form local amorphous regions. In the unimplanted samples, NiSi is seen to grow with square root of time. This disagrees with the linear rate previously reported by Coe et al [4] (also shown in Fig. 11a). For the implanted samples, the NiSi growth is again proportional to the square root of time, but is slower than for the unimplanted case and is practically identical for both the 2 and $3 \times 10^{16} \text{ O/cm}^2$ cases. NiSi growth continues until all

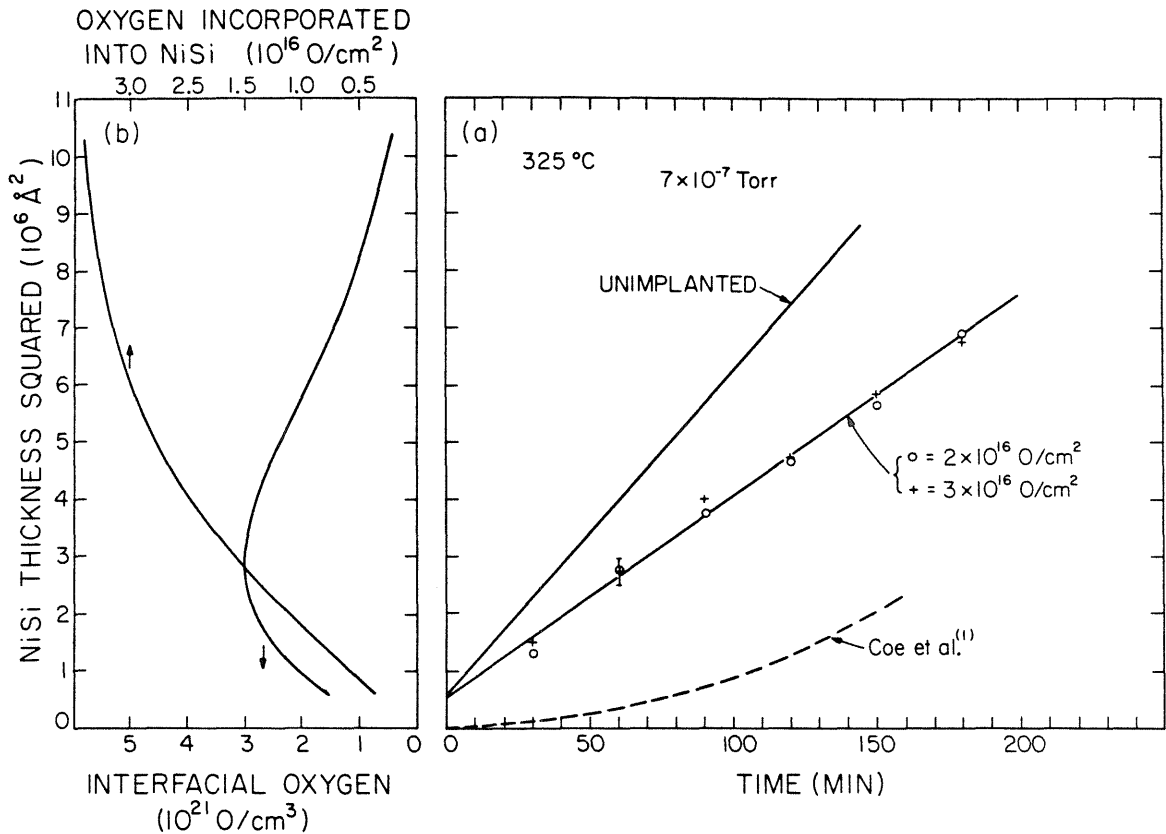


Fig. 11. (a) A plot of NiSi thickness squared versus annealing time at 325°C for unimplanted samples and samples implanted with 2 and $3 \times 10^{16} \text{ O/cm}^2$. Growth is uniformly proportional to square root of time in both cases. Also shown for comparison is a calculated curve of NiSi growth using Coe et al [1], results reporting a linear time-dependence.

(b) The total oxygen incorporated into the NiSi and the concentration of oxygen present at the NiSi side of the $\text{Ni}_2\text{Si-NiSi}$ interface as a function of NiSi thickness squared. These curves were calculated from the initial oxygen distribution. They illustrate that depth dependences of oxygen have little effect on the time dependence of NiSi growth.

of the Ni_2Si layer has been consumed. These results were reproduced with samples prepared fully independently to within the uncertainty resulting from the furnace setting. The nonzero intercepts for the NiSi thickness squared in both the implanted and unimplanted cases indicate that an initial amount of NiSi was present before annealing.

Figure 12a shows the oxygen distribution obtained by the $^{16}\text{O}(d,\alpha)^{14}\text{N}$ nuclear reaction technique for the as-implanted sample. The implanted oxygen is seen to have an approximately Gaussian distribution with a range $R_p \sim 1200 \text{ \AA}$ and a width $\Delta R_p \sim 550 \text{ \AA}$. Both values are near the estimated ones ($\sim 1000 \text{ \AA}$ and $\sim 450 \text{ \AA}$). The total amount of oxygen in this peak (350 to 2200 \AA) is $2.74 \times 10^{16} \text{ O/cm}^2$ and agrees well with that obtained by charge integration. The boundaries of the initial amount of NiSi present in the as-implanted sample as determined from the intercept of Fig. 11a are shown as vertical dashed lines. A small amount of the implanted oxygen reaches this layer. Fig. 12b shows the oxygen distribution after the Ni_2Si film has fully reacted to form NiSi. The oxygen remains approximately Gaussian; however, R_p and ΔR_p are less than before ($\sim 925 \text{ \AA}$ and $\sim 400 \text{ \AA}$, respectively). The total amount of oxygen in this peak (250 \AA to 1700 \AA) is $3.42 \times 10^{16} \text{ O/cm}^2 \sim 25\%$ larger than the as-implanted oxygen peak. The large surface peaks shown one-tenth actual size in both spectra is most likely due to surface oxidation of the samples during processing.

2. Discussion

These results may be explained in terms of the asymmetries present in the chemical affinities of oxygen to the reacting species and in the initial location of the oxygen relative to the moving species. Marker experiments have shown that Ni is the diffusing species in NiSi formation

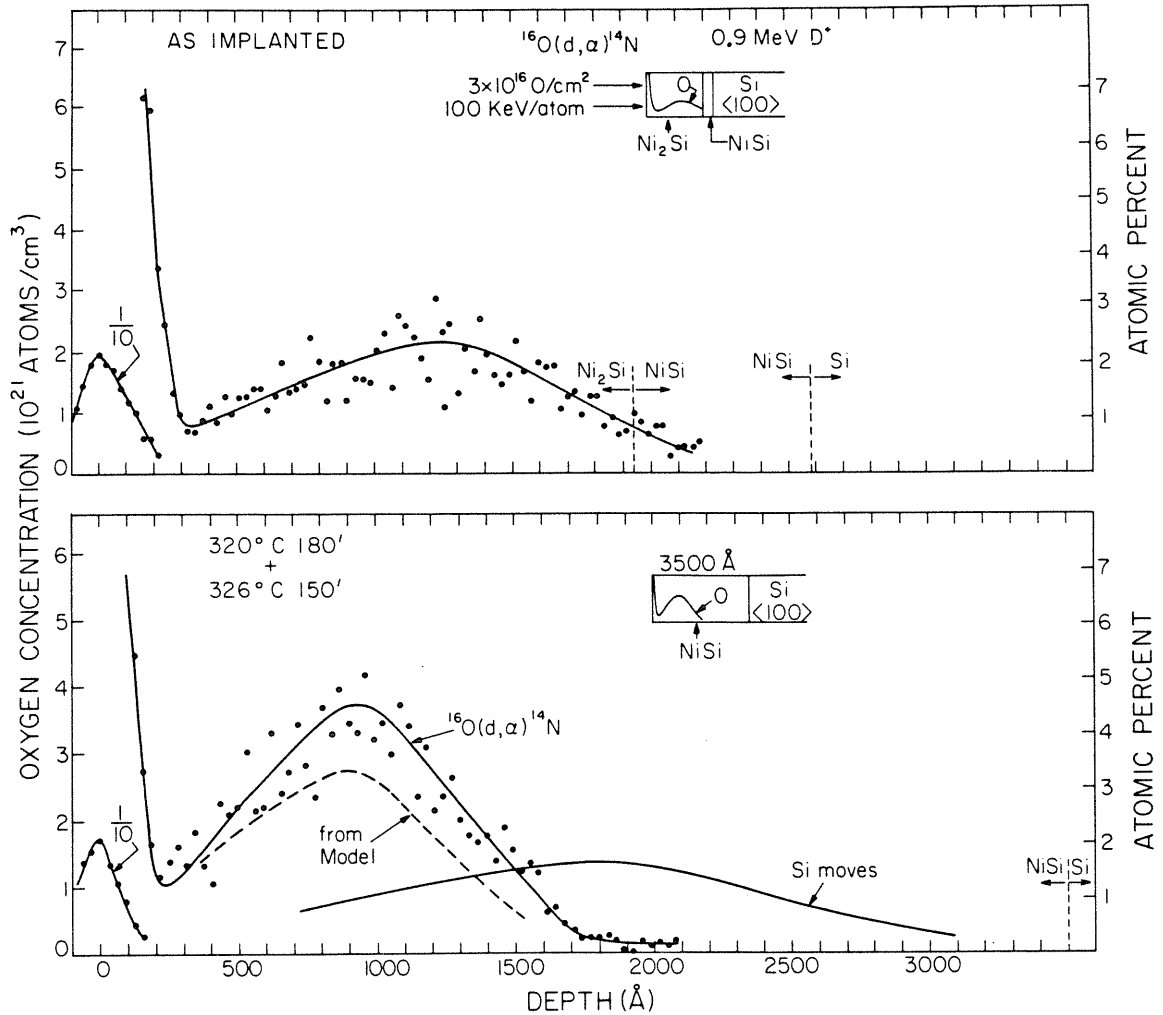


Fig. 12. (a) Oxygen distribution obtained by $^{16}\text{O}(d,\alpha)^{14}\text{N}$ nuclear reaction for the as-implanted sample. The broad peak located at ~ 1200 \AA is due to the implanted oxygen. The boundaries between Ni_2Si , the initial NiSi present and the Si substrate are shown as vertical dashed lines.

(b) Oxygen distribution obtained by $^{16}\text{O}(d,\alpha)^{14}\text{N}$ nuclear reaction after the Ni_2Si film has been completely reacted to form NiSi . The peak of the oxygen distribution is located at ~ 950 \AA and agrees very well with the calculated curve from the model.

[9], [10]. Oxygen bonds weakly to Ni ($\Delta G_f^\circ(\text{NiO}) = -51.7$ kcal/mol) as compared with Si ($\Delta G_f^\circ(\text{SiO}_2) = -204.8$ kcal/mol [5]). Thus oxygen initially located in Ni_2Si finds itself in a medium containing both the moving species with which it only weakly bonds and the stationary species with which it forms strong bonds. The difference in chemical affinity suggests that the oxygen will initially bond to the Si and will remain so throughout NiSi formation.

In Fig. 12b we show a theoretical curve (dashed line) calculated on this assumption from the as-implanted oxygen distribution (solid line shown in Fig. 12a). This curve matches very well to the measured oxygen distribution. Evidently, the oxygen has been incorporated into the NiSi film without an interfacial accumulation taking place. This ability of oxygen to form an inert oxide that is incorporated in the Si without interfacial effects suggests an interesting possibility to use oxygen as a diffusion marker. Since each oxygen atom is tightly bound to two Si atoms and these are tied to the silicon lattice, this array of atoms is not expected to move relative to the Si lattice even though considerable mass transport may take place around it. The lack of segregation effects in the present case would seem to verify this picture. Assuming Si rather than Ni as the diffusing species in NiSi formation, we calculate the third curve ("Si moves") on Fig. 12b. The clear difference between the two predicted curves provides an independent verification that within our experimental sensitivity it is only the Ni that moves. While oxide inclusions have been used before as a diffusion marker during bulk diffusion [18], [19], the use of ion implanted oxygen to form an inert oxide may open this possibility to studies of thin films as well.

The origin of the disagreement between the square root of time growth rate measured here and the linear growth rate reported by Coe et al [3] is not known. One evident difference appears to lie in the annealing ambient of forming gas (90% N₂ - 10% H₂) in the latter case. After annealing a sample in forming gas, however, we found nearly the same NiSi growth as in the vacuum annealed samples. Linear growth, instead of square root growth, will result if the interfacial reactions are slowed down. It is well known that impurities introduced during film deposition or annealing can interfere with silicide reactions. We suspect this to have happened in the case of Coe et al [3].

The slowing of NiSi growth in the implanted samples may be due to various effects. The presence of oxygen may be expected to slow down the reaction. Since the kinetics remains transport-limited, oxygen interference with the interfacial reaction must be insignificant, but oxygen may alter the diffusion of Ni through the NiSi layer. The amount of oxygen present on the NiSi side of the NiSi-Ni₂Si interface and the total amount of oxygen incorporated in the NiSi film are shown in Fig. 10b. These curves were calculated based on the as-implanted oxygen distribution. The lack of correlation of the NiSi growth with either of these parameters shows that the presence of oxygen per se is not a plausible explanation for the reduced kinetics. This conclusion is further supported by the observation that a 50% increase in oxygen does not affect the resulting kinetics. Structural damage caused to the Ni₂Si film by the ion implantation process is another factor to be considered in regards to the slowing of the NiSi growth for the implanted samples. The X-ray diffraction measurements indicate a structural change after implantation. However, any amorphous regions present will recrystallize in only a few

seconds at 325°C [20]. This can result in a further change in Ni₂Si structure. What effect a change in Ni₂Si structure has on the resulting NiSi structure is not known. However, it is known that the initial structure of the Si substrates affects the structure and the kinetics of the first phase Ni₂Si formed upon annealing [2]. A similar effect may be present here in the second phase of NiSi as well. Finally, it is conceivable that both structural alterations of the Ni₂Si and the presence of oxygen simultaneously affect the reaction, and in different ways. Further studies using additional diagnostic techniques, and in particular TEM, are required to settle these questions.

The implantation of 2 to 3×10^{16} O/cm² reduces the reaction kinetics slightly. Strictly speaking, a marker should not alter the reaction, but in the present case, the oxygen performs as a valid marker nevertheless. Mass transport should not take place through a truly inert marker. Thus the presence of marker material can only decrease the number of available diffusion paths. This is not expected to alter the identity of the moving species. Therefore, we speculate that an inert marker will perform properly even if it causes a reduction in the growth rate so long as the phase formed is unaltered. In the present case, we find that noticeable interference by the marker can be tolerated. This relaxation of the requirements placed on the marker could be useful in further marker studies of thin film reactions.

F. SUMMARY AND CONCLUSION

We have investigated the effects of oxygen on Ni_2Si formation by implanting oxygen initially into the Ni film and by implanting oxygen initially into the Si substrate. We found that if oxygen is initially in the Ni, oxygen continuously accumulates at the Ni- Ni_2Si interface during annealing and ultimately a barrier to further Ni diffusion is formed. The XPS measurements show that the chemical form of the oxygen at the Ni- Ni_2Si interface is SiO_2 . It is the formation of SiO_2 at the Ni- Ni_2Si interface that prevents Ni from entering the Ni_2Si . Once the Ni supply is cut off, the second phase NiSi begins to form. When the oxygen is initially in the Si, it is incorporated into the Ni_2Si without barrier formation. The decrease in oxygen density parallels that of Si as the Si reacts to form Ni_2Si , indicating that the oxygen remains bound to Si during Ni_2Si formation. We propose a model in which the moving species Ni binds with the impurity oxygen much more weakly than does the stationary species Si. Oxygen will therefore react with the Si at the Ni- Ni_2Si interface to form a barrier of SiO_2 , whereas oxygen initially in Si will remain tied to the Si during Ni_2Si formation.

We have also investigated the effects of oxygen on the formation of the second phase NiSi by implanting oxygen initially into the Ni_2Si film. We found that NiSi grows with square root of time in both implanted and unimplanted samples. The slowing is uncorrelated with the amount of oxygen suggesting that a structural change due to ion implantation is the cause. During NiSi formation oxygen initially present in the Ni_2Si layer

is incorporated into the NiSi film without interfacial accumulation, however the oxygen is seen to move toward the surface. This motion is explained in terms of a simple model based on the chemical affinity of oxygen to Si and Ni and the fact that Ni is the diffusing species in NiSi growth. The shift in the peak of the oxygen distribution during NiSi formation enables the implanted oxygen to act as a diffusion marker, thus confirming Ni as the diffusing species in NiSi growth. The use of implanted oxygen as a diffusion marker in thin film studies is explored briefly.

REFERENCES

- [1] K. N. Tu, W. K. Chu, and J. W. Mayer, *Thin Solid Films*, 25, 403 (1975)
- [2] J. O. Olowolafe, M-A. Nicolet, and J. W. Mayer, *Thin Solid Films*, 38, 143 (1976)
- [3] C. Canali, F. Catellini, G. Ottaviani, and M. Prudenziati, *Appl. Phys. Lett.*, 33, 187 (1978)
- [4] D. J. Coe and E. H. Rhoderick, *J. Phys. D: Appl. Phys.*, 9, 965 (1976)
- [5] R. Pretorius, J. M. Harris and M-A. Nicolet, *Solid-State Elect.*, 21, 667 (1978)
- [6] W. K. Chu, S. S. Lau, J. W. Mayer, H. Muller, and K. N. Tu, *Thin Solid Films*, 25, 393 (1975)
- [7] R. Pretorius, C. L. Ramiller, S. S. Lau, and M-A. Nicolet, *Appl. Phys. Lett.*, 30, 501 (1977)
- [8] R. Pretorius *J. Electrochem Soc.*, 128, 107 (1981)
- [9] T. G. Finstad, J. W. Mayer, and M-A. Nicolet, *Thin Solid Films*, 51, 391 (1978)
- [10] T. G. Finstad, *Phys. Stat. Sol. (a)*, 63, 223 (1981)
- [11] J. F. Gibbons, W. S. Johnson, and S. W. Mylroie, *Projected Range Statistics*, Dowden, Hutchinson and Ross, Stroudsburg, Penna. (1975)
- [12] F. J. Grunthaler and J. M. Maserjian, *IEEE Trans. Nuc. Sci.*, NS-24, 2108 (1977)
- [13] W. K. Chu, J. W. Mayer, and M-A. Nicolet, *Backscattering Spectrometry*, Academic Press, N.Y. (1978)
- [14] H. C. Kim, R. F. Seiler, D. F. Herring, and K. W. Jonas, *Nuc. Phys.*, 57, 526 (1964)
- [15] F. J. Grunthaler, P. J. Grunthaler, R. P. Vasquez, B. F. Lewis, J. Maserjian, A. Madhukar, *J. Vac. Sci. Tech.*, 16, 1443 (1979)
- [16] J. M. Hill, D. G. Royce, C. S. Fadly, L. F. Wagner, and F. J. Grunthaler, *Chem. Phys. Lett.*, 44, 225 (1976)
- [17] D. R. Penn, *J. Electron Spectrosc. Relat. Phenom.*, 9, 29 (1976)
- [18] G. S. Hartley, *Trans. Faraday Soc.*, 42, 6 (1946)
- [19] H. Foll and P. S. Ho, *J. Appl. Phys.*, 52, 5510 (1981)
- [20] M. Maenpaa, private communication (1981)

CHAPTER IV

IMPLANTED OXYGEN IN Pt SILICIDE FORMATION

A. INTRODUCTION

Platinum silicide formation commands an important role in integrated circuit technology where it is used to form ohmic and Schottky contacts in silicon devices. For impurity-free Pt films deposited on Si and annealed in vacuum, a uniform layer of Pt_2Si first begins to grow at the Pt-Si interface [1],[2],[3]. The thickness of this layer increases with the square root of time indicating diffusion-limited growth. Marker experiments have shown that Pt is the diffusing species in Pt_2Si formation [4],[5]. The Pt_2Si layer will continue to form as long as there is a supply of unreacted Pt. When all of the Pt film is consumed, a layer of PtSi nucleates and grows, converting the Pt_2Si to PtSi [1],[3]. The simultaneous presence of Pt, Pt_2Si and PtSi is not observed. It is known, however, that this growth sequence can be greatly altered by the presence of impurities [1], [6]-[12]. Impurities introduced into the Pt film during deposition [7]-[9] or during annealing [6],[12] have been found to prevent a Pt metal layer from forming silicide. Thus Pt, Pt_2Si and PtSi can then be simultaneously present. It has also been observed that impurity oxygen and Al accumulate at the Pt- Pt_2Si interface during annealing [2],[6]-[10]. From these observations it has been postulated that impurities in the metal may stop the supply of Pt to the Pt_2Si -Si interface, thus allowing PtSi to nucleate and grow [1].

In our previous work on the effects of impurity oxygen on Ni silicide formation [13],[14],[15] (Chapter III), we modeled the effects of the impurity oxygen in terms of two parameters. The first is the initial location of the impurity relative to the moving species and the second is the chemical affinities of the oxygen relative to the Ni and Si.

In this chapter we apply this model to explain and clarify the effects of impurity oxygen on Pt silicide formation. We also present experimental results, using ion implantation, to control the initial position and amount of the oxygen.

B. EXPERIMENTAL PROCEDURES

Commercially prepared and polished Si <100> wafers (Wacker) were cleaned ultrasonically with TCE, acetone and methanol, and etched for 1 min. in 1:1 HF:H₂O immediately prior to loading into an oil-free e-beam evaporation system. Pt films of ~ 2000 Å were evaporated onto the silicon substrate at ~ 17 Å/sec with the vacuum kept $\leq 9 \times 10^{-7}$ torr during the evaporation. Half of the wafers were then implanted with either 1.0 or 2.0×10^{16} O/cm² at 180 keV per atom. According to range tables [16] this places the peak oxygen concentration (0.9 and 1.8 at. % respectively) at $R_p \sim 970$ Å into the Pt with $\Delta R_p \sim 670$ Å.

The wafers used in the kinetic study were diced and loaded into a quartz-tube vacuum-annealing furnace. Unimplanted and implanted samples were annealed simultaneously at 290°C with a background pressure of $\sim 5 \times 10^{-7}$ torr. The silicide composition and growth kinetics were studied with 2.0 MeV ⁴He⁺ backscattering [17]. The detector angle was 170° with the He₊ beam incident 5° from the sample normal. An identification of the phases by X-ray diffraction was not performed since the Pt/Si system has been extensively studied before [18]. Instead, the phases were identified from the composition ratios determined from the backscattering spectra. The oxygen distribution was measured by the ¹⁶O(d,α)¹⁴N nuclear reaction (Chapter II).

A detector angle of 164° and sample tilt angle of 55° with respect to the incident beam were used. The cross section reported by Kim et al was used to calculate the oxygen concentration [19].

After implantation, samples examined by XPS were cleaned by a 20-minute plasma oxidation at a pressure of ~ 50 m torr. This step is required to remove a carbon overlayer which we attribute to contamination by diffusion pump oil during the ion implantation step [20]. The Pt oxide that had formed during the oxidation was etched off in a dry box maintained under a N_2 atmosphere by spinning the sample at 3600 rpm and adding dropwise 500 $\mu\ell$ of 1:10 HF in ethanol followed by a 1000 $\mu\ell$ ethanol rinse. The sample inlet port of the spectrometer is connected directly to the N_2 dry box and, consequently, no further oxygen contamination occurred after etching. After loading into the XPS system [21], initial measurements of the Pt 4f, Si 2p and O 1s core levels were taken. The samples then were annealed in situ at a pressure of 2×10^{-9} torr until the Pt-Pt₂Si interface was within the depth range accessible to the analyzer (≤ 50 Å). Samples were initially heated to 325°C. This temperature turned out to be insufficient to bring the Pt-Pt₂Si within the depth range of the analyzer for the samples implanted with 2.0×10^{16} O/cm². For these samples additional annealing at 377°C was required. During annealing the sample was monitored using the O 1s core level for samples implanted with 1.0×10^{16} O/cm² and the Si 2p line for samples implanted with 2.0×10^{16} O/cm². Annealing was stopped after the intensity of the core line being monitored had reached a plateau. Following annealing the samples were cooled to 25°C to allow extended final measurements of the Pt 4f, Si 2p and O 1s core level binding energies. After XPS analysis, the sample composition and oxygen distributions were measured by BS and the $^{16}O(d,\alpha)^{14}N$ nuclear reaction.

C. EXPERIMENTAL RESULTS

Figure 1 illustrates the formation of Pt_2Si and PtSi for unimplanted samples and for samples implanted with $2.0 \times 10^{16} \text{ O/cm}^2$ half way through the Pt film. Initially Pt_2Si grows with square root of time indicating that the reaction process is transport-limited for both implanted and unimplanted samples. The growth rate agrees with published values [2]. In the unimplanted samples Pt_2Si continues to grow with square root of time until all of the unreacted Pt is consumed. Subsequently, after a slight delay, the second phase PtSi nucleates and begins to grow, also with square root of time. In the implanted samples, the Pt_2Si growth first slows and then finally halts after 80 minutes, at which time $\sim 1580 \text{ \AA}$ of Pt_2Si have formed. The PtSi phase then begins to form at the expense of the Pt_2Si .

Backscattering spectra show that the amount of unreacted Pt left on the surface is unchanged by subsequent annealing at 290°C for up to 300 minutes. The increase in PtSi and decrease in Pt_2Si shown in Fig. 1 also corresponds to a constant amount of Pt shared between the silicides. The the total amount of Pt in the Pt_2Si and PtSi remains constant during the transformation of Pt_2Si to PtSi . While the growth rate of the PtSi is slower than in the unimplanted case, the growth still remains proportional to the square root of the annealing time.

Fig. 2a shows the as-implanted oxygen profile obtained from the $^{16}\text{O}(\text{d},\alpha)^{14}\text{N}$ nuclear reaction technique. The intense peak at the sample surface is due to an oxidized layer which forms during sample handling. The low broad peak located in the Pt is due to the implanted oxygen. The peak of the oxygen distribution is located at $\sim 1100 \text{ \AA}$ (R_p) which is

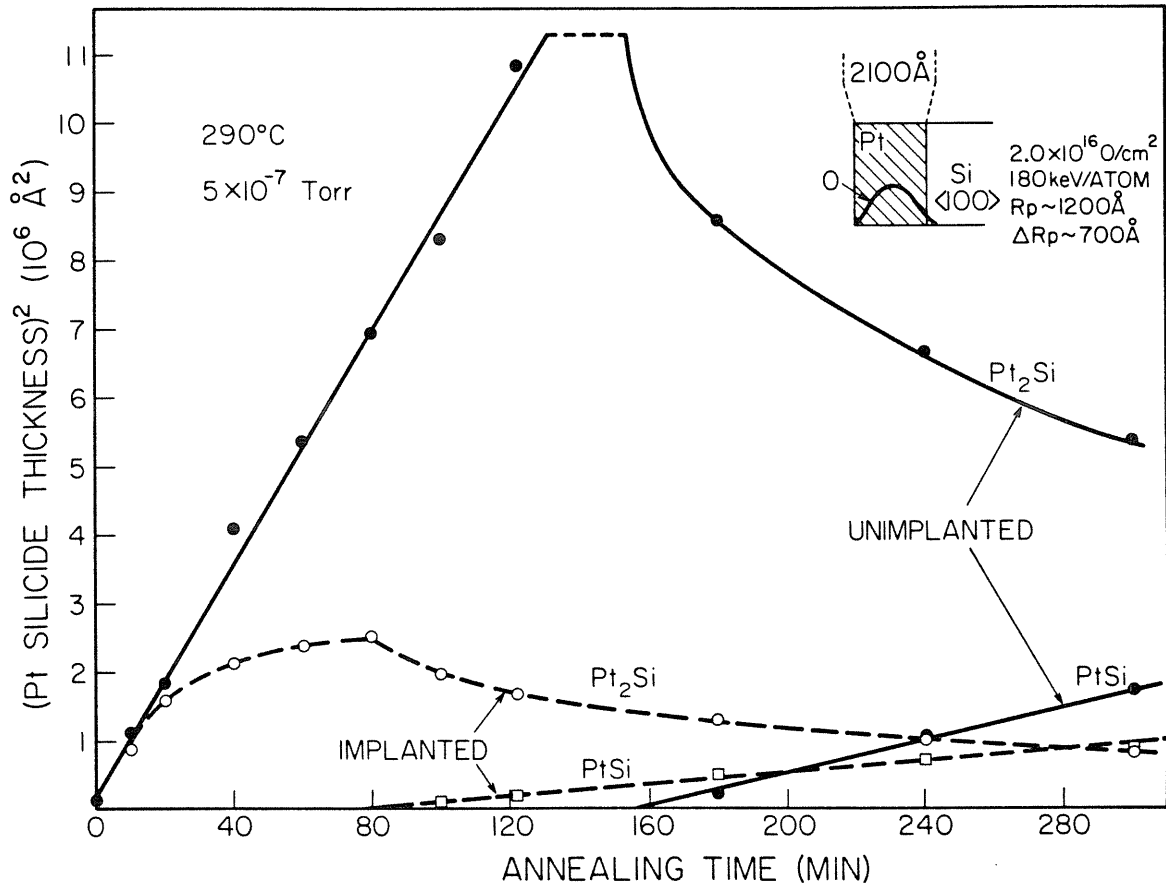


Fig. 1. Plot of Pt silicide thickness squared versus annealing time at 290°C for unimplanted samples and for samples implanted with 2.0×10^{16} O/cm². Barrier formation in the implanted sample halts Pt₂Si growth before all Pt is consumed. The total amount of Pt in Pt₂Si and PtSi is conserved in the implanted samples indicating that further diffusion of Pt into the silicide layers is completely blocked.

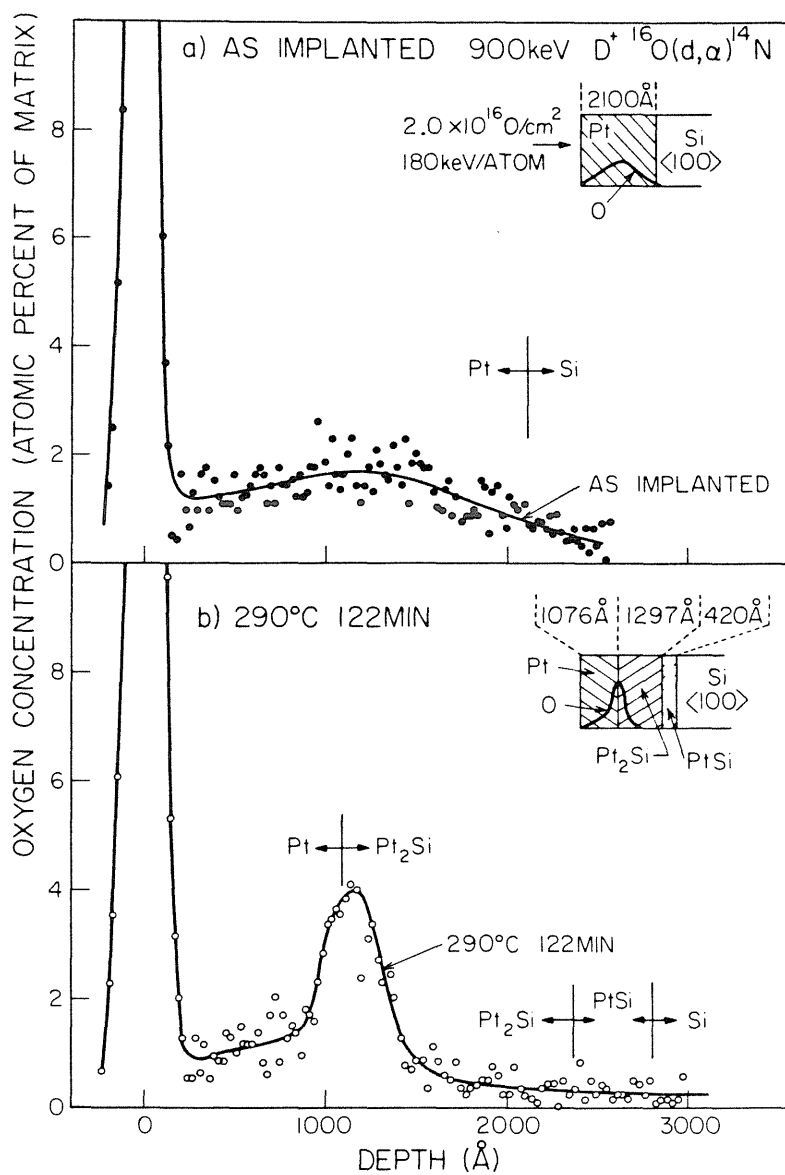


Fig. 2. Oxygen distributions obtained by the $^{16}\text{O}(d,\alpha)^{14}\text{N}$ nuclear reaction for: (a) the as-implanted sample, (b) after annealing at 290°C for 122 min. in vacuum. The dashed lines are interface positions independently determined from $^4\text{He}^+$ backscattering spectra. After annealing the oxygen distribution peaks at the Pt-Pt₂Si interface. The amount of oxygen beneath the surface remains constant after annealing, indicating that oxygen from the ambient does not reach the Pt-Pt₂Si interface.

slightly deeper than $R_p \sim 970$ calculated from the range tables [16]. However, $\Delta R_p \sim 700 \text{ \AA}$ is very close to the calculated value of 670 \AA . The total amount of oxygen in this peak (from 250 \AA to 2400 \AA) is calculated to be $2.0 \times 10^{16} \text{ O/cm}^2$, which agrees fortuitously well with that obtained by charge integration during ion implantation. The positions of the Pt/Si, Pt/Pt₂Si, Pt₂Si/PtSi, and PtSi/Si interfaces in Fig. 2 have been determined independently using $^4\text{He}^+$ backscattering. Fig. 2b shows the oxygen distribution after annealing the implanted sample for 122 minutes at 290°C . From Fig. 1 this corresponds to the point where the transport of the unreacted Pt remaining on the sample surface has been blocked. The growth of PtSi has begun at the Pt₂Si-Si interface. The oxygen distribution is seen to peak at the Pt-Pt₂Si interface. The total amount of oxygen beneath the surface (from 300 \AA to 1800 \AA) is again $2.0 \times 10^{16} \text{ O/cm}^2$, indicating that no additional oxygen from the ambient has been introduced during the annealing. The total amount of oxygen near the Pt-Pt₂Si interface (from 900 \AA to 1400 \AA) amounts to $1.2 \times 10^{16} \text{ O/cm}^2$.

Fig. 3 shows the oxygen distribution obtained using the $^{16}\text{O}(d,\alpha)^{14}\text{N}$ nuclear reaction for the XPS sample implanted with $2.0 \times 10^{16} \text{ O/cm}^2$ after annealing. The surface peak is again most likely due to surface oxidation during exposure to the atmosphere prior to $^{16}\text{O}(d,\alpha)^{14}\text{N}$ measurements. The low broad peak located from ~ 1000 to $\sim 2500 \text{ \AA}$ ($1.6 \times 10^{16} \text{ O/cm}^2$) is most likely due to further redistribution of the oxygen that was located at the Pt-Pt₂Si interface when Pt diffusion was first halted during Pt₂Si formation (325° annealing, cf. Fig. 2). The bulk of this oxygen has not been brought within the depth range accessible to the XPS system. A new feature is the peak located at the Pt₂Si-Si interface ($\sim 4000 \text{ \AA}$). The total amount of oxygen in this peak (~ 3000 to $\sim 5000 \text{ \AA}$) is $9.4 \times 10^{15} \text{ O/cm}^2$.

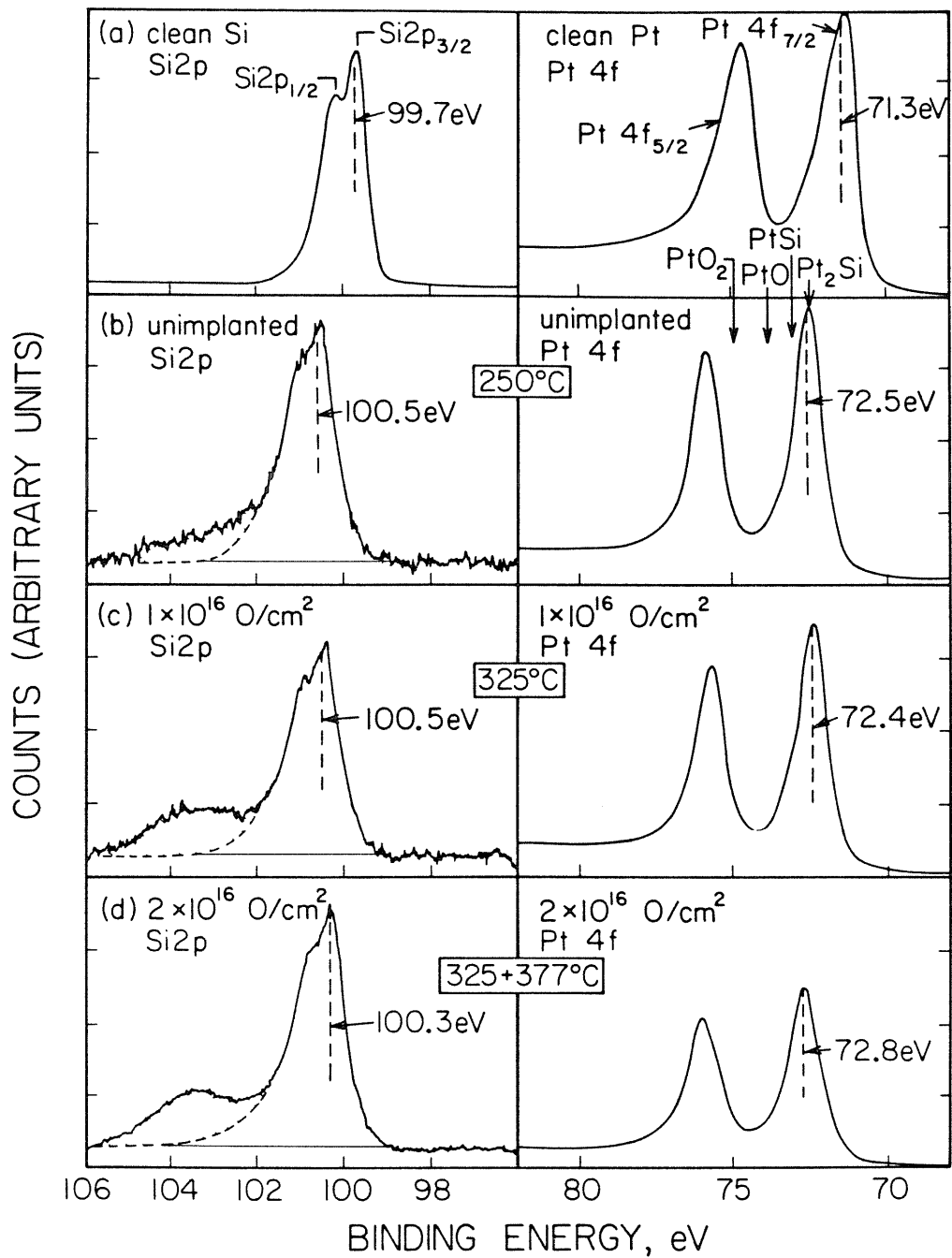


Fig. 3. The Si2p and Pt 4f spectra for (a) clean Si and Pt and after in situ annealing, (b) unimplanted samples, annealed at 250°C, (c) samples implanted with 1.0×10^{16} O/cm² annealed at 325°C (d) samples implanted with 2.0×10^{16} O/cm² annealed at 325°C and 377°C.

A detailed study of the Pt₂Si growth rate in the samples implanted with 1.0×10^{16} O/cm² was not done. However, a delay of the Pt-Pt₂Si interface in reaching the surface during in situ annealing for the XPS measurements was not observed. Thus barrier formation, which would have prevented the Pt-Pt₂Si interface from coming within ~ 50 Å of the surface, did not take place.

Fig 4. shows the Pt and Si core level spectra obtained after in situ annealing for an unimplanted sample and for samples implanted with 1.0 and 2.0×10^{16} O/cm². Clean Si substrate and Pt metal spectra are also shown for comparison (Fig. 4a). The Pt 4f_{7/2} core level is found at 71.3 eV for Pt metal.

This line is broadened and highly asymmetric due to electron-hole pair formation around the Fermi energy accompanying photoemission [22]. After annealing this core level has shifted upfield by 1.2 eV to 72.5 eV and the FWHM has decreased to 1.2 eV for both unimplanted samples (Fig. 4b) and samples implanted with 1.0×10^{16} O/cm² (Fig. 4c). This binding energy agrees with the value reported previously for Pt₂Si [23]. We have also found Pt₂Si formation in these samples using ⁴He backscattering. The final Pt 4f_{7/2} core level obtained from the sample implanted with 2.0×10^{16} O/cm² (Fig. 4d) falls at 72.8 eV which is half-way between the previously reported values [23] for Pt₂Si (72.5 eV) and PtSi (73.0 eV). This suggests that the sample surface consists of a distribution of both silicides.

The FWHM of this line has also increased slightly (0.1 eV) to 1.3 eV compared to the other samples. This slight broadening may also result from an inhomogeneous surface consisting of both silicides. The Pt 4f_{7/2}

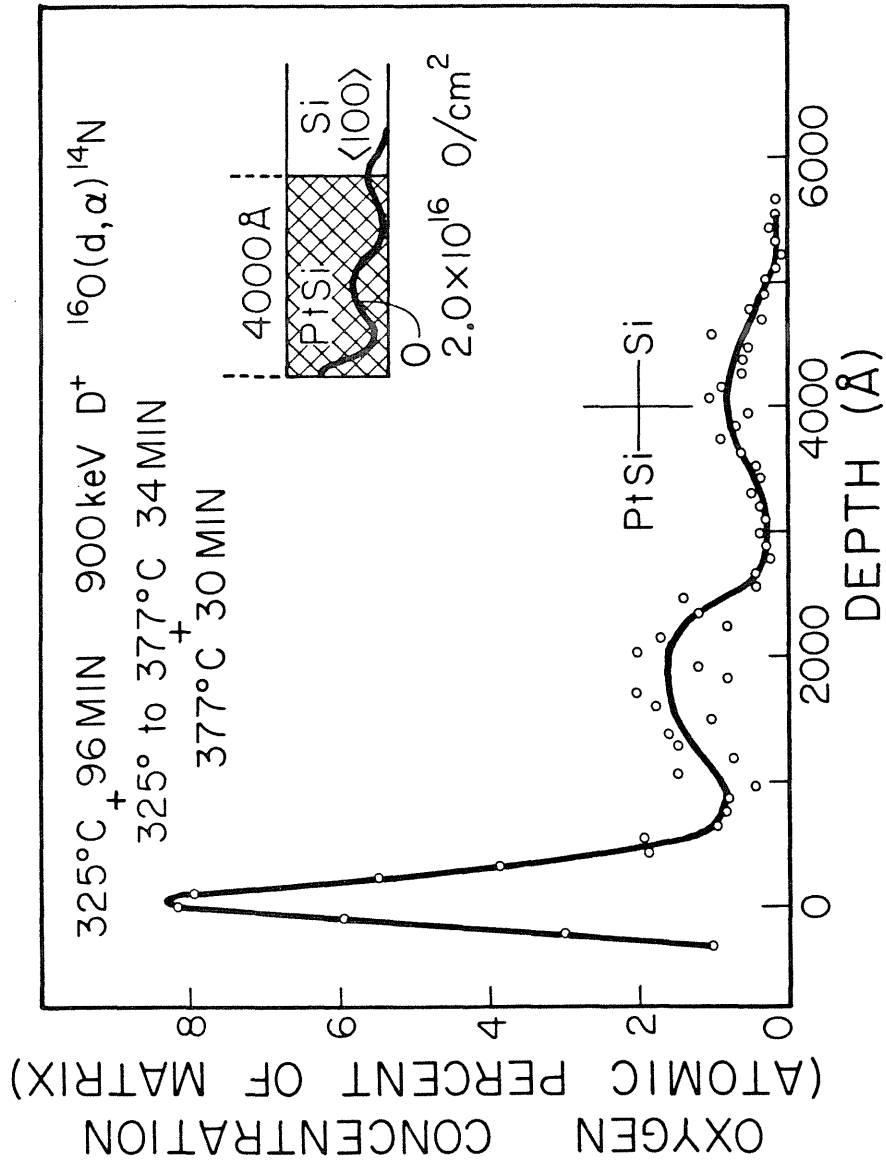


Fig. 4. Oxygen distribution obtained by the ¹⁶O(d,α)¹⁴N nuclear reaction for the XPS sample implanted with 2.0 × 10¹⁶ O/cm² after barrier breakdown. The oxygen initially forming the barrier has been dispersed into the sample (1000 Å to 2500 Å). The presence of oxygen at the PtSi-Si interface is also seen.

binding energies for the oxides PtO and PtO₂ are also indicated on this figure [24].

The corresponding Si 2p signals for the unimplanted and implanted samples are shown in the left-hand panels of Fig. 4. The doublet structure is due to the $2p_{3/2,1/2}$ spin-orbit coupling. The Si $2p_{3/2}$ binding energy is 100.5 eV for both Pt₂Si and PtSi [23]. Thus the position of the Si $2p_{3/2}$ line for unimplanted samples (Fig. 4b) and for samples implanted with 2.0×10^{16} O/cm² (Fig. 4c) does agree with the Pt₂Si previously assigned using the position of the Pt 4f core level along with the back-scattering.

In the samples implanted with 2.0×10^{16} O/cm² (Fig. 4d) the major peak is a result of contributions from both Pt₂Si and PtSi. Since the Si $2p_{3/2}$ binding energy is the same for both silicides the inhomogeneity of the surface composition as previously determined from the Pt 4f spectra does not lead to additional complexity in the Si 2p signal. Table 1 summarizes the binding energies and full widths observed for the unimplanted and implanted samples as well as Pt, Pt₂Si and PtSi samples for comparison. A broad low intensity distribution is observed to the left of the dominant Si 2p signal for each sample (shaded areas). This peak is due to intermediate oxidation states of Si. Evidently a residual amount of oxygen is present in the unimplanted samples. The intensity of this distribution relative to the Si 2p silicide signal increases with increasing oxygen dose (Table 1). The ratios of the integrated intensity of the oxygen 1s line (not shown in Fig. 3) to that of the shaded Si 2p oxide peak normalized using a thick thermal SiO₂ layer on Si are also summarized in Table 1.

D. DISCUSSION

The growth of Pt_2Si and PtSi in the unimplanted samples is that previously observed for impurity-free Pt films annealed in vacuum [2]. Pt_2Si grows with square root of time until all free Pt is consumed. This exhausts the supply of free Pt to the Pt_2Si interface and allows PtSi to nucleate and grow. After a slight delay that may represent a nucleation time, PtSi begins to grow, also with square root of time. The simultaneous presence of Pt, Pt_2Si and PtSi is not observed. For the samples implanted with oxygen, Pt_2Si growth ceases before all of the unreacted Pt is consumed. Evidently the presence of the implanted oxygen results in the formation of a barrier to further Pt diffusion. This diffusion barrier remains impenetrable during subsequent annealing so that the total amount of Pt in the Pt_2Si and PtSi remains constant during the transformation of Pt_2Si to PtSi . Fig. 2 shows that it is the build-up of oxygen at the Pt- Pt_2Si interface that prevents further Pt diffusion. The accumulation of oxygen at this interface and the subsequent formation of a reaction barrier have been reported previously by other workers [7],[10].

In the XPS sample implanted with 1.0×10^{16} O/cm² barrier formation did not take place. Thus the threshold dose necessary for the barrier is between 1 and 2×10^{16} O/cm². An improved estimate of the amount of oxygen required may be found from the amount of oxygen near to the Pt- Pt_2Si interface once the diffusion of Pt has halted. From Fig. 2, this dose is 1.2×10^{16} O/cm². This is much higher than the value of 2 to 4×10^{15} O/cm² reported recently by Nava et al [10]. The study by Nava et al differs from ours in two major ways: first, their Pt films are sputtered unlike ours that were evaporated Pt films. It is well known that

sputtering may incorporate large amounts of the sputtering gas or other impurities into the metal film during deposition. Thus the rather low value quoted by Nava et al may represent only the additional amount of impurity oxygen necessary for barrier formation, above the amount of impurities already present. Second, Nava et al uses AES for impurity profiling; but an AES signal is difficult to quantify, especially when the host matrix is also changing. Thus we believe that $\sim 1.2 \times 10^{16}$ O/cm² represents the threshold oxygen dose necessary for barrier formation. This value is also close to that observed for Ni (see Chapter III).

The chemical nature of this reaction barrier has been reported to be SiO₂ as well as PtSiO₄ [26]. The possibility of participation of either Pt silicates or Pt oxides in the barrier can be eliminated by examination of the Pt 4f spectra in Fig. 4. The Pt 4f binding energies for PtO (73.8 eV and PtO₂ (74.8 eV) are well distinguishable from the energies observed for Pt₂Si and PtSi [23],[24]. No indication of the presence of these oxides can be found in the Pt 4f spectra. If the Pt 4f signal from PtSiO₄ or some other Pt oxide were only slightly shifted from the Pt silicide peaks, then the presence of these species should be manifested as an increase in the full width at half maximum (FWHM) of the Pt 4f core line as the oxygen implant dosage increases; this is not the case (see Table 1). The Pt 4f_{7/2} binding energy for the sample, however, falls midway between the energy observed for bulk Pt₂Si and PtSi, which suggests that the slight broadening of the FWHM by ~ 0.1 eV is the result of an inhomogeneous surface consisting of both silicides. The formation of PtSiO₄ or other Pt suboxides can thus be ruled out by the lack of any dependence of the FWHM of the Pt 4f_{7/2} signal upon the oxygen implant

dosage. The Si 2p spectrum in Fig. 4 immediately suggests that the formation of Si oxides is of major importance in the reaction barrier.

The absolute binding energy of the Si 2p oxide peak cannot be used to establish the precise stoichiometry of the Si oxide for two reasons. First, the contribution of final state relaxation energy to the chemical shift is different for a Si oxide--say, SiO_2 --in a metallic matrix as compared to bulk SiO_2 (an insulating matrix). A thin layer of stoichiometric SiO_2 sandwiched within a metallic silicide/metal structure would be expected to fall at a lower binding energy than bulk SiO_2 . Secondly, the flexibility of the Si-O-Si bond angle results in a measurable structure-induced charge transfer [26]. The Si 2p binding energy of SiO_2 in α -quartz, where the bond angle is 144° , is expected to be greater than the binding energy of a strained oxide where the bond angle distribution is less than 144° . Since any Si oxide formed in the silicide reaction barrier is likely to be in a strained environment, it is impossible to ignore and difficult to estimate the magnitude of any strain-induced charge transfer.

To estimate stoichiometry of the Si oxides observed in Fig. 4b-d we have therefore used the ratio of the intensities of the O 1s line (not shown in Fig. 4) to the shaded Si oxide signal normalized using a thick thermal SiO_2 layer on Si (Table 1). The use of such a standard assumes that samples with similar electron escape depth are compared. Since the SiO_x layer is of finite thickness while the SiO_2 standard is effectively infinitely thick, we also need to assume that the escape depth of an electron from the Si 2p level is approximately the same as that for the O 1s level. This approximation that the escape depth is independent of

the electron kinetic energy for these two core levels results in $\sim 10\%$ error in the stoichiometry of the Si oxides. The O/Si ratio for the unimplanted sample was found to be 0.9, indicating that nominally SiO is present. Both implanted samples yield an oxygen-to-silicon ratio of 1.5, corresponding to Si_2O_3 . Since XPS examines a relatively large area of the sample which is most likely nonuniform laterally as well as in depth, these stoichiometries should be considered as an average of the oxide layer present. The large full width of the Si oxide peak suggests that, in fact, a distribution of suboxides is present.

The presence of only Si suboxide is not surprising for unimplanted samples since the total amount of oxygen initially present in the Pt film is most likely too small to form even one monolayer of SiO_2 (1.6×10^{15} O/cm²). The samples implanted with 1.0×10^{16} O/cm² contain much more oxygen than the unimplanted samples yet still less than the threshold dose necessary to form a barrier. The effect of this additional oxygen is to form additional oxides of Si at the Pt-Pt₂Si interface. Thus this buildup of Si suboxides is the precursor to the actual barrier formation.

The presence of enough oxygen to form a barrier will undoubtedly enable the Si to take on a full coordination of oxygen and thus form SiO_2 . Such a dose dependence of Si oxide formation has been shown directly in the Ni-Si system (Chapter III). In addition, it is known from Auger studies of the formation of PtSi in an O₂ ambient that oxygen forms SiO_2 with Si even in the presence of a thin layer of unreacted Pt [6]. Thus we propose that the final chemical form of the oxygen is SiO_2 .

The two major parameters previously identified in our study of impurity oxygen in the Ni-Si system (Chapter III) are the initial location of the impurity oxygen relative to the moving species and the relative chemical affinities of the oxygen to the reacting species. To apply these parameters to the present case we note that marker experiments have shown that Pt is the moving species during Pt₂Si formation [4],[5]. Thus oxygen initially present in the Pt film is located in the moving species. It is also known that oxygen forms weak bonds with Pt ($\Delta H_f^\circ(\text{PtO}, \text{Pt}_3\text{O}_4, \text{PtO}_2) = -17.0, -16.8, -32.1 \text{ kcal/mol}$) as compared to Si ($\Delta H_f^\circ(\text{SiO}_2) = -205.5 \text{ kcal/mol}$) [27]. By taking into account these asymmetries in initial location and in chemical affinities, the effect of the implanted oxygen can be modeled as shown in Fig. 5.

The implanted oxygen is initially distributed in the Pt with an approximately Gaussian profile. Presumably the implanted oxygen binds with the Pt to form complexes that are immobile in Pt during annealing. As Pt diffuses into the Pt₂Si, these complexes meet with the advancing Pt-Pt₂Si interface. Because of their weak binding to oxygen these Pt complexes are reduced by Si to form Si oxides and free Pt metal. This model predicts that the Si present at the Pt-Pt₂Si interface will be oxidized a step at a time as it encounters oxygen atoms in the Pt. This is verified by the presence of Si suboxides in the XPS data. As oxygen-bearing Pt diffuses into the Pt₂Si, Si takes on its full coordination of oxygen, forming SiO₂. When sufficient SiO₂ has accumulated at the Pt-Pt₂Si interface, Pt can no longer diffuse to the Pt₂Si-Si interface to maintain the formation of Pt₂Si. The results show that the threshold oxygen dose necessary for barrier formation is about $1.2 \times 10^{16} \text{ O/cm}^2$. The cessation of the Pt

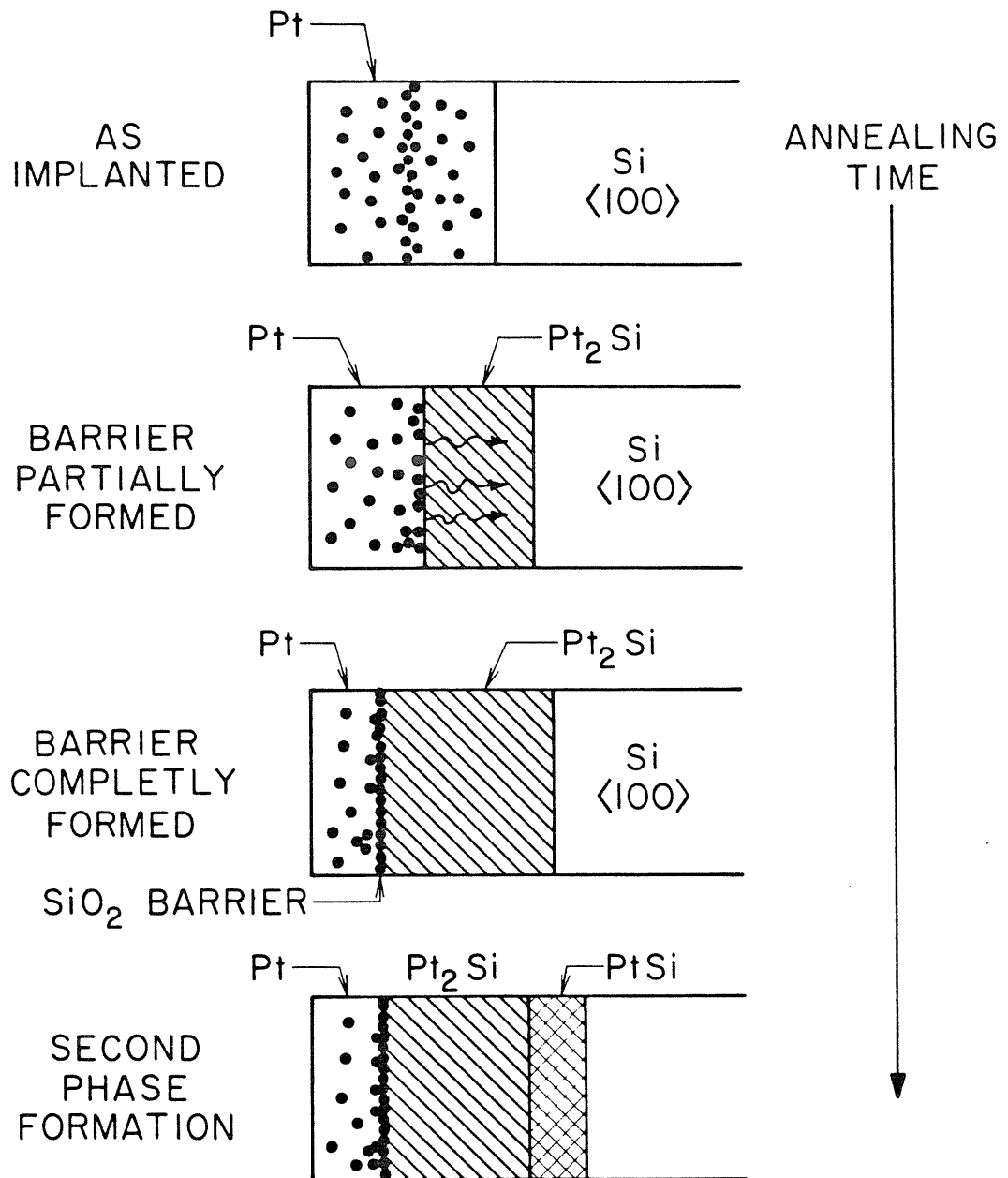


Fig. 5 Model of SiO_2 barrier formation. The black dots represent oxygen atoms. Upon annealing, Pt diffuses into the silicide, (curved arrows), exposing the oxygen to Si at the $\text{Pt-Pt}_2\text{Si}$ interface. Oxygen reacts with the Si and forms SiO_2 . When all Pt diffusion paths are blocked, the second phase PtSi begins to form.

supply then allows the next phase PtSi to nucleate and grow, converting the Pt₂Si to PtSi.

The growth rate of PtSi is slower in the implanted samples than in the unimplanted samples. However, the implanted oxygen is rejected from the silicide so that the Pt₂Si film contains little oxygen. This slower growth of the second phase has also been observed for ion implanted Ni films on Si substrates (Chapter III). In that case it was concluded that structural changes due to ion implantation rather than impurity effects were responsible. A similar situation may also exist in the present case.

The 2×10^{16} O/cm² XPS sample shows the effects of barrier breakdown at high temperatures. An examination of the sample surface with optical microscopy shows the sample to be laterally nonuniform. This is also confirmed by backscattering measurements. XPS measurements show that the Pt 4f signal falls at an energy intermediate between PtSi and Pt₂Si (Fig. 4d); both phases are present on the surface. Evidently very nonuniform silicide growth takes place after barrier breakdown. The final oxygen distribution (Fig. 3) shows that the oxygen initially forming the barrier has not been brought to the sample surface. Instead, this oxygen remains buried and has been dispersed over a wide range of depths. This is also consistent with nonuniform silicide growth. Thus the observation of Si suboxides (Fig. 4d) is most likely due to Si bonding with oxygen in the Pt that did not take part in barrier formation along with fragments of the barrier exposed to the surface due to the nonuniformity of the final silicide growth.

The origin of the oxygen at the PtSi-Si interface (Fig. 3) is not known. We speculate that since the implanted oxygen is nearly all

accounted for by the distribution from 1000 to 2700 Å, the additional oxygen at the PtSi-Si interface comes from exposure to air. This would indicate that the final silicide after barrier failure is no longer a continuous layer. Further studies using additional techniques, in particular using ^{18}O to differentiate between implanted and atmospheric oxygen, are required to settle this question.

E. CONCLUSION

We have investigated the effects of oxygen on Pt₂Si formation from a thin Pt film on a Si substrate by implanting oxygen into the Pt film. We found that oxygen accumulates at the Pt-Pt₂Si interface during annealing and for oxygen doses above the threshold dose of about 1.2×10^{16} O/cm², forms a barrier to the Pt diffusion. It is the formation of SiO₂ at the Pt-Pt₂Si interface that prevents Pt from entering the Pt₂Si. Once the Pt supply is cut off, the second phase PtSi nucleates and grows. These results can be understood using two asymmetries present, one being in the chemical affinities of oxygen relative to the reacting species and the other in the initial location of the oxygen relative to the moving species.

TABLE I

Sample	Pt 4f _{7/2} Binding Energy(ev)	Pt 4f _{7/2} FWHM(ev)	Si 2p _{3/2} Binding energy(ev)	Relative Si 2p oxide intensity	O:Si ratio	H _f ^o (b) (kcal/ mol)
unimplanted	72.5 (a)	1.2 (a)	100.5 (a)	0.16 (a)	0.9 (a)	-
1x10 ¹⁶ Ocm ²	72.4 (a)	1.2 (a)	100.5 (a)	0.28 (a)	1.5 (a)	-
2x10 ¹⁶ O/cm ²	72.8 (a)	1.3 (a)	100.3 (a)	0.34 (a)	1.48 (a)	-
Si	-	-	99.7 (a)	-	-	0
Pt	71.3 (a)	1.5 (a)	-	-	-	0
Pt ₂ Si	72.5 (c)	1.2 (c)	100.5 (c)	-	-	-20.7
PtSi	73.0 (c)	1.1 (c)	100.5 (c)	-	-	-15.8
PtO	73.8 (d)	-	-	-	-	-17.0
PtO ₂	74.8 (d)	-	-	-	-	-32.1
SiO ₂	-	-	102.8 (a)	0.46 (a)	2 (a)	-205.5

(a) This work;

(b) R. Pretorius, J.M. Harris and M-A. Nicolet, *Solid-State Elect.* 21, 667, (1978);

(c) P.J. Grunthaner and F. J. Grunthaner and A. Madhukar, *J. Vac Si. Tech.*, to appear

(d) K. S. Kim, N. Winograd and R. E. Davis, *J. Am. Chem. Soc.* 93, 6296, (1971)

REFERENCES

- [1] C. Canali, F. Catellani, G. Ottaviani, and M. Prudenziati, *Appl. Phys. Lett.*, 33, 187 (1978)
- [2] C. Canali, C. Catellani, M. Prudenziati, W. H. Waldin, and C. A. Evans Jr., *Appl. Phys. Lett.*, 31 43 (1977)
- [3] G. Ottaviani, *J. Vac. Sci. Tech.*, 16 1112 (1979)
- [4] R. Pretorius, *J. Electrochem Soc.*, 128 107 (1981)
- [5] R. Pretorius, A. P. Botho and J. C. Lombaard, *Thin Solid Films*, 79 61 (1981)
- [6] R. J. Blattner, C. A. Evans, Jr., S. S. Lau, J. W. Mayer and B. M. Ullrich, *J. Electrochem Soc.*, 122 1732 (1975)
- [7] J. B. Bindell, J. W. Colby, D. R. Wonsidler, J. M. Poate, D. K. Conley and T. C. Tisone, *Thin Solid Films*, 37 441 (1976)
- [8] C. A. Crider, J. M. Poate and J. E. Rowe, in *Proceedings of the Symposium on Thin Film Interfaces and Interactions*, edited by J. E. F. Baglin and J. M. Poate, The Electrochemical Soc., Princeton, N.J., Vol. 80-2, p. 135, (1980)
- [9] C. A. Crider, J. M. Poate, *Appl. Phys. Lett.*, 36 417 (1980)
- [10] F. Nava, S. Valeri, G. Majni, A. Cembali, G. Pignatelli, and G. Queirolo, *J. Appl. Phys.* 52 6641 (1981)
- [11] P. Joubert, P. Auvroy and L. Henry, *Thin Solid Films* 79 235 (1981)
- [12] M. Severi, E. Gabilli, S. Guerri, and G. Celloti, *J. Appl. Phys.* 48 1998 (1977)
- [13] D. M. Scott, P. J. Grunthaner, B. Y. Tsaur, M-A. Nicolet and J. W. Mayer, in *Proceedings of the Symposium on Thin Film Interfaces and Interactions*, J.E.E. Baglin and J. M. Poate, eds., The Electrochem. Soc., Princeton, NJ, Vol. 80-2, p. 148, (1980)
- [14] D. M. Scott and M-A. Nicolet, *Nuc. Inst. Meth.* 182/183 655 (1981)
- [15] D. M. Scott and M-A. Nicolet, *Physica Status Solidi(a)* 66 773 (1981)
- [16] J. F. Gibbons, W. J. Johnson and S. W. Mylroie, *Projected Range Statistics* Dowden, Hutchinson and Ross, Stroudsburg, PA (1975)
- [17] W. K. Chu, J. W. Mayer, and M-A. Nicolet, *Backscattering Spectrometry*, Academic Press, NY (1978)
- [18] K. N. Tu and J. W. Mayer in *Thin Films - Interdiffusion and Reactions*, J. M. Poate, K. N. Tu and J. W. Mayer eds., John Wiley, NY (1978)

- [19] H. C. Kim, R. F. Seiler, D. F. Herring and K. W. Jones, *Nuc. Phys.*, 57 526 (1964)
- [20] P. J. Grunthaner, F. J. Grunthaner, D. M. Scott, M-A. Nicolet and J. W. Mayer, *J. Vac. Sci. Tech.*, In Press
- [21] F. J. Grunthaner, P. J. Grunthaner, R. R. Vasquez, B. S. Lewis, J. Macerjian and A. Madhukar, *J. Vac. Sci. Tech.* 16 1443 (1979)
- [22] G. K. Wertheim and P. H. Citrin, in *Photoemission in Solids I*, eds., M. Cardona and L. Ley, Springer-Verlag 197 (1978)
- [23] P. J. Grunthaner, F. J. Grunthaner and A. Madhukar, *J. Vac. Sci. Tech.*, to appear
- [24] K. S. Kim, N. Winograd and R. E. Davis, *J. Am. Chem. Soc.* 93 6296 (1971)
- [25] S. Danyluk and G. E. McGuire, *J. Appl. Phys.* 45, 5141 (1974)
- [26] F. J. Grunthaner, P. J. Grunthaner, R. P. Vasquez, B. E. Lewis, J. Maserjian and A. Madhukar, *Phys. Rev. Lett.* 43, 1683 (1979)
- [27] R. Pretorius, J. M. Harris and M-A Nicolet, *Solid-State Elect.* 21, 667 (1978)

CHAPTER V

OXYGEN IN Pd₂Si FORMATION

A. INTRODUCTION

The silicide of the near-noble metal Pd, in addition to Ni and Pt silicides, is extensively used to form contacts to semiconductor devices. This silicide contact is also formed by a solid-phase reaction between the metal and the Si. Small amounts of impurities either initially present or incorporated during annealing can dominate the reactions of Ni and Pt with Si ([1]-[6], Chapters III,IV), however Pd silicide formation has much less sensitivity than Pt or Ni silicide formation to impurities [5],[7],[8]. A thin oxide layer formed by boiling the Si wafer in H₂O, HNO₃ or H₂O₂ will not prevent Pd silicide formation [5],[7],[8]. An understanding of the relative immunity of Pd silicide formation to the presence of impurities is important to a general understanding of impurity effects in metal silicide reactions. In this chapter we study the effects of implanted oxygen on the growth of Pd silicide.

In previous work we have shown that the effects of implanted oxygen on both Ni and Pt silicide formation can be explained in terms of a model using only two parameters ([1],[9], Chapters III and IV). The first parameter is the relative chemical affinities of the oxygen to the reacting species. The second parameter is the location of the impurity relative to the moving species. While marker experiments have shown that Ni and Pt are the dominant diffusing species during their silicide formation [10],[11], both Si and Pd move during Pd silicide formation [11],[12],[13]. The chemical affinity of oxygen to Si ($\Delta H_f^\circ(\text{SiO}_2) = -205.5$

kcal/mole) is much greater than for either Ni, Pt or Pd ($\Delta H_f^\circ(\text{NiO}) = -58.4$ kcal/mole, $\Delta H_f^\circ(\text{PtO}) = -17.0$ kcal/mole, and $\Delta H_f^\circ(\text{PdO}) = -21.0$ kcal/mole) [14]. When the impurity oxygen is initially located in the Ni or Pt, the metal diffusion will expose the oxygen to Si at the metal-silicide interface.

Due to the large chemical affinity of oxygen and silicon, the oxygen will react with the Si to form SiO_2 . As the metal-silicide interface moves through the Ni or Pt film, this SiO_2 builds up until a barrier to further metal diffusion is formed. For the case of oxygen initially located in a Pd film on a Si substrate, the model suggests that while Pd diffusion may still expose the oxygen to Si at the Pd- Pd_2Si interface and lead to a build-up of oxygen there, the simultaneous diffusion of Si through the Pd_2Si will lead to the incorporation of the oxygen into the silicide without the build-up of oxygen at the interface and the formation of a barrier. In this chapter we verify this prediction and extend our model to include Pd_2Si formation.

B. EXPERIMENTAL

Commercially prepared and polished Si <100> wafers were cleaned ultrasonically with TCE, acetone and methanol and rinsed in doubly distilled H₂O. The wafers were then given a 1 min. etch in a 1:1 HF:H₂O solution just prior to loading into our oil-free E-beam evaporation system. Palladium films ~ 2000 Å thick were then deposited at a rate of ~ 20 Å/sec with the background pressure kept below 8×10^{-7} torr during the evaporation. Half of the wafers were then implanted with 2.0×10^{16} O/cm² at 130 keV/atom. According to range tables [15], this corresponds to a $R_p \sim 1010$ Å and a $\Delta R_p \sim 570$ Å, with the peak of the oxygen distribution ~ 2.0 at. %. The samples were then diced and loaded into a quartz tube vacuum annealing furnace. Implanted and unimplanted samples were annealed simultaneously at 250°C with the vacuum kept ~ 5×10^{-7} torr.

The silicide composition and growth kinetics were studied by 2.0 MeV ⁴He⁺ backscattering spectrometry. The detector angle was 170° with the He⁺ beam along the sample normal. The oxygen distribution was measured by the ¹⁶O(d,α)¹⁴N nuclear reaction technique [Chapter II]. The detector angle was 164° with the O⁺ beam incident at 55° to the sample normal. The cross-section used was that measured by Kim et al [16].

C. EXPERIMENTAL RESULTS

Figure 1 shows a plot of Pd₂Si thickness squared versus annealing time for an annealing temperature of 250°C. In both unimplanted samples and samples implanted with 2.0×10^{16} O/cm², Pd₂Si grows proportionally to the square root of annealing time. The growth rate is the same in both the implanted and unimplanted cases and agrees with published data [8]. The nonzero intercept at zero annealing time indicates an initial amount of Pd₂Si present before annealing. Figure 2a shows the oxygen distribution obtained by the $^{16}\text{O}(d,\alpha)^{14}\text{N}$ nuclear reaction for the as-implanted sample. The implanted oxygen is seen to have an approximately Gaussian distribution with a range $R_p \sim 1250$ Å and width $\Delta R_p \sim 600$ Å. These values are near the ones estimated from range tables [15] (~ 1010 Å and ~ 570 Å). The peak oxygen concentration is ~ 1.75 at. % as compared to the estimated 2.0 at. %. The total amount of oxygen beneath the surface (from 200 Å to 2500 Å) is 1.7×10^{16} O/cm² as compared to 2.0×10^{16} obtained by charge integration during implantation. Figure 2b shows the oxygen distribution for a sample annealed at 250°C for 100 min. The relatively sharp peak located at ~ 2500 Å in the Pd₂Si was not present in the unimplanted samples and is due to the redistribution of the implanted oxygen. The total amount of oxygen in this peak is 1.9×10^{16} O/cm² which agrees well with that in the as-implanted sample. The large surface peak is due to the incorporation of $\sim 7.1 \times 10^{16}$ O/cm² over three times the implanted dose, during annealing. This oxygen extends over 1000 Å into the Pd₂Si, but apparently has no effect on the growth kinetics of Pd₂Si. The surface of both implanted and unimplanted samples appeared a dark brown due to this accumulation of oxygen.

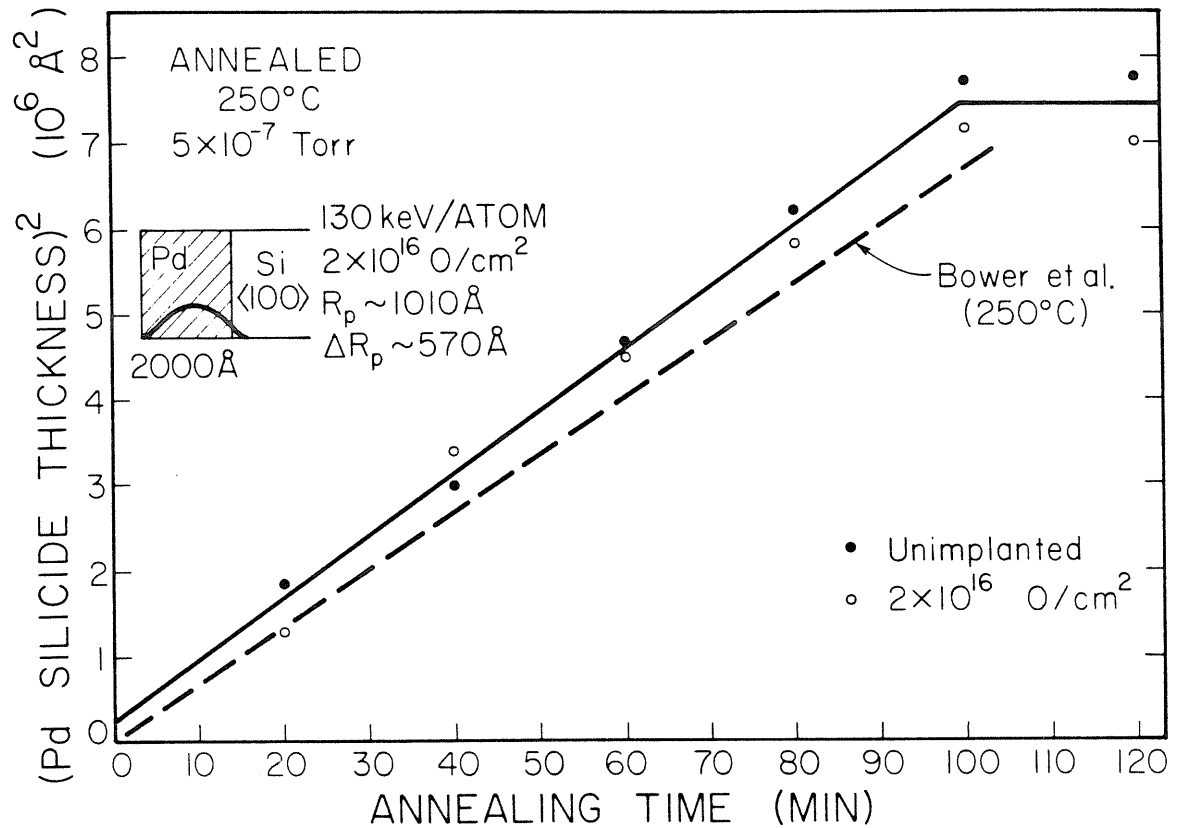


Fig. 1 Plot of Pd₂Si thickness squared versus annealing time at 250°C for unimplanted samples and samples implanted with 2.0×10^{16} O/cm² half-way through the Pd film. Identical behavior is seen in both cases. The dashed line is extrapolated from Bower et al [8] and agrees well with our measurement.

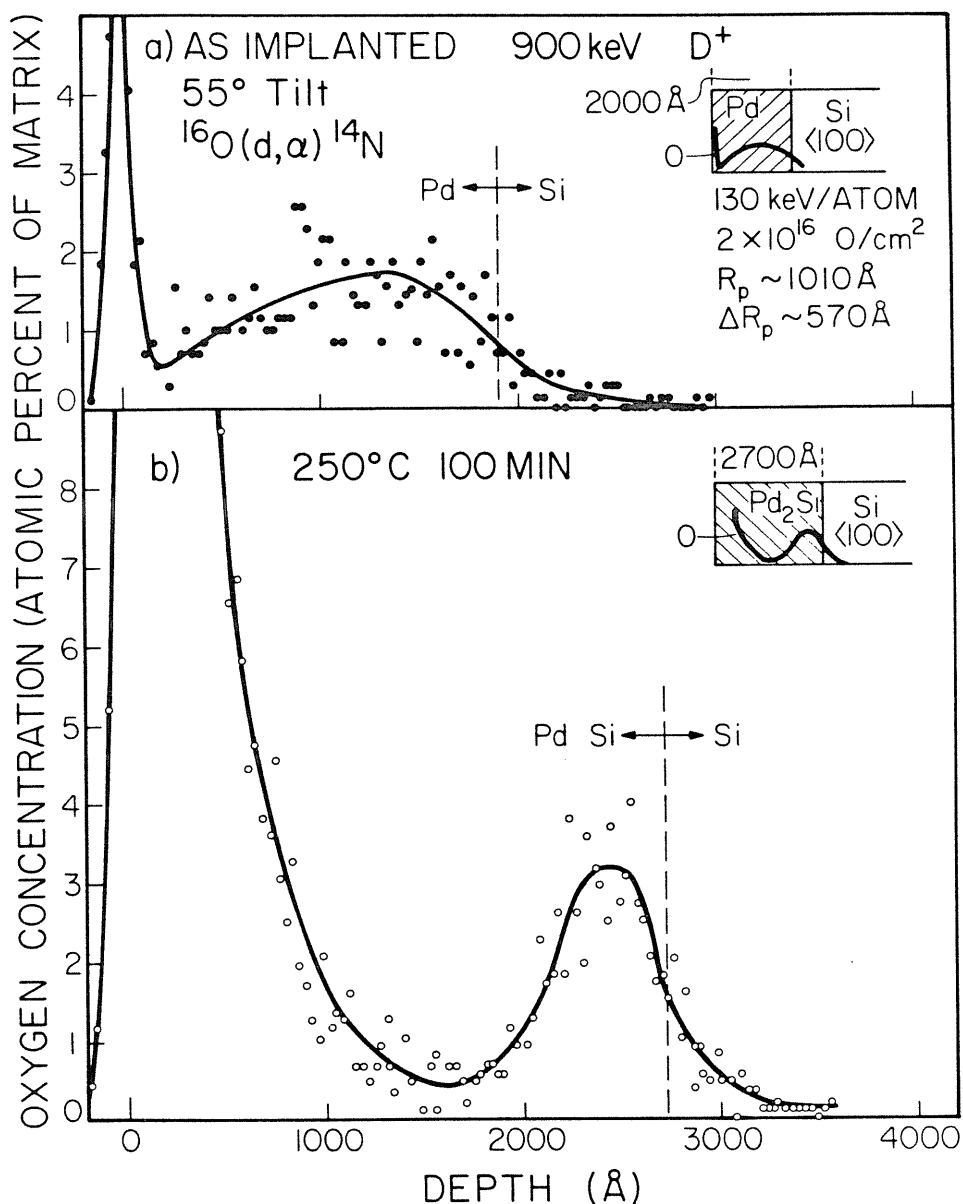


Fig. 2 Oxygen distribution obtained by the $^{16}O(d, \alpha)^{14}N$ nuclear reaction for a sample: (a) as-implanted, and (b) after annealing at 250°C for 100 min. The dashed lines are interfacial positions determined independently by $^4He^+$ backscattering spectrometry. After annealing, the oxygen has accumulated near, but not at the Pd_2Si -Si interface.

D. DISCUSSION

In the cases of Ni and Pt silicide formation, 1.2×10^{16} O/cm² present in the metal film is sufficient to halt formation of the metal rich phases Ni₂Si, Pt₂Si before all of the unreacted metal has been consumed, (Chapters III and IV). In the present case 2.0×10^{16} O/cm² initially present in the Pd film has no effect on the growth rate of Pd₂Si. Even the incorporation of 7.1×10^{16} O/cm², extending over 1000 Å into the silicide, is insufficient to alter the reaction kinetics. Thus Pd₂Si formation is indeed highly insensitive to oxygen initially present in the Pd film or picked up during annealing. Marker experiments have shown that both Pd and Si move during Pd₂Si formation [11]-[13]. Evidently the presence of amounts of oxygen as substantial as 9×10^{16} O/cm², equivalent to ~ 190 Å of SiO₂ if present as a layer, does not lead to the formation of a diffusion barrier to either species during annealing.

The redistribution of the implanted oxygen after annealing is also different from that observed during Ni and Pt silicide formation (Chapters III & IV). In the present case an interfacial accumulation does not take place. Instead, the oxygen moves deeper into the sample, near but not at the Pd₂Si-Si interface, and accumulates into a distribution of narrowed depth. Thus the implanted oxygen does not remain stationary with respect to the Pd distribution during annealing. Interfacial drag or segregation is not responsible for this since the movement of the Pd-Pd₂Si interface is opposite to that of the oxygen displacement and the Pd₂Si-Si interface motion is away from the implanted oxygen. Thus the implanted oxygen is mobile relative to the Pd distribution at the annealing temperature

(250°C). Implanted oxygen is not mobile relative to a Ni or Pt film during annealing at even higher temperatures (~ 300°C) (Chapters III & IV) without interfacial effects.

The oxygen not only moves deeper into the sample during annealing, it also accumulates in a relatively narrow region. Diffusion alone can only broaden the initial distribution. Evidently the oxygen accumulates at a sink. The nature of this sink can be inferred from the chemical affinities of the oxygen relative to the reacting species. The chemical affinity of oxygen to Si ($\Delta H_f^\circ(\text{SiO}_2) = -205.5 \text{ kcal/mol}$) much exceeds that between oxygen and Pd ($\Delta H_f^\circ(\text{PdO}) = 21.0 \text{ kcal/mol}$) or between Pd and Si ($\Delta H_f^\circ(\text{Pd}_2\text{Si}) = -20.7 \text{ kcal/mol}$) [14]. Thus as previously shown for the cases of Pt and Ni, (Chapters III & IV) oxygen present at the Pd-Pd₂Si interface will oxidize the Pd₂Si to form free Pd and Si oxides. Since Si oxides are not mobile relative to either Pd or Pd₂Si further motion of the oxygen will not take place. Thus we conclude that the sink must be the Si present at the Pd-Pd₂Si interface.

Our results can be modeled as shown in Fig. 3. The implanted oxygen is initially distributed in the Pd in an approximately Gaussian shape. In the early stages of the annealing, Pd₂Si begins to form. Oxygen is mobile in Pd at the annealing temperature and begins to diffuse throughout the Pd. As this oxygen comes in contact with the Si at the Pd-Pd₂Si interface, the oxygen will react with the Si there to form SiO₂ due to the large chemical affinity between oxygen and Si. The Si at the Pd-Pd₂Si interface acts as a sink for the implanted oxygen. However SiO₂ is not mobile relative to either element or the silicide. Thus, as SiO₂ forms by the diffusion of oxygen to the Pd-Pd₂Si interface, it is incorporated into

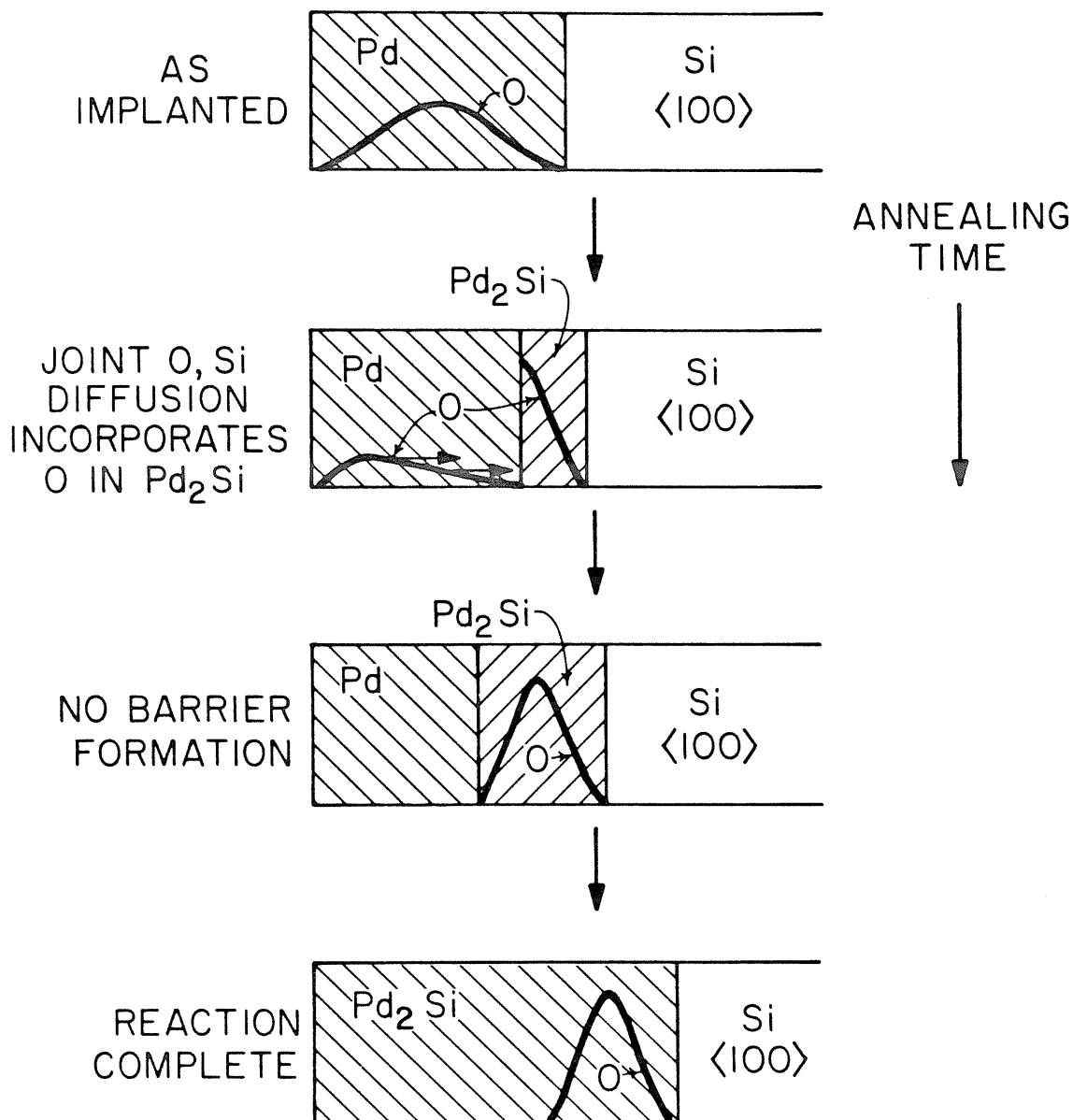


Fig. 3 Model of oxygen in Pd₂Si growth. The initial oxygen distribution is approximately Gaussian. Upon annealing the implanted oxygen diffuses throughout the Pd film as Pd₂Si growth begins. Oxygen diffusing to the Pd-Pd₂Si interface reacts with Si there to form SiO₂. The Si at the Pd-Pd₂Si interface acts as a sink for the oxygen. The joint diffusion of Si incorporates the SiO₂ into the growing Pd₂Si without barrier formation taking place.

the growing Pd_2Si by the Si diffusion. Thus, barrier formation does not take place as in the case of Ni and Pt. The sharpness of the oxygen distribution after annealing shows that the diffusion rate of the implanted oxygen to the Pd-Pd₂Si interface is fast compared to Pd₂Si growth. This joint diffusion of both Si and oxygen is responsible for the relative immunity of Pd₂Si formation to impurities. Interfacial accumulation and subsequent blocking of the diffusion paths does not take place. Our results confirm that neither implanted oxygen nor oxygen picked up during annealing impedes the Pd₂Si growth.

The ability of oxygen to form an inert oxide that is incorporated into the Pd₂Si layer without interfacial effects suggests the interesting possibility to use the oxygen as a diffusion marker. Since each oxygen atom is tightly bound to two Si atoms and these are tied to the silicide lattice, this array of atoms is not expected to move relative to the silicide lattice even though considerable mass transport may take place around it. Thus we can reinterpret the experiment as in the case of oxygen in NiSi formation (Chapter III) and use the implanted oxygen to determine the relative diffusion rates of Si and Pd during Pd₂Si formation.

Since oxygen is immobile in Pd₂Si (by assumption) the Si to Pd transport ratio can only be determined once the oxygen is incorporated in the Pd₂Si. The Pd₂Si layer containing the oxygen becomes the marker region. Thus the shift in position of the oxygen distribution identifying this region after Pd₂Si formation relative to that just after incorporation into the Pd₂Si determines the Pd to Si transport ratio. Direct measurements of the position of the oxygen distribution just after

incorporation into the Pd_2Si have not been made, however limits may be inferred from the shape of the final oxygen distribution (Fig. 3). For the case where the width of the oxygen distribution remains unchanged after incorporation into the Pd_2Si , we may take the FWHM (550 Å) to be the width of the initial marker layer. This gives 0.014 as the Pd to Si atomic transport ratio. This case is also consistent with the assumption that oxygen is immobile in Pd_2Si . The other, extreme case is obtained by taking the oxygen to be initially incorporated into a Pt_2Si layer of negligible width located at the Pd-Si interface. This assumption yields a Pd to Si transport ratio of 0.24. Thus we obtain Si as the dominant diffusing species during Pd_2Si formation. This is a different result than that reported by Chu et al [12] using an inert gas marker and that reported by Pretorius et al [13] using a $^{31}\text{Si}^*$ marker. The origin of this disagreement is not known. However in his paper Chu [12] states that very little marker displacement occurred during Pd_2Si growth, and therefore on the basis of energy loss considerations he concludes that both Pd and Si are moving. We speculate after a close inspection of his paper that the origin of the disagreement lies in that his Ar marker was initially placed in the Si substrate at a depth Pd_2Si formation could not reach. Thus a marker shift would not occur.

The $^{31}\text{Si}^*$ radioactive marker experiment of Pretorius et al, [11], [13] on the other hand cannot distinguish between the case where both the metal and the Si move and the case where only Si moves by both substitutional and interstitial means. Both his and our results can be explained if we assume that some component of both types of Si diffusion are present

during Pd₂Si growth. The resolution of the questions raised by the interpretation that Si is the diffusing species as suggested by our facts must await further experiments.

In our model of the effects of oxygen or Pd₂Si formation, the effects of Pd diffusion are virtually eliminated due to the high mobility of the implanted oxygen in the Pd film. Thus our model is consistent with only Si moving during Pd₂Si formation as found here and with both Pd and Si moving as reported previously [11],[12],[13].

E. CONCLUSION

We have investigated the effects of oxygen on Pd₂Si formation by implanting oxygen initially into the Pd film. We found that the oxygen is incorporated into the Pd₂Si near the Pd₂Si-Si interface without a diffusion barrier being formed. The implanted oxygen has no effect on the growth of Pd₂Si. We propose a model in which implanted oxygen is mobile in Pd. Oxygen will therefore diffuse to the Pd-Pd₂Si interface upon annealing, react and form SiO₂ with the Si there. Simultaneously Si diffuses through the Pd₂Si and forms additional silicide at that interface, thereby incorporating the SiO₂ into Pd₂Si, so that no SiO₂ barrier is formed. This model fits a general conceptual model proposed previously.

Our results can also be interpreted to show that Si is the dominant diffusing species during Pd₂Si formation rather than both Pd and Si as previously reported. It is shown that this is not necessarily in contradiction with the other marker experiments thus the statement that both Pd and Si move during Pd₂Si growth may need reconsidering.

REFERENCES

- [1] D.M. Scott, P.J. Grunthaner, B.Y. Tsaur, M-A Nicolet and J.W. Mayer, in *Proceedings of the Symposium on Thin Film Interfaces and Interactions*, J.E.E. Baglin and J. M. Poate, eds., (The Electrochemical Society, Princeton, vol. 80-2, 148) (1980)
- [2] R.J. Blattner, C.A. Evans, Jr., S.S. Lau, J.W. Mayer and B.M. Ullrich, *J. Electrochem. Soc.* 122, 1732 (1975)
- [3] J.B. Bindell, J.W. Colby, D.R. Wonsidler, J.M. Poate, D.K. Conley and T.C. Tisone, *Thin Solid Films*, 37, 441 (1976)
- [4] C.A. Crider, J.M. Poate, and J.E. Rowe, in *Proceedings of the Symposium on Thin Film Interfaces and Interactions*, J.E.E. Baglin and J. M. Poate, eds. The Electrochemical Society, Princeton, vol. 80-2, 135 (1980)
- [5] H. Foll and P.S. Ho, *J. Appl. Phys.* 52, 5510 (1981)
- [6] P. Joubert, P. Auvray and L. Henry, *Thin Solid Films*, 79, 235 (1981)
- [7] S.S. Lau and W. F. van der Weg, in *Thin Films - Interdiffusion and Reactions*, J.M. Poate, K.N. Tu and J. W. Mayer, eds. (John Wiley, NY, 450, (1978)
- [8] R.W. Bower, D. Sigurd and R.E. Scott, *Solid State Electron.* 16, 1461 (1973)
- [9] D.M. Scott and M-A. Nicolet, *Nucl. Instr. & Meth.* 182/183, 65 (1981)
- [10] K.N. Tu, W.K. Chu, and J.W. Mayer, *Thin Solid Films*, 25, 40 (1975)
- [11] R. Pretorius, *J. Electrochem Soc.* 128, 107 (1981)
- [12] W.K. Chu, S.S. Lau, J.W. Mayer, H. Muller and K.N. Tu, *Thin Solid Films*, 25, 393 (1975)
- [13] R. Pretorius, C.L. Ramiller and M-A. Nicolet, *Nucl. Instr. & Meth.* 149, 629 (1978)
- [14] R. Pretorius, J.M. Harris and M-A. Nicolet, *Solid State Elect.* 21, 667 (1978)
- [15] J.F. Gibbons, W.S. Johnson and S.W. Mylroie, *Projected Range Statistics*, (Dowden, Hutchenson & Ross, Stroudsburg, PA) (1975)
- [16] H.C. Kim, R.F. Seiler, D.F. Herring, and K.W. Jones, *Nuc. Phys.* 57, 526 (1964)

CHAPTER VI

GENERAL MODEL

A. INTRODUCTION

The silicides of Ni, Pd and Pt are not the only ones presently used to form contacts to semiconductor devices. An understanding of the role of impurities in the formation of these other silicides is also important to avoid unwanted effects. It is also important to understand the effects of impurities other than oxygen on silicide formation. A systematic experimental determination of these effects for each system and impurity is both time consuming and difficult.

In this chapter we present a general framework in which such future work on silicides can be cast. We also make some predictions of impurity effects, especially on barrier formation.

1. Model

Generalizing from the results of our study on the effects of impurity oxygen on the formation of the silicides of Ni, Pt and Pd, (Chapters III to V), we can identify two major parameters that determine the effect of impurities on metal silicide formation. The first is the initial location of the impurity relative to the moving species. Second is the chemical affinities of the impurity element relative to the reacting species. If we assume that the most stable compound the impurity forms will constitute a diffusion barrier if accumulated at an interface, and if one ignores the ambivalent cases (both species moving, comparable chemical affinity of impurity with both species), there are four distinct

combinations of initial position of the impurity relative to the moving species and of the degree of chemical affinity with respect to the two species (Table 1). Only in the case where the impurity is initially located in the moving species and the moving species has a low chemical affinity with the impurity can a barrier build up during annealing as a result of both chemical reaction and physical accumulation. The case of impurity oxygen initially present in a Ni or Pt film on a Si substrate is an example of this combination (Chapters III and IV). In the other three combinations, barriers can form only by redistribution and build up (segregation, interface drag) of the impurity at an interface; a chemical reaction is not associated with the barrier formation. Oxygen initially present in Si during Ni_2Si formation (Chapter III) is an example where the impurity is initially in the stationary species and is strongly bound there. No barrier is formed however since SiO_2 is not rejected from the silicide, but incorporated in it. The case where oxygen is initially present in the Pd film during Pd_2Si formation (Chapter V) is an example where the impurity is initially located in the stationary species and is weakly chemically bound there. Again, no barrier is formed as the SiO_2 is incorporated into the silicide without an interfacial accumulation taking place. The remaining case, where the impurity is initially located in the moving species and is strongly chemically bound there, has not yet been investigated. Oxygen initially present in Si during Pd_2Si formation may be an example of this combination. We expect on the basis of this model that a buildup of SiO_2 at the Pd_2Si -Si interface will take place due to segregation during Pd_2Si formation. It is not known however, whether such an accumulation of SiO_2 , not chemically bound to the Si in the silicide,

constitutes a diffusion barrier. The resolution of this question must be experimentally determined.

We have tested the predictions of this general treatment for the case of impurity N in the Ni-Si system [1],[2]. Since Ni is the moving species and N does not form a stable nitride with Ni although it forms a very strong nitride with Si ($\Delta H_f^\circ(\text{Si N}_4) = -179.3 \text{ kcal/mol}$ [3]), we predict that the influence of N should parallel that of oxygen on Pt and Ni silicide formation. This is indeed the case. A minor difference however is that N is mobile in Ni at the annealing temperatures of $\sim 300^\circ\text{C}$ and thus N is not carried by Ni diffusion. Nitrogen impurity in Ni thus behaves much like oxygen in Pd films. In fact, barrier formation takes place so fast due to N diffusion that no measurable Ni_2Si forms. Other, preliminary, results supporting the conclusions of this model will be briefly presented in the next chapter.

TABLE 1

		Location	
		Moving	Stationary
Binding Energy	High	Segregation Pd/(Si+O)?	Incorporation: Ni/(Si + O) Ni/(Si + N)
	Low	Barrier Formation: (Ni + O)/Si (Pt + O)/Si (Ni + N)/Si	Incorporation: (Pd+O)/Si

REFERENCES

- [1] L. Wielunski, D.M. Scott, M-A. Nicolet and H. von Seefeld, *Appl. Phys. Lett.* 38, 106 (1981)
- [2] D.M. Scott, L. Wielunski, H. von Seefeld and M-A. Nicolet, *Nucl. Inst. Meth.* 182/183, 661 (1981)
- [3] L.D. Hodgman, R.L. Weast, R.S. Shankland and S.M. Selby, *Handbook of Chemistry and Physics*, Chemical Rubber, Cleveland, (1961)

CHAPTER VII

SUMMARY OF ADDITIONAL WORK

A. INTRODUCTION

The culmination of the work presented thus far is the general conceptual model presented in Chapter VI. This model may prove applicable to impurity elements other than oxygen or silicide formation. Two such elements of special concern are C and N since both are everpresent contaminants in semiconductor processing. We have, therefore, begun to investigate the effects of these two impurity elements on silicide formation.

In this chapter we present a brief summary of work on the effects of N on Ni_2Si formation along with brief summaries of preliminary work on the effects of N on Pt and Pd silicide formation and on the effects of C on the formation of Ni and Pt silicide.

In the case of sufficient oxygen initially present in a Ni or Pt film, we have shown that a barrier to metal diffusion will form during silicide growth (Chapters III and IV). Since metal silicides are used extensively to form contacts to semiconductor devices, an interesting question is that of the change in the contact properties of the silicide due to this barrier formation. In this chapter we also present a brief summary of preliminary work on the effects of O and N on the contact properties of Ni silicide.

B. N IN Ni, Pt AND Pd SILICIDE FORMATION

The chemistry between N and Si is quite different from that between N and Ni, Pt or Pd. N forms a very stable nitride with Si ($\Delta H_f^\circ(\text{Si}_3\text{N}_4) = -179.3$ kcal/mol [1]); however, no Pt or Pd nitrides are known [2]. The Ni nitride Ni_3N has been reported to be very unstable, decomposing at only 190°C in vacuum [2]. Thus N has a much greater chemical affinity to Si than to these metals. This asymmetry in the chemistry of N relative to the reacting species suggests that impurity N will effect the silicide formation of these metals in a manner similar to that previously observed for oxygen (Chapters III to V); i.e., formation of a barrier to Ni or Pt diffusion will take place only if sufficient N is initially located in the metal film; N will have little effect on Pd_2Si formation, etc.

1. N Effects on Ni Silicide Formation

We have studied the effects of implanted N on Ni_2Si formation using $^4\text{He}^+$ backscattering spectroscopy and the $^{14}\text{N}(d,\alpha)^{12}\text{C}$ nuclear reaction [3], [4]. Ni films 1.5 to 4.0 kÅ thick were evaporated on Si $\langle 100 \rangle$ and $\langle 111 \rangle$ substrates; were implanted with N^+ into the Ni film and through the Ni film into the substrate; and were thermally annealed in vacuum at temperatures from 290 to 450°C for various times. The two cases behave as expected. For the N initially located in the Ni film on Si $\langle 100 \rangle$ substrates the $^{14}\text{N}(d,\alpha)^{12}\text{C}$ nuclear reaction shows that the N profile changes its distribution from an as-implanted Gaussian located in the Ni film to a peak positioned at the Ni-Si interface without loss of N. Barrier formation takes place for a threshold dose ϕ_{th} of about 9×10^{15} N/cm^2 , independent of the film thickness (≤ 4000 Å). One difference between oxygen and N is that N is mobile in Ni at the annealing temperature ($\geq 290^\circ\text{C}$) and

redistributes quickly to the Ni-Si interface preventing appreciable Ni_2Si formation. At a dose of $5 \times 10^{16} \text{ N/cm}^2$ the reaction between Ni and Si is completely halted for annealing temperatures below $\sim 375^\circ\text{C}$. Changing the substrate orientation to $\langle 111 \rangle$ raises ϕ_{th} to between 1.0 and $2.0 \times 10^{16} \text{ N/cm}^2$.

For the N initially located in the Si substrate the growth rate of Ni_2Si is retarded but not suppressed. Thus the effects of impurity N on Ni silicide formation are consistent with the predictions of our model [3],[4].

2. N Effects on Pt Silicide Formation

We have made preliminary measurements on the effects of implanted N on the formation of Pt_2Si using backscattering spectroscopy. Pt films $\sim 2500 \text{ \AA}$ thick were evaporated onto Si $\langle 100 \rangle$ substrates, then implanted with N to a depth of $\sim 600 \text{ \AA}$ with doses ranging from 0.5 to $5.0 \times 10^{16} \text{ N/cm}^2$. The samples were then annealed in vacuum at 300°C for various times.

The growth of Pt_2Si is halted before all of the Pt is consumed for N doses $\geq 2 \times 10^{16} \text{ N/cm}^2$. The amount of unreacted Pt left after cessation of Pt_2Si growth increases with increasing N dose. Pt_2Si growth in samples with N doses $\leq 1.0 \times 10^{16} \text{ N/cm}^2$ is not impeded and takes place as in unimplanted samples. Evidently a barrier to Pt diffusion forms in those samples with $\geq 2.0 \times 10^{16} \text{ N/cm}^2$. The threshold N dose is between 1 to $2 \times 10^{16} \text{ N/cm}^2$.

While the redistribution of the N during annealing and the chemical state of the N has yet to be determined, the results so far support the predictions of our model.

3. N in Pd Silicide Formation

We have made only preliminary measurements of the effects of N on Pd₂Si formation using backscattering spectrometry. Pd films ~ 2000 Å thick were evaporated onto Si <100> substrates than implanted with four N doses ranging from 0.5 to 5.0 × 10¹⁶ N/cm² to a depth ~ 600 Å into the Pd film. These samples were then annealed at 250°C in vacuum for various times.

A detailed examination of the backscattering spectra taken for these samples reveals no detectable effects on Pd₂Si formation by the N implantation. This result is consistent with that observed previously in the case of impurity oxygen and is also consistent with our model.

C. C IN Ni AND Pt SILICIDE FORMATION

The chemistry of C in the Ni-Si or Pt-Si systems is not clear. It is known that C forms a stable carbide SiC [1] with Si and does not form any compounds with Pt [2]. A nickel carbide Ni₃C does exist, but is thermodynamically unstable [2]. Thus C forms a stable carbide with Si but not with Ni or Pt. However, SiC has a heat of formation ΔH_f° of only -26.7 kcal/mol [1]. This is close to the heats of formation of Ni and Pt silicides ($(\Delta H_f^\circ(\text{Ni}_2\text{Si}, \text{NiSi}, \text{Pt}_2\text{Si}, \text{PtSi}) = -31.5, -20.4, -20.7, -15.8$ kcal/mole)[5]. Since it is also known that SiC is attacked by molten Ni or Pt [2] and thus at least at high temperatures SiC may not be stable in the presence of Ni or Pt, we are unable to predict the chemistry of C relative to the reacting species as required by our model. Hence no prediction of the effects of impurity C on the formation of Ni or Pt silicides can be made. Therefore an experimental determination of these effects becomes of increased interest.

1. C Effects on Ni Silicide Formation

We have made preliminary measurements on the effects of implanted C on Ni silicide formation using backscattering spectroscopy. Ni films ~ 1500 Å thick evaporated onto Si <100> substrates were implanted with 3.0×10^{16} C/cm² halfway into the film, then thermally annealed in vacuum at 290°C for various times.

Formation of a barrier to Ni diffusion does not take place during annealing. The effect of the implanted C is to slow the rate of Ni₂Si formation $((\text{Ni}_2\text{Si thickness})^2/\text{annealing time})$ to ~ half the unimplanted rate. The Ni₂Si growth rate remains, however, proportional to the square

root of time. The width of the Ni_2Si -Ni interface appears slightly larger than in unimplanted samples, indicating some lateral nonuniformity in Ni_2Si growth. Evidently a SiC diffusion barrier does not form at concentrations at which N or O does.

2. C Effects on Pt Silicide Formation

We have made preliminary measurements on the effects of implanted C on Pt_2Si formation using backscattering spectroscopy. Pt films $\sim 1100 \text{ \AA}$ thick were evaporated onto Si $\langle 100 \rangle$ substrates, implanted with $3.0 \times 10^{16} \text{ C/cm}^2$ halfway through the Pt film then annealed in vacuum at 275°C for various times.

We found that Pt_2Si continues to grow proportionally to the square root of time, but at a rate $((\text{Pt}_2\text{Si thickness})^2/\text{annealing time}) \sim$ half of that observed for unimplanted samples. Formation of a barrier to Pt diffusion did not take place during annealing. The width of the Pt- Pt_2Si interface remains sharp, indicating that Pt_2Si has formed uniformly. There is a dip in the Pt signal at the Pt- Pt_2Si interface for samples in which Pt_2Si growth has nearly reached the Pt surface. This may indicate that the implanted C is rejected from the Pt_2Si and has built up at the Pt- Pt_2Si interface during Pt_2Si formation. As in the Ni_2Si case, evidence of a SiC barrier is absent.

D. DIFFUSION BARRIER EFFECTS ON CONTACT RESISTIVITY OF NICKEL SILICIDE

We have made preliminary measurements of the contact resistivities of Ni silicide contacts to shallow junction solar-cell-type silicon substrates. The substrates were solar cells; 1-10 Ωcm p-type $\langle 100 \rangle$ silicon wafers with a P diffused n^+ -layer. Ni films of $\sim 1400 \text{ \AA}$ were evaporated onto these substrates and implanted with either $2 \times 10^{16} \text{ O/cm}^2$ or $2 \times 10^{16} \text{ N/cm}^2$. Patterns conforming to the transmission line model (TLM) [6],[7] were defined by conventional photolithography using the lift-off technique. The samples were then annealed in vacuum from 290 to 625°C for various times.

1. O Effects on Contact Resistivity

For the case of impurity oxygen in the Ni-Si system, we have shown that a barrier of SiO_2 forms during Ni_2Si formation that prevents complete consumption of the Ni layer. Thus the contact becomes $n^+\text{Si-Ni}_2\text{Si-SiO}_2$ barrier-Ni after annealing. Using the TLM [6],[7] we measured the sheet resistance of the n^+ layer to be $37.4 \text{ } \Omega/\square$ for the implanted samples, which agrees well with $36.0 \text{ } \Omega/\square$ measured for the unimplanted samples. The measured values of the contact resistivity P_c are also close: $P_c = 70 \text{ } \mu\Omega\text{cm}^2$ for the implanted case and $\rho_c = 28 \text{ } \mu\Omega\text{cm}^2$ for the unimplanted case. Evidently the presence of the SiO_2 barrier to Ni diffusion has only a small effect on the contact resistivity.

2. N Effects on Contact Resistivity

For the case of impurity N in the Ni-Si system we have shown that a barrier to Ni diffusion forms before appreciable Ni_2Si can form. Thus the contact becomes $n^+\text{Si-N barrier-Ni}$. We found that the sheet resistance of

the n^+ layer to be $\sim 32 \Omega/\square$ in both implanted and unimplanted samples.

The contact resistivity P_c was found to be $\sim 90 \mu\Omega\text{cm}^2$ in the implanted samples and $\sim 150 \mu\Omega\text{cm}^2$ for unimplanted samples. The lower value observed in the implanted samples may result from improved contact adhesion found after implantation. Thus while N completely blocks N diffusion, the presence of this barrier has little effect on the contact resistivity.

REFERENCES

- [1] R. C. Weast, *Handbook of Chemistry and Physics*, (Chemical Rubber, Cleveland) D-69 (1969)
- [2] M. Hansen and K. Anderko, *Constitution of Binary Alloys*, McGraw-Hill, New York, (1958)
- [3] D. M. Scott, L. Wielunski, H. von Seefeld and M-A. Nicolet, *Nucl. Inst. Meth.*, 182/183, 661 (1981)
- [4] L. Wielunski, D. M. Scott, M-A. Nicolet and H. von Seefeld, *Appl. Phys. Lett.*, 38, 106 (1981)
- [5] R. Pretorius, J. M. Harris and M-A. Nicolet, *Solid-State Elect.*, 21, 667 (1978)
- [6] H. H. Berger, *J. Electrochem. Soc.: Solid-St. Sci. Tech.*, 119, 507 (1972)
- [7] H. H. Berger, *Solid-St. Electron.*, 15, 145 (1972)

CHAPTER VIII

CONCLUSION AND OUTLOOK

A. CONCLUSION

We have used three complimentary techniques, BS, NRA and XPS to investigate the effects of impurity oxygen on the formation of the silicides of Ni, Pt and Pd by thermal annealing of a thin film of the metal deposited on a Si substrate. We found that oxygen initially present in a Ni or Pt film continuously accumulates at the metal-metal silicide interface during annealing. Ultimately a barrier to further metal diffusion is formed. It is the formation of SiO_2 at the metal-metal silicide interface that prevents the metal from entering the silicide. Once the metal supply is cut off, the second phase (NiSi or PtSi) begins to form. When the oxygen is initially present in a Pd film on a Si substrate, we found that this barrier formation does not take place. Instead the oxygen is incorporated into the Pd_2Si during annealing without an interfacial accumulation taking place. The implanted oxygen has little effect on the growth of Pd_2Si . We also found the impurity oxygen to be incorporated both into Ni_2Si for the case of impurity oxygen initially located in the Si substrate and into NiSi for the case of the impurity oxygen initially located in the Ni_2Si film. These results are summarized in Table 1.

We propose a model in which oxygen bonds to Si much more strongly than to either Ni, Pt or Pd. Since Ni and Pt are the moving species during silicide formation, oxygen initially present in the metal will be

exposed to, and react with, the Si at the metal-metal silicide interface to form a barrier of SiO_2 , whereas oxygen initially present in Si or Ni_2Si will remain tied to the Si during silicide formation. The same asymmetry in chemical affinities is also present between oxygen relative to Pd and Si. However since Si is moving during Pd_2Si formation, the SiO_2 formed at the Pd-Pd₂Si interface is incorporated into the Pd₂Si by Si diffusion. Thus barrier formation does not take place.

Generalizing from these cases we propose a model in which only two parameters determine the effect of an impurity element on metal silicide formation. The first parameter is the initial location of the impurity element relative to the moving species. The second is the chemistry of the impurity element relative to the reacting species. If we ignore the ambivalent cases (both species moving, comparable chemical affinities) there are four distinct combinations of initial position and chemical affinity of the impurity relative to the reacting species. We show that only the case where the impurity element is initially in the moving species and this moving species has a low chemical affinity to the impurity can a barrier build up during annealing as a result of both chemical reaction and physical accumulation, e.g., O in a Ni or Pt film on a Si substrate. We have tested the predictions of this general treatment for the cases of impurity N in Ni_2Si , Pt_2Si and Pd_2Si formation and also for impurity C in Ni_2Si and Pt_2Si formation (Table 1). We show that the effects of impurity N on the formation of these silicides are consistent with the predictions of the model. The case of impurity C in Ni_2Si and Pt_2Si is an ambivalent case as C, Ni and Pt have comparable chemical affinities to Si. Thus this model is unable to predict the effects of impurity C on Ni or Pt silicide formation. Experimentally we show that

formation of a barrier does not take place during either Ni_2Si or Pt_2Si formation for C initially present in the metal films. Finally, we have shown that the formation of an oxygen or N diffusion barrier during Ni_2Si formation has little effect on the contact resistivity of nickel silicide.

B. OUTLOOK

At the conclusion of this study, interesting unanswered questions remain. It would be most desirable, for example, to complete the work started on the effects of impurity C since the model breaks down for this case. An investigation of practical importance is that of determining the contact resistivity of silicides found in the presence of impurities. Two questions regarding the diffusion barrier itself are: (1) What is the physical form of the barrier? i.e., is the barrier located at grain boundaries? and (2) What is the effect of temperature on the barrier stability? These possibilities for further studies indicate the direction for future work in an area in which only the first step has been taken.

TABLE 1
Summary of Results

System	Impurity		Silicide Formed	Moving Species	Result (a)
	Element	Location			
Ni-Si	0	Ni	Ni ₂ Si	Ni (b,c)	Barrier
	0	Si	Ni ₂ Si	Ni (b,c)	Incorporation
	0	Ni ₂ Si	NiSi	Ni (d)	Incorporation
Pd-Si	0	Pd	Pd ₂ Si	Si (a),Pd(b)	Incorporation
Pt-Si	0	Pt	Pt ₂ Si	Pt (e)	Barrier
Ni-Si	N	Ni	Ni ₂ Si	Ni (b(c))	Barrier
	N	Si	Ni ₂ Si	Ni (b,c)	Incorporation
Pd-Si	N	Pd	Pd ₂ Si	Si (a),Pd(b)	Incorporation
Pt-Si	N	Pt	Pt ₂ Si	Pt (e)	Barrier
Ni-Si	C	Ni	Ni ₂ Si	Ni (b,c)	No barrier
Pt-Si	C	Pt	Pt ₂ Si	Pt (e)	No barrier

(a) this work

(b) W. K. Chu, S. S. Lau, J. W. Mayer, H. Muller and K. N. Tu, *Thin Solid Films*, 25, 393 (1975)

(c) R. Pretorius, C. L. Ramiller, S. S. Lau, and M-A. Nicolet, *Appl. Phys. Lett.*, 30, 501 (1977)

(d) T. G. Finstad, J. W. Mayer, and M-A. Nicolet, *Thin Solid Films*, 51, 391 (1978)

(e) R. Pretorius, *J. Electrochem. Soc.*, 128, 107 (1981)